

## **INFORMATION TO USERS**

This manuscript has been reproduced from the microfilm master. UMI films the text directly from the original or copy submitted. Thus, some thesis and dissertation copies are in typewriter face, while others may be from any type of computer printer.

**The quality of this reproduction is dependent upon the quality of the copy submitted.** Broken or indistinct print, colored or poor quality illustrations and photographs, print bleedthrough, substandard margins, and improper alignment can adversely affect reproduction.

In the unlikely event that the author did not send UMI a complete manuscript and there are missing pages, these will be noted. Also, if unauthorized copyright material had to be removed, a note will indicate the deletion.

Oversize materials (e.g., maps, drawings, charts) are reproduced by sectioning the original, beginning at the upper left-hand corner and continuing from left to right in equal sections with small overlaps. Each original is also photographed in one exposure and is included in reduced form at the back of the book.

Photographs included in the original manuscript have been reproduced xerographically in this copy. Higher quality 6" x 9" black and white photographic prints are available for any photographs or illustrations appearing in this copy for an additional charge. Contact UMI directly to order.



Bell & Howell Information and Learning  
300 North Zeeb Road, Ann Arbor, MI 48106-1346 USA  
800-521-0600



Copyright

by

Joseph Chen-Yu Wang

1998

**A One Dimensional Model of Convection in Iron Core  
Collapse Supernovae**

APPROVED BY

SUPERVISORY COMMITTEE:

Supervisor:

Jay Wheeler  
Walter Truran  
Adam Burrows  
John S. DeLoach  
Paul Shenko

**A One Dimensional Model of Convection in  
Iron Core Collapse Supernovae**

by

**Joseph Chen-Yu Wang, S.B., M.A.**

**Dissertation**

Presented to the Faculty of the Graduate School of

The University of Texas at Austin

in Partial Fulfillment

of the Requirements

for the Degree of

**Doctor of Philosophy**

**The University of Texas at Austin**

December 1998

**UMI Number: 9937155**

**Copyright 1998 by  
Wang, Joseph Chen-Yu**

**All rights reserved.**

---

**UMI Microform 9937155  
Copyright 1999, by UMI Company. All rights reserved.**

**This microform edition is protected against unauthorized  
copying under Title 17, United States Code.**

---

**UMI**  
300 North Zeeb Road  
Ann Arbor, MI 48103

# Acknowledgments

I would like to thank my wife Suchen Liao and my daughter for their support and patience through my graduate studies. Furthermore, I also thank my mother, Luan Luan Wang, and my brother and sister, Ruth and Daniel for their encouragement. My dissertation supervisor, Craig Wheeler, and dissertation committee Adam Burrows, John Scalo, Paul Shapiro, and Ethan Vishniac, all deserve thanks for their invaluable time and help. In addition, I would also like to thank Itamar Lichtenstadt, Alexei Khokhlov, and Stephen Bruenn for their ideas, comments, and suggestions.

Finally, I would like to dedicate this dissertation to Confucius and my departed father, Ming Kang Wang, without whose direction and love of knowledge this dissertation would never have existed.

JOSEPH CHEN-YU WANG

*The University of Texas at Austin  
December 1998*

# **A One Dimensional Model of Convection in Iron Core Collapse Supernovae**

Publication No. \_\_\_\_\_

Joseph Chen-Yu Wang, Ph.D.

The University of Texas at Austin, 1998

Supervisor: J. Craig Wheeler

Although convection is agreed to exist within the newly formed neutron stars in core collapse supernovae, its role remains unclear. Much of the uncertainty concerning the role of convection may be attributed to the fact that the main tools for the investigation of convection in these supernovae are multi-dimensional codes. While these codes provide insight into the role of convection in supernova, their computationally intensive nature makes it impractical to run these codes repeatedly under different physical assumptions and to explore the physics of the late time evolution of the iron core collapse.

A one dimensional algorithm for modeling time-dependent convection was developed by treating the convectively unstable zones as two streams. Models using this algorithm were run using various parameters. A series of models were run including different types of neutrinos and different convective

effects. Without convection, the shock stalled at a radius of  $2 \times 10^7$  cm. No qualitative differences that would aid the supernova explosion were observed when convection was included.

In models containing all neutrino species, an entropy spike developed in the immediate post shock region. In contrast to interpretations which attribute this spike to radiative heating by neutrinos, the spike in the current models are believed to be caused by shock heating. Comparison of models containing different neutrino species suggests that a “heating dilemma” exists, in that for a shock evolving quasi-statically whose post-shock region is in hydrostatic equilibrium, increased post shock entropy is associated with a smaller shock stall radius. Therefore higher entropies behind the shock in these conditions correspond to model failure rather than to successful explosions. This correlation also appears to produce an inverse relationship between root mean square radiated neutrino energy and shock stall radius.

# Contents

<b>Acknowledgments</b>	<b>iv</b>
<b>Abstract</b>	<b>v</b>
<b>List of Tables</b>	<b>xi</b>
<b>List of Figures</b>	<b>xii</b>
<b>Chapter 1 Introduction</b>	<b>1</b>
1.1 Physics of core collapse . . . . .	4
1.1.1 The prompt shock . . . . .	5
1.1.2 The delayed shock . . . . .	6
1.2 Convective instabilities in supernovae . . . . .	10
1.2.1 Observational evidence for convection in 1987A . . . . .	12
1.2.2 $Y_e$ driven convection . . . . .	14
1.2.3 Salt-finger mixing . . . . .	14
1.2.4 Prompt convection . . . . .	16
1.2.5 Neutrino-driven convection . . . . .	17
1.2.6 Hot bubble convection . . . . .	19
1.2.7 Late-time inner-core Ledoux convection . . . . .	20

1.2.8	H-He instability . . . . .	20
1.2.9	Need for a one dimensional code . . . . .	21
<b>Chapter 2</b>	<b>The supernova shock</b>	<b>25</b>
2.1	The shock . . . . .	26
2.2	The stalled shock . . . . .	31
2.3	The revived shock . . . . .	32
2.4	Conclusion . . . . .	38
<b>Chapter 3</b>	<b>The convective model</b>	<b>40</b>
3.1	Physical requirements . . . . .	40
3.2	Review of convective algorithms . . . . .	42
3.2.1	Standard mixing length theory . . . . .	42
3.2.2	Non-local mixing length theory . . . . .	44
3.2.3	Moment models . . . . .	44
3.2.4	Turbulent diffusion models . . . . .	46
3.2.5	Two-stream models . . . . .	46
3.3	Review of numerical work . . . . .	47
3.4	The convective model . . . . .	48
3.4.1	The entropy and composition fluctuation equations . .	52
3.4.2	The velocity fluctuation equation . . . . .	54
3.4.3	Asymmetry parameter . . . . .	56
3.4.4	Coupling with the neutrinos . . . . .	57
3.4.5	Energy conservation . . . . .	58
3.4.6	Braking parameter . . . . .	58
3.4.7	Turbulent pressure . . . . .	59
3.4.8	Boundary conditions and initial perturbations . . . . .	59

3.4.9	Summary of equations and parameters . . . . .	61
3.5	Analytic limits . . . . .	62
3.6	Extensions to the model . . . . .	63
3.6.1	Radiative damping extensions . . . . .	64
<b>Chapter 4</b>	<b>Numerical implementation</b>	<b>66</b>
4.1	Numerical implementation . . . . .	66
4.2	The non-convective implementation . . . . .	66
4.2.1	Hydrodynamics . . . . .	67
4.3	Neutrino transport algorithm . . . . .	69
4.3.1	Multi-group flux limited diffusion . . . . .	69
4.3.2	Neutrino matter coupling . . . . .	72
4.4	Neutrino differencing algorithm . . . . .	79
4.5	Switch on criterion . . . . .	86
4.6	Splitting algorithm . . . . .	87
4.7	Merging algorithm . . . . .	88
4.8	Computational hardware . . . . .	89
4.9	Computational tests . . . . .	90
<b>Chapter 5</b>	<b>Results and discussion</b>	<b>100</b>
5.1	Model runs . . . . .	100
5.2	The non-convective models . . . . .	101
5.3	Comparison with electron neutrino only models . . . . .	117
5.4	The heating dilemma . . . . .	139
5.4.1	Resolving the heating dilemma . . . . .	141
5.5	Neutrino energy . . . . .	142
5.6	Convective models . . . . .	143

5.7	Convective models with nonstandard parameters . . . . .	161
5.8	Analysis of the convective models . . . . .	165
<b>Chapter 6 Conclusion</b>		<b>169</b>
6.1	Future Application of the Convective Algorithm . . . . .	171
6.2	Applicability of this model to other astrophysical convection problems . . . . .	172
6.3	Further research . . . . .	172
<b>Bibliography</b>		<b>175</b>
<b>Vita</b>		<b>188</b>

# List of Tables

1.1	Summary of convective instabilities in core collapse supernovae	11
1.2	Translation table . . . . .	13
3.1	Parameters in the convective model . . . . .	61
5.1	List of model runs . . . . .	101

# List of Figures

1.1	Optical depth of neutrinos . . . . .	9
2.1	Time versus radius assuming hydrostatic equilibrium . . . . .	33
2.2	Time versus radius for given entropy . . . . .	35
2.3	Energy versus time and entropy. Numbers in the plot are explosion energies in $10^{51}$ ergs . . . . .	36
4.1	Sedov blast wave density evolution . . . . .	93
4.2	Sedov blast wave pressure evolution . . . . .	94
4.3	Sedov blast wave radius $^{5/2}$ versus time evolution . . . . .	95
4.4	Sedov blast wave density transient evolution . . . . .	96
4.5	Sedov blast wave pressure transient evolution . . . . .	97
4.6	Neutrino propagation test . . . . .	99
5.1	Shock radius versus time - Non-convective - All neutrino species	102
5.2	Velocity evolution - Non-convective - All neutrino species . .	104
5.3	Early entropy evolution - Non-convective - All neutrino species	105
5.4	Entropy versus mass evolution - Non-convective - All neutrino species . . . . .	106

5.5	Entropy versus radius evolution - Non-convective - All neutrino species . . . . .	107
5.6	Entropy versus log radius evolution - Non-convective - All neutrino species . . . . .	108
5.7	$Y_e$ evolution - Non-convective - All neutrino species . . . . .	109
5.8	Radius versus mass evolution - Non-convective - All neutrino species . . . . .	111
5.9	Density evolution - Non-convective - All neutrino species . . . . .	112
5.10	Neutrino heating/cooling - Non-convective - All neutrino species . . . . .	113
5.11	Neutrino heating/cooling - Non-convective - All neutrino species . . . . .	114
5.12	Temperature - Non-convective - All neutrino species . . . . .	116
5.13	Neutrino energy versus time - Non-convective - All neutrino species . . . . .	118
5.14	Neutrino luminosity versus time - Non-convective - All neutrino species . . . . .	119
5.15	Neutrino energy versus radius - Non-convective - All neutrino species . . . . .	120
5.16	Shock versus time - Non-convective - Electron neutrino only . . . . .	122
5.17	Velocity evolution - Non-convective - Electron neutrino only . . . . .	123
5.18	Entropy evolution - Non-convective - Electron neutrino only . . . . .	124
5.19	Entropy evolution - Non-convective - Electron neutrino only . . . . .	125
5.20	Entropy evolution - Non-convective - Electron neutrino only . . . . .	126
5.21	$Y_e$ evolution - Non-convective - Electron neutrino only . . . . .	127
5.22	Comparison of entropy versus mass profiles . . . . .	128
5.23	Comparison of entropy versus radius profiles . . . . .	129

5.24 Neutrino heating/cooling - Non-convective - Electron neutrino only	131
5.25 Neutrino heating/cooling - Non-convective - Electron neutrino only	132
5.26 Velocity evolution - Non-convective - Electron neutrino only	133
5.27 Radii evolution - Non-convective - Electron neutrino only	134
5.28 Density evolution - Non-convective - Electron neutrino only	135
5.29 Neutrino energy versus time - Non-convective - Electron neutrino only	136
5.30 Neutrino luminosity versus time - Non-convective - Electron neutrino only	137
5.31 Neutrino energy versus radius - Non-convective - Electron neutrino only	138
5.32 Convective velocity versus mass evolution - Convective - All neutrino species	144
5.33 Convective velocity evolution versus radius - Convective - All neutrino species	145
5.34 Velocity evolution - Convective - All neutrino species	146
5.35 Entropy evolution - Convective - All neutrino species	147
5.36 $Y_e$ evolution - Convective - All neutrino species	148
5.37 Convective luminosity - Convective - All neutrino species	149
5.38 Shock versus time - Convective - All neutrino species	151
5.39 Neutrino heating/cooling - Convective - All neutrino species	152
5.40 Neutrino heating/cooling - Convective - All neutrino species	153
5.41 Neutrino energy versus time - Convective - All neutrino species	154

5.42 Neutrino Luminosity versus time - Convective - All neutrino species . . . . .	155
5.43 Convective velocity evolution - Convective - Electron neutrinos only . . . . .	156
5.44 Entropy evolution - Convective - Electron neutrino only . . . . .	157
5.45 Entropy versus radius evolution - Convective - Electron neutrinos only . . . . .	158
5.46 Convective luminosity - Convective - Electron neutrinos only . . . . .	159
5.47 Entropy versus radius evolution - Convective with braking and turbulent pressure - All neutrino species . . . . .	162
5.48 Entropy evolution - Convective with neutrino advection - All neutrino species . . . . .	163
5.49 Shock radius versus time - Convective with neutrino advection - All neutrino species . . . . .	164
5.50 Neutrino energy versus time - Convective with neutrino advection - All neutrino species . . . . .	166
5.51 Neutrino luminosity versus time - Convective with neutrino advection - All neutrino species . . . . .	167

# Chapter 1

## Introduction

One of the most fascinating yet frustrating challenges in astrophysics is the modeling of the first few seconds after collapse of an iron core collapse supernova. The correct modeling of this phase of supernova is vital for the complete understanding of a variety of phenomena including nucleosynthesis, neutrino interactions, and compact objects such as black holes and neutron stars.

Core collapse supernovae are believed to generate most of the heavy elements in the Universe. Hence the correct modeling of the mechanism for these supernova explosions is critical for understanding both the creation and distribution of elements as well as for the overall chemical evolution of the Milky Way galaxy and the Universe as a whole. The lack of a successful numerical model to bridge the gap between models of supernova progenitors and nucleosynthetic calculations means that there is not a good understanding of the relationship between different progenitor models and nucleosynthetic yields (Burrows 1996, 1997). Although models exist that calculate the nucleosynthetic abundances from an iron-core collapse (Woosley & Weaver 1995; Hartmann, Woosley, & El Eld 1985; Thielemann, Nomoto, & Hashimoto 1996;

Rayet et al. 1995; Thielemann, Hashimoto, & Nomoto 1990) the lack of understanding of the early phases of the core collapse requires these models to begin with an artificial velocity push or a large injection of thermal energy as an artificial initial condition in their calculation. Although models with these conditions allow for nucleosynthetic predictions, they are unsatisfactory in that these conditions are not derived from the physics of the core collapse and because varying the strength of the initial shock does have an effect on the calculated nuclear yields (Aufderheide, Baron, & Thielemann 1991). In addition, it is still unclear whether r-process elements may be formed within core collapse supernovae (Woosley & Hoffman 1992; Takahashi, Witt, & Janka 1994 ; Woosley et al. 1994; Hoffman, Qian, & Woosley 1995 ; Meyer & Brown 1997 ) or whether neutrino interactions with nuclei can produce rare isotopes such as  $^{11}B$  and  $^{19}F$  (Woosley et al. 1990; Woosley & Haxton 1989).

The high temperatures, pressures, and densities which occur within core collapse supernova may allow them to be used as a laboratory for high energy physics in order to support or refute various theories. Core collapse supernova produce large numbers of neutrinos and are the only objects outside the solar system for which neutrinos have been detected. Neutrinos from 1987A are significant since they set limits on the mass (Burrows 1988; Chiu & Chan 1988) and magnetic moment of the electron neutrino (Lattimer and Cooperstein 1988; Barbieri and Mohapatra 1988; Blinnikov and Okun 1988) as well as masses of electron antineutrinos (Loredo & Lamb 1989) and of the tau neutrino (Loredo & Lamb 1991; Takahara & Sato 1988 ). It has been suggested that the details of a supernova explosion are affected by the existence or non-existence of a neutrino mass (Fuller et al. 1992), which, in turn, has cosmological implications. The explosion may also be affected by the existence or non-

existence of particles such as the majoron and axion (Choi & Santamaria 1990; Choi, Kang, & Kim 1989; Fuller et al. 1992). The density at the centers of proto-neutron stars exceeds nuclear density. This high density may affect neutrino cross-sections either through long range correlations (Burrows & Sawyer 1998) or by ion screening effects (Bruenn & Mezzacappa 1998) and may produce unusual forms of matter such as pion or kaon condensates (Brown & Bethe 1994) or strange matter (Anand et al. 1997; Benvenuto & Horvath 1989). The primary difficulty in using supernovae as laboratories for high energy or high density physics is that early phase core collapse models are not yet sufficiently well developed enough to calculate the results of competing theories and to distinguish between different particle theories.

In addition, iron core collapse and the possible collapse of the iron core into a black hole has been suggested as sources of gravitational radiation either from asymmetries resulting from the rotation of the collapsing core (Burrows, Hayes, & Frxeyll 1995; Bonnell & Pringle 1995; Trofimenko & Gurin 1991) or from convection within the protoneutron star (Mueller & Janka 1997) As with the cases involving high energy and high density physics, the main limitation to the use of supernova to explore the physics of gravitational radiation is the lack of understanding of the mechanisms of core collapse.

Core collapse results in some of the more exotic objects in astronomy such as black holes and neutron stars. A model of the first few seconds of core collapse may provide answers to a number of intriguing questions. For example, it is not clear which progenitors leave black holes and which ones leave neutron stars and what the mass function for these remnant objects is (Timmes, Woosley, & Weaver 1996). Moreover, the supernova explosion may determine the mass of the remnant object and may provide an explanation for

why pulsar masses appear to cluster at a fixed value (Thorsett et al. 1993) while the observed black hole candidates in X-ray binaries appear to have much larger masses of between 3 and 16 solar masses (Van Paradijs & McClintock 1995). There is also a population of high velocity pulsars the velocities of which have been attributed to asymmetric supernova explosions. (Janka & Mueller, 1994; Brandt & Podsiadlowski 1995; Fryer, Burrows, & Benz 1996; Van Den Heuvel & Van Paradijs 1997)

## 1.1 Physics of core collapse

Despite valiant efforts, there are no satisfactory models of the first several seconds of iron core collapse. Much of the difficulty in developing these models results from the rich and complex physics which influences this phenomenon. Among the physical processes affecting core collapse are neutrino interactions, general relativity, nuclear equations of state, convection, rotation, and magnetism. In addition, there is variation in the structures of progenitor models used as initial conditions for collapse calculations (Burrows 1997). This rich set of physical processes and the fact that these processes may be interacting with each other in complex ways also leads to considerable theoretical uncertainty. It is still unclear which processes are important and which processes are incidental and how variations in the physical processes during the collapse affect the dynamics of the explosion.

Despite these uncertainties, there is general agreement on some basic points. To begin with, it is generally agreed that core collapse supernova are the result of the collapse of a massive star at the end of its evolutionary lifespan. This paradigm has not only resulted in models of Type II supernova

spectra, light curves, and nucleosynthesis (Woosley & Weaver 1995; Timmes et al. 1996; Rayet et al. 1995) that match observations, but also is supported by the observations of supernova 1987A whose progenitor was observed before the explosion. (Testor 1988; West et al. 1987). When the mass of the iron core in a progenitor exceeds approximately 1.4 solar masses, the interior of the star can no longer be supported, and the star begins to collapse. During the course of the collapse, approximately  $10^{53}$  ergs of potential energy is released. This far exceeds the observed kinetic energy of this form of supernova which is approximately  $10^{51}$  ergs. However, it is believed the bulk of energy of collapse is radiated away in the form of neutrinos and is therefore unavailable to power the explosion. This belief is supported by observations of neutrinos from supernova 1987A.

When the collapse begins, it can be accurately modeled as a homologous contraction (Yahil 1983). This phase of the collapse is known as the “infall phase” and ends when the density of the inner core rises to nuclear densities. This causes the core to suddenly stiffen. Because the infall material is falling at speeds approaching the sound velocity, the stiffening of the core causes a shock wave to begin to propagate outward. The process by which the inner core reaches maximum density and rebounds, thereby causing a shock wave to begin propagating outward is known as “core bounce.”

### 1.1.1 The prompt shock

As the shock travels out it begins to weaken as it dissociates iron nuclei and more importantly as neutrino losses remove energy from behind the shock (Mezzacappa et al. 1998). In so-called “prompt shock” (Colgate & White

1964) models, these losses are unable to prevent the shock from moving outward, and the shock escapes the iron core and the star and produces an explosion (Bruenn 1989; Myra 1989; Burrows & Lattimer 1985). For a prompt shock model to succeed, two conditions must be fulfilled. First, there must be a large homologous core, which is to say that the shock must begin to form near the outside of the iron core. Secondly, the iron core itself must be relatively small. These two conditions insure that the shock does not have to travel through a large section of the iron core and thereby lose excessive energy through nuclear dissociation. Unfortunately, the consensus now is that prompt shock models will not work because they require iron cores which are unrealistically small (Mezzacappa et. al. 1998). Instead of escaping the star, the shock in current models stalls, becoming an accretion shock which remains relatively fixed in radius as material from above continues to move across the shock front.

### 1.1.2 The delayed shock

The failure in developing successful prompt shock models has lead to interest in “delayed shock” models of Burrows & Lattimer (1985) and Bethe and Wilson (1985). In these models, the shock stops propagating outward and becomes an accretion shock; however, neutrino radiation from the interior of the shock heats the material directly behind the shock. This causes the shock to revive and to begin moving outward in radius. In contrast to the mechanism of Colgate (1968) in which neutrino heating occurs on timescales of a few milliseconds, the delayed shock mechanism invoked in more recent models envisions neutrino heating occurring over a timescale of several hundred

milliseconds (Mezzacappa et al. 1998).

### **Concepts used with delayed models**

Within the delayed shock paradigm are a number of concepts which have been used in the literature to describe models. One of these concepts are “neutrinospheres,” which are the locations in the proto-neutron star where the material becomes optically thin to a given type of neutrinos. More specifically, a neutrinosphere for a type of neutrino is the location where the optical depth  $\tau$  of that neutrino type falls below  $\tau = 2/3$ . Below the neutrinosphere, the neutrinos are trapped and only slowly diffuse outward. Above the neutrinosphere, they begin to stream freely. This concept is particularly important since most groups who work with multidimensional models and many who work with one dimensional collapse do not calculate the neutrino energy spectrum, but rather approximate the neutrino spectrum as a function of the temperature at the neutrinosphere, where the neutrinos become decoupled from the matter. This thermal spectrum is generally modified by a “pinch factor” to take into account non-thermal effects such as Doppler shifting and different opacities for different energy neutrinos.

Some caution should be taken in dealing with the neutrinosphere. The neutrinosphere is conceived of as the radius within the proto-neutron star where the neutrino radiation field becomes decoupled from the matter. The actual situation is likely to be considerably more complicated, because neutrinos of different energy have very different scattering and absorption cross sections, and therefore different optical depths. In the actual star there is not a single radius which can be considered to be the neutrinosphere, rather one has different neutrinospheres for neutrinos of different energy. The degree to

which this is true is illustrated in figure 1.1 which plots the optical depths of neutrinos of different energy in a typical collapse calculation. As can be seen, there is not a clearly defined radius which can be considered the neutrinosphere. The degree to which the neutrinosphere can be treated as a single radius is a topic of current research.

Another important concept found in delayed shock models is the gain radius. The gain radius lies inside of the shock and marks the point beyond which neutrino heating occurs. Within the gain radius there is a net loss in neutrino energy. Between the gain radius and the shock, there is net energy gain due to neutrino heating. The gain radius comes about because neutrino emission is a highly sensitive monotonically increasing function of temperature while neutrino absorption is relatively insensitive to temperature. As one moves outward through the proto-neutron star, the temperature decreases. This implies that the neutrino emission decreases while the absorption stays relatively constant. When one moves past the gain radius, the neutrino emission drops below the neutrino absorption rate and the material gains neutrino energy.

One final concept which is found in delayed shock models is that of “critical luminosity.” For a delayed shock model to generate a successful explosion, there needs to be a certain amount of energy deposited behind the shock through neutrino interactions. For a collapse model of a given structure, the energy deposition rate should increase as the neutrino luminosity increases. If the neutrino luminosity exceeds a critical value, there should be a successful explosion. Using quasi-static models of the supernova, Burrows and Goshy (1993) and Shigeyama (1995) have derived analytic criteria to calculate the value and form of the critical luminosity function, given the infall rate.

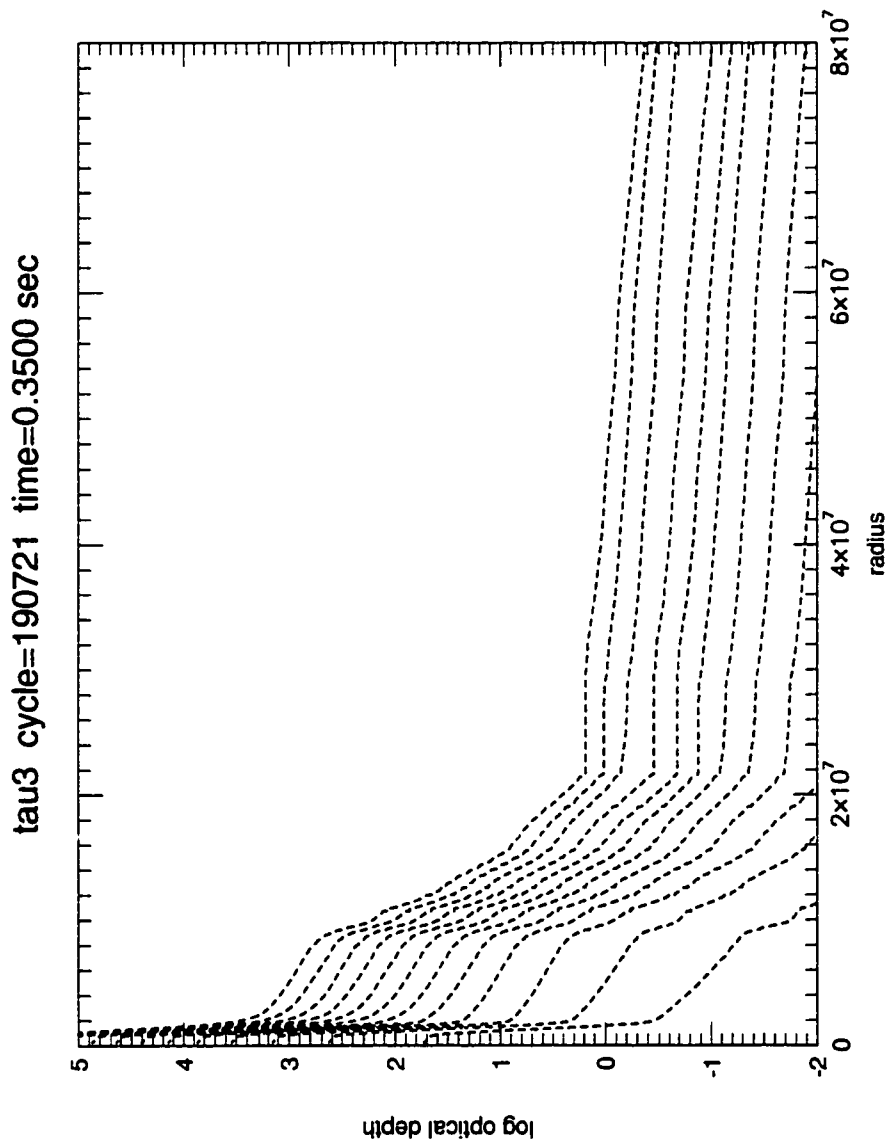


Figure 1.1: Optical depth of neutrinos

## **Results of delayed models**

The success of delayed shock models has been disappointing. One group has reported successful explosions which give rise to a high-entropy, low density, radiation-dominated bubble (Bethe & Wilson 1985). This bubble is particularly of interest since it has been suggested as a possible site for the formation of r-process elements (Meyer et al. 1992). However, the explosions generated by Wilson and Mayle (1993) are less energetic than observed supernovae, and in general, the neutrino flux has not been sufficient in one dimensional models to revive the shock and cause an explosion (Myra et al. 1987; Bruenn & Mezzacappa 1994).

## **1.2 Convective instabilities in supernovae**

In an effort to more consistently generate core collapse supernova explosions, there has been interest in the role of convection in core collapse. Convectively unstable regions follow naturally from the delayed shock model. The dissipation of the shock leads to a convectively unstable gradient as does the fact that a convective unstable gradient is needed for heating to exceed cooling in steady state accretion (Burrows 1997). Moreover, observations of supernova 1987A have provided evidence of convective instabilities in proto-neutron stars.

In this section, the observational evidence for convection in core collapse supernova is presented, and the literature concerning the theoretical role of convection is reviewed. A review of the literature is made complicated because of the existence of several convective zones, and the fact that some convective instabilities are observed in some simulations but not others. In addition,

	driving force	location	time
$Y_e$ driven	negative $Y_e$ gradient caused by deleptonization due to neutrino emission	0.0 to 0.2 solar masses	starts 5 to 10 msec after bounce
double diffusive	positive $Y_e$ gradient and negative $s$ gradient due to neutrino emission	0.4 to 0.6 solar masses	starts 5 to 10 msec after bounce
prompt	negative $s$ gradient caused by weakening of shock	0.8 to 1.2 solar masses	starts 5 to 10 msec after bounce
neutrino driven	negative $s$ gradient caused by neutrino heating of material	1.3 to 1.4 solar masses	starts 20 to 30 msec after bounce
hot bubble	pressure-density instability caused by rapid neutrino heating at the based of zone	1.3 to 1.4 solar masses	several hundred msec after bounce
H-He convection	pressure-density instability caused by shock hitting H-He boundary	10 solar masses	several hours after bounce

Table 1.1: Summary of convective instabilities in core collapse supernovae

the terminology used to describe convection is confused with authors using different terms for the same process and the same term to describe different processes. Therefore, one of the purposes of this section will be to define a consistent terminology to describe convective processes in this dissertation and to relate this terminology to the terms used by other authors. A summary of how the terminology of the dissertation relates to the terminology used by other authors is given in table 1.2.

### **1.2.1 Observational evidence for convection in 1987A**

There are two pieces of observational evidence which indicate the existence of convective instabilities in supernova 1987A, which are reviewed by Arnett et al. (1989) and McCray (1993). The first is the early detection of spectral lines in X-rays and  $\gamma$ -rays associated with  $^{56}\text{Co}$ . This element is generated from  $^{56}\text{Ni}$  which is produced deep within the silicon layer. Without mixing to move this material into optically thin layers, it would not be visible until at least a year after the explosion.

The other piece of evidence of large scale mixing in type II supernova consists of high velocity spectral lines which have been observed in the infrared for  $^{56}\text{Fe II}$  and in gamma rays for  $^{56}\text{Co}$ . These lines have not been reproduced in simulations which include only Rayleigh-Taylor instabilities at the hydrogen-helium interface. It has therefore been concluded that instabilities were preceded by earlier instabilities deeper in the supernova core (Herant & Benz 1992).

This Work	(Mezzacappa, Calder, Bruenn et al. 1997)	(Burrows, Hayes and Fryxell 1995)	(Mueller Janka 1995)	& (Miller, Wilson & Mayle 1993)	(Herant, Benz & Colgate 1992; Herant, Benz, Hix & Colgate 1994)
early ye-driven convection	lepton - driven convection below the neu- trinosphere				Lepton-gradient driven instabil- ity
salt-finger mix- ing	Neutron fingers			salt-finger mix- ing, convection below the neu- trinosphere	
prompt convec- tion	Entropy-driven convection below the neu- trinosphere	inner entropy- driven convec- tion	convection inside the proto- neutron star	convection above the neu- trinosphere	Entropy- gradient driven instability
neutrino-driven convection	neutrino-driven convection above the neu- trinosphere	outer entropy- driven convec- tion	convection in the hot-bubble region		
late-time Ledoux con- vection			Ledoux convec- tion within the proto-neutrino star		
H-IIe convection		Rayleigh-Taylor instabilities in the stellar envelope			

Table 1.2: Translation table

### **1.2.2 $Y_e$ driven convection**

In addition to the observational evidence for convection, theoretical models of core collapse supernova also suggest a number of sites in which convection occurs. One of the first papers to deal with the topic of convection in supernovae was that of Epstein (1979) who pointed out that as neutrinos leave the inner layers of the neutron star a gradient in the electron mass fraction  $Y_e$  is formed which is unstable to convection. Epstein postulated that this leptonic overturn would produce hydrodynamic motions that would power the shock. This leptonic overturn was the topic of several papers in the late-1970's and early-1980's (Bruenn, Buchler and Livio 1979), but interest in this form of convection waned after two items were pointed out. First, the region of the instability was small since the negative  $Y_e$  gradient was stabilized by the positive  $S$  gradient in most of the core of the proto-neutron star. Second, the equation of state for much of the inner core resulted in  $\frac{\partial Y_e}{\partial \rho}$  being positive, thereby causing a negative  $Y_e$  gradient to be a stable configuration rather than an unstable one (Lattimer & Masurek 1983).

### **1.2.3 Salt-finger mixing**

Another form of mixing which has been invoked in core collapse supernova is the salt-finger instability, also known as the neutrino-finger, double-diffusive, or thermohaline instability (Wilson & Mayle 1993). This instability occurs when there is a positive entropy gradient and a composition gradient in which the material with denser composition is on top. In this instability, the heat diffuses out of a fluid element faster than composition. As the fluid elements reach thermal equilibrium, the composition difference between a fluid element

and its surroundings causes a buoyancy force, which cause downward moving fluid elements to move even further downward and upward moving fluid elements to move even further upward. The name “salt-finger” derives from an example of this mixing in geophysics when the warm and fresh waters of the Mediterranean move on top of the cold and salty waters of the North Atlantic.

Wilson and Mayle (1988) have reported that this form of convection is essential for their models to achieve an explosion, albeit one which has half the energy of observed supernovae. The effect of salt-finger mixing in their models is to increase the temperature and the lepton fraction at the neutrinosphere. The increase in temperature causes an increase in both neutrino emission and neutrino energy while the increase in the lepton fraction allows more electron captures to take place thereby increasing the neutrino flux. Because this form of convection is important to their models, they are careful to distinguish between “convection under the neutrinosphere” as they classify this convection and “convection above the neutrinosphere” which they consider largely unimportant to the explosion.

This form of convection is difficult to study because it occurs deep within the proto-neutron star. In this region, the Courant condition makes it difficult to perform multi-dimensional simulations. However, the two dimensional simulations of Keil, Janka, and Mueller (1995) which studied conditions within the supernova down to the center of the star have failed to find this form of convection. Furthermore, Dineva and Bruenn (1996) have argued that neutrino processes cause diffusion in composition to occur more rapidly than thermal diffusion. Under these circumstances, the gradients required for salt finger mixing to occur are reversed, and the inner core of the proto-neutron star is stable to salt finger mixing.

### 1.2.4 Prompt convection

Another region of convection occurs behind the stalled shock. As the shock stalls, the material behind the shock is heated less and less, and this produces a negative entropy gradient that will drive convection.

This form of convection was first pointed out by Burrows (1987) and has been the topic of both one-dimensional (Bruenn & Mezzacappa 1994) and two dimensional (Herant and Benz 1996; Burrows, Hayes & Fryxell 1995; Janka & Mueller 1995; Mezzacappa et al. 1998) calculations. Although researchers tend to agree that there is a negative entropy gradient, there is some difference in opinion as to the subsequent evolution of the convection generated by this gradient. In the two dimensional calculations of Mezzacappa et al. (1996), transfer of heat between fluid elements suppresses the convection. By contrast, in the two dimensional calculations of Janka and Mueller (1996),  $Y_e$  driven convection causes the convective region which is initially generated by the negative energy gradient to move inward and to encompass the entire proto-neutron star after about one second.

The role of this convection remains uncertain. Bethe, Brown and Cooperstein (1987) used analytic arguments to conclude that convection in this region reduces the pressure behind the shock and hurts the explosion. However, convection would bring hot material to the shock and thereby support it. Some two dimensional models suggest that prompt convection may aid in the evolution of the explosion. Herant, Benz and Colgate (1992) report explosions in their two dimensional models based on smooth particle hydrodynamics (SPH). In their simulations, the upwelling hot material and downwelling cool material are clearly separated, and convection allows for the transport of a large

amount of energy without temperature increases and corresponding neutrino energy losses.

Herant, Benz and Colgate (1992) regard convection as an open cycle “convective engine” in which cool material moves from behind the shock to the hot protoneutron star where it is heated and returned near the shock. Because some of the energy is transported by convection rather than by neutrino radiation, the energy can be transported without large increases in temperature in the proto-neutron star, and therefore energy losses due to neutrinos can be reduced. Furthermore, they conclude that prompt convection will continue to feed energy into the shock until an explosion is achieved, and therefore provides a robust mechanism for an explosion.

On the other hand, Bruenn and Mezzacappa (1994) argue that convection is largely irrelevant for the explosion. Mezzacappa et al. (1998) claim through a numerical code and through some analytic arguments that horizontal thermal transfer suppressed prompt convection. In two-dimensional simulations in which the neutrino flux was modeled using results from a one-dimensional multi-group neutrino code, They also conclude that convection does not much affect the progression of the explosion.

### 1.2.5 Neutrino-driven convection

Because neutrino heating is maximized at the base of the negative entropy gradient, it is possible that neutrino heating will cause this gradient to persist and to continue to driven convective motions. Janka and Mueller (1995, 1996) report a zone of neutrino-driven convection to be a region separate from the prompt convection zone. However, other two dimensional simulations re-

port a single large convective zone (Herant, Benz and Colgate 1992; Herant, Benz, Hix and Colgate 1994). Also, there is some confusion in terminology. Janka and Mueller label the region of neutrino-driven convection as “hot bubble convection.” Because there are qualitative differences between neutrino-driven convection region and the “hot bubble” found in the one dimensional simulations of Wilson and Mayle (1993), we retain the label “neutrino-driven convection.”

In a two-dimensional model using the piecewise-parabolic method (PPM), Burrows, Hayes and Fryxell (1994) report that including convection can convert an unsuccessful explosion into a successful one. By varying the neutrino flux at the inner boundary and comparing one-dimensional and two-dimensional calculations, Janka and Mueller (1995) report that neutrino driven convection reduces the neutrino luminosity necessary to generate an explosion by about 20%. Instead of calculating the evolution of each neutrino energy group using an algorithm such as multi-group flux limited diffusion or by calculating the full Boltzmann equation, both Burrows and Janka characterize the neutrinos at a given shell and angle in terms of the number density of neutrinos and a single temperature. From these quantities, the neutrino reaction rates are calculated. Although, this simplification in algorithm is needed in order to make the calculations computationally tractable, it has been unclear what impact more accurate modeling of neutrino interactions would have on these results.

Burrows, Hayes and Fryxell (1995) and Janka and Mueller (1995, 1996) do not find an accumulation of energy behind the shock, but instead note two important effects that result from convective instabilities. First, convective instabilities allows material to remain within the neutrino heating region for a

longer period of time than with a one dimensional code. This allows for greater neutrino heating of the incoming material and for the shock to equilibrate at a larger radius. Second, the convection flattens the entropy gradient thereby enlarging the gain radius. In addition, Burrows (1995) suggests that convection through the neutrinosphere may increase the neutrino flux.

The parameter study by Janka and Mueller (1995, 1996) suggests that convection does not provide a robust mechanism for an explosion. Unlike the models of Burrows et al., they did not find that there is a boiling phase lasting for a few hundred milliseconds before an explosion.

### 1.2.6 Hot bubble convection

In simulations of Wilson and Mayle (1988), neutrino heating behind the shock produces a radiation dominated bubble whose density is low, on the order of  $1 \times 10^5 \text{ cm/sec}^3$ , and whose entropy is high, on the order of 50 – 100 Boltzmann units and which appears several hundred milliseconds after bounce. This region is of special interest for nucleosynthesis since it has been hypothesized as a region which is the source of r-process elements. Material within this region is unstable to pressure-density instabilities, and it has been suggested that convection in this region may serve to regulate the strength of the explosion, (Colgate 1968) and that material in this region may fall back onto a neutron star and convert it into a black hole.

The hot bubble observed by Wilson and Mayle has not, however, been observed by any other groups in either one dimensional or multi-dimensional simulations. While some multi-dimensional simulations such as those by Janka and Mueller (1995, 1996) contain pockets of entropy as high as 20 or 30, none

has reported the high entropies of order 50 and the low densities observed by Wilson and Mayle and assumed in hot-bubble r-process models (Woosley et al. 1994; Meyer et. al 1992).

### **1.2.7 Late-time inner-core Ledoux convection**

Yet another region of convection was first pointed out in the one dimensional simulations of Burrows (1987) and observed in the more recent simulations of Janka and Mueller (1995). In these simulations the inner boundary of the region of prompt convection gradually moves inward over the course of several hundred milliseconds. The movement is produced as the inner core decreases in both entropy and electron fraction, and causes the gradients to become unstable to the Ledoux criterion for convection. In the simulations of Janka and Mueller the entire core becomes convective one second after bounce. In order to distinguish this regime of convection from others, this dissertation will denote it as “late-time inner-core Ledoux convection.” The theoretical implications of this form of convection are currently unclear. There is speculation that this convection may increase the neutrino luminosity (Janka and Mueller 1995).

### **1.2.8 H-He instability**

One final region of convective instability deserves mention. As the shock moves outward and encounters the Hydrogen-Helium interface, a region is generated in which the density gradient and the pressure gradient are opposite directions (Hachisu et al. 1990). This mixing region is necessary to explain the velocities of Nickel-57 observed in supernova 1987A (Herant and Benz 1992),

and numerical simulations suggest that to reproduce the observations in Supernova 1987A, the Rayleigh-Taylor convection must be seeded with density and velocity fluctuations that occur as a result of convection at earlier times. This H-He convection therefore provides a potential means of testing models of early convection.

H-He convection is important observationally, because it allows material from deep within the supernova to be moved to regions in which they can be observed. Nevertheless, this convection occurs several hours into the explosion and simulations of this form of convection assume that a successful explosion is already under way. Because this convection does not occur in the early phase of the supernova, it will not be considered further in this dissertation.

### **1.2.9 Need for a one dimensional code**

To summarize the current state of affairs, there is the general consensus that core collapse supernova models without convection will not explode (Wilson & Mayle 1993; Bruenn & Mezzacappa 1994; Baron & Cooperstein 1993). Furthermore, there are strong reasons, both observational and theoretical, for believing that convection in some form does occur in core collapse. What remains unclear is the role of convection in the iron core collapse, in particular, whether convection helps the explosion, hurts the explosion, or has no effect.

Much of the difficulty in clarifying the role of convection in core collapse lies in the conflicting results obtained by different research groups. These conflicting outcomes, in turn, are the results of differing physical assumptions. These various assumptions include different hydrodynamic algorithms, different initial models, different neutrino algorithms, and different equations of

state. Furthermore, the components of a model for core collapse supernova may interact in complex ways with each other. These facts make it difficult to compare results between research groups and to understand the interactions between convection and the other physical processes occurring within core-collapse supernova.

This situation would be much clarified if many different models of core collapse supernovae with varying physical assumptions could be calculated. Ideally, there would be a set of codes which would allow for the rapid modeling of the core collapse process in which convection could be simulated with a wide variety of initial conditions and physical assumptions. These codes would allow for the calculations of large numbers of models with differing assumptions and conditions which would then shed light on the role of convection within core collapse and the interaction between convection and other physical processes.

Unfortunately, most numerical work on the role of convection in supernova has been done with two dimensional codes. While these models have provided a considerable amount of insight in the role of convection, they suffer from the disadvantage of requiring a large amount of computer time. Moreover, their complexity makes it rather difficult to introduce different physical assumptions and algorithms into the code. This makes it difficult to run these codes repeatedly with various physical assumptions as well as making it difficult to incorporate convection into numerical models which include other computationally intensive elements, such as nucleosynthesis models or more accurate neutrino interaction models.

In addition, the computational resources necessary for these codes make their use in studying the later time evolution of core collapse supernovae problematic. It is suspected that the later stages of the core collapse may have some

interesting physical phenomenon such as a hot bubble (Wilson and Mayle 1988, 1993) which may be a possible site for r-process nucleosynthesis (Meyer et al. 1992; Woosley et al. 1994) or fall back due to a reverse shock (Houck & Chevalier 1991). Indeed, observations suggest some interesting phenomena exist in this phase of core collapse supernovae. From these observations, there are indication that all of the iron core and perhaps much of the silicon core must not be ejected, (Timmes et al. 1996) for if they were, there would be a far higher abundance of iron isotopes other than Iron-56 than are observed. The lack of these isotopes indicates that either the time at which the infalling matter separates from the ejected material is on the order of a second after bounce so that the whole iron core can fall through the shock or that substantial fallback occurs when the shock is in the silicon or oxygen layers of the collapsing star. Clearly there may be some interesting physics here, but without an efficient one dimensional numerical model with convection, this phase is outside the reach of current multi-dimensional numerical models.

Finally, there is a large body of one-dimensional codes which have been designed to study nucleosynthesis (Woosley & Weaver 1995; Hashimoto, Nomoto, & Shigeyama 1989; Thielmann et al. 1996) and to attempt to more accurately model neutrino-matter interactions by calculating the full Boltzmann equation (Mezzacappa & Bruenn 1993a, 1993b, 1993c) or by a radiation relaxation model (Eastman & Pinto 1993). The multi-dimensional nature of most supernova convection calculations makes it difficult to incorporate the results of these calculations within the existing one-dimensional codes.

The work that is done thus far with simulating convection in one dimensional models has involved the use of standard mixing length theory. In coupling a mixing length convection algorithm to a one dimensional code,

Bruenn and Mezzacappa (1994) and Bruenn and Dineva (1996) find that convection had little effect on the explosion, while Wilson and Mayle (1993) find that a mixing length theory treatment of salt-finger mixing generates a successful explosion. Unfortunately, standard mixing length theory is unsuited for simulations of core collapse supernova because it assumes that convection is a steady state time-independent process when convection in core collapse occurs on the same time scales as the evolution of the collapse.

The purpose of this dissertation was to develop a prescription for including convection in one dimensional codes in the context of collapse supernovae. This prescription has been incorporated within a one dimensional supernova code and the results compared with multi-dimensional simulations. The parameters within the convective model were varied in order to gain an understanding of how such factors as the strength and location of convection affects the iron core collapse. Finally, the one dimensional model was run for an extended duration in order to probe epochs of the supernova evolution which cannot practically be investigated by multi-dimensional codes due to computational limits.

# Chapter 2

## The supernova shock

In order to gain a greater understanding of core collapse supernova explosions, analytic and semi-analytic techniques have also been devised to model the early phases of the iron core collapse. Bethe, Brown, and Cooperstein (1987) used the virial theorem and the assumption of hydrostatic equilibrium to calculate a quantity called the “net ram”, which can be used to find the pressure behind the shock. They conclude that convection weakens the explosion. Burrows and Goshy (1993) derived a set of ordinary differential equations describing steady state infall and find that above a certain neutrino luminosity there is no solution for these equations. They conclude that this luminosity represents a critical neutrino luminosity which is necessary for an explosion. Shigeyama (1995) expanded the steady state infall equations and calculated a family of curves that specify the neutrino luminosity needed for a successful explosion.

These semi-analytic models show the power of such techniques to elucidate the physics of a complex problem, but they naturally have limitations. They require the assumption of either hydrostatic equilibrium or steady state infall and therefore cannot describe the behavior of the supernova shock once

it has revived. The formulations of Burrows and Goshy and that of Shigeyama assume that the only heating processes are those due to neutrino interactions and do not take into account the effect of convection. They cannot directly incorporate the findings of multidimensional supernova calculations where convection plays a major role (Herant et al. 1994; Burrows, Hayes & Fryxell 1995; Janka & Mueller 1996)

In this chapter, an alternative semi-analytic model of the revival of core-collapse supernova shocks is derived. This model is used to find the conditions under which an explosion with energies consistent with observed supernovae is produced. The model requires as input a pre-supernova stellar model, a prescription for how either the entropy or the velocity behind the shock evolves over time, and the location of the shock at a particular time. From these inputs, we can calculate the trajectory of the shock and estimate the total energy released in the explosion as well and the velocity of the shock when it leaves the iron core. The input quantities can be adapted from multidimensional calculations, and the output quantities can be compared with nucleosynthetic calculations to constrain the possible input conditions of such models.

## 2.1 The shock

An analogy for our model of the shock propagating in the supernova is that of a flame moving up a rope which is being lowered at a prescribed rate. The movement of the flame relative to the rope is affected only by its local environment and is independent of the rate at which the rope is being lowered. To calculate the motion of the flame in the lab frame, one first looks at the motion of the flame with respect to the rope and then does a coordinate transforma-

tion using the known speed of the rope. In this analogy the supernova shock is the flame and the infalling material is the rope. Because the material in front of the shock is moving at supersonic speeds, it is unaware of the approaching shock and unaffected by events occurring near the shock. The motion of the unshocked material is therefore independent of the motion of the shock. The motion of shock in the frame of the unshocked material is determined by the Hugoniot shock jump conditions and is only directly affected by the local environment of the shock.

To quantify this model, we calculate the conditions within the infalling material as determined by a progenitor structure. The assumption is made that at time  $t = 0$  pressure support is lost near the center of the progenitor star and that information about the loss of this pressure support will propagate outward at the local sound speed. When this information reaches a mass shell, we assume that it begins to free fall and will continue to do so until it hits the shock.

The equation of motion for the the infalling material is therefore

$$\left( \frac{dr}{dt} \right)_m = - \sqrt{\frac{2gm}{r} - \frac{2gm}{r_0}} \quad (2.1)$$

where  $r$  is the radius at a given time,  $r_0$  is the initial radius of the shell, and  $m$  is the mass interior to a given radius. The solution for this equation is

$$J\left(\frac{r}{r_0}\right) = - \sqrt{\frac{2gm}{r_0^3} t_{infall}} \quad (2.2)$$

where

$$J(x) = \frac{\pi}{2} - \sin^{-1}(1-x)^{1/2} - [x(1-x)]^{1/2} \quad (2.3)$$

and  $t_{\text{infall}}$  is the time after the material has begun falling. The infall trajectories for material at different radii are identical functions rescaled by the mass and radius of the infalling material.

After the center of the supernova has lost pressure support, there is a delay for information about the loss of pressure support to reach a shell and for the shell to begin to infall. This time delay is given by

$$t_{\text{infall}}(r) = \int_0^r \frac{1}{c_s(r)} dr, \quad (2.4)$$

where  $c_s$  is the speed of sound at a given radius within the progenitor model.

The thermodynamic quantities for the material in front of the shock can be calculated from the infall trajectories and from the initial structure. Once we find the radii of all of the mass shells at a certain time, we can calculate the density of the material immediately preceding the shock to be

$$\rho_1(r, t) = \frac{1}{4\pi r_{\text{shock}}(t)^2} \frac{dm}{dr}. \quad (2.5)$$

Because of its low density and low fraction of free baryons, the infalling material is not affected by the outward neutrino flux (Shigeyama 1995). Furthermore, there are no entropy producing processes within the infall material nor are there any processes which would substantially change the electron fraction of the material. To a good approximation the entropy  $s_1$  and the electron fraction  $Y_{e1}$  for a given mass shell are the same as that of the initial model. The pressure  $p_1$  and internal energy  $e_1$  of the material in front of the shock can then be calculated using the equation of state.

The motion of the shock is determined by the Hugoniot shock jump conditions which express the conservation of mass, momentum, and energy.

These shock jump conditions can be written in the frame of the shock as

$$\rho_1 v_1 = \rho_2 v_2, \quad (2.6)$$

$$p_1 + \rho_1 v_1^2 = p_2 + \rho_2 v_2^2, \quad (2.7)$$

$$e_1 + \frac{p_1}{\rho_1} + \frac{v_1^2}{2} = e_2 + \frac{p_2}{\rho_2} + \frac{v_2^2}{2}, \quad (2.8)$$

where subscript 1 denotes material in front of the shock and subscript 2 denotes material that has already fallen through the shock, and  $\rho$ ,  $v$ ,  $e$ , and  $p$  denotes density, velocity, energy density, and pressure. Neutrino processes will cause  $Y_e$  to decrease once the material has fallen though the shock. In the current model, the assumption is made that the material directly behind the shock has just fallen through and has therefore not been substantially deleptonized, hence  $Y_{e2} = Y_{e1}$ .

To close the system of equations, one further quantity behind the shock must be specified for all time. This quantity can be the entropy  $s_2$  or the velocity  $v_2$ . Once these quantities are specified, conditions on both sides of the shock can be solved from the equation of state and the Hugoniot condition (Landau & Lifshitz 1987) that

$$c_1 - c_2 + (1/\rho_1 - 1/\rho_2) \frac{p_1 + p_2}{2} = 0, \quad (2.9)$$

in which  $e_1$ ,  $\rho_1$ , and  $p_1$  are fixed from the infall equations. The post-shock density  $\rho_2$  can be found from the above conditions using an iterative Newton-Raphson method. New trial values of  $e_2$  and  $p_2$  are calculated at the end of each iteration using the equation of state and the new trial value for density  $\rho_2$  along with the specified value for entropy  $s_2$ . The solutions are iterated until they converge to a value for  $\rho_2$ .

Once the densities and pressures on both sides of the shock are known, the velocity of the material in the reference frame of the shock by using the

shock jump conditions can be calculated. These equations are

$$v_1 = \frac{1}{\rho_1} \sqrt{\frac{p_2 - p_1}{1/\rho_1 - 1/\rho_2}}, \quad (2.10)$$

$$v_2 = \frac{1}{\rho_2} \sqrt{\frac{p_2 - p_1}{1/\rho_1 - 1/\rho_2}}. \quad (2.11)$$

Since the velocity of the preshock material is known both in the reference frame of the shock and in the rest frame of the star, the shock velocity can be calculated from

$$v_{\text{shock}} = \frac{dr}{dt} = v_1 - \sqrt{\frac{2gm}{r} - \frac{2gm}{r_0}}. \quad (2.12)$$

The motion of the shock in Lagrangian coordinates can be calculated from the rate of infall of material through the shock.

$$\frac{dm}{dt} = \frac{dm}{dr} v_1 = 4\pi r^2 \rho_1 v_1 \quad (2.13)$$

One of the features of this model is that the motion of the supernova shock is affected only by conditions within the infalling material and those immediately behind the shock. Events deeper within the supernova affect the shock only to the extent that they affect the conditions directly behind the shock. Expressed in a different way, events behind the shock which do not change the conditions directly behind the shock will not change the shock trajectory. This can be seen from the shock equations in that the only quantities in these equations involve material falling into the shock or material immediately behind the shock. A proper knowledge of the conditions behind the shock requires a full global solution of the post-shock structure and evolution, but the current model can be used to gain physical insight without a complete solution. In particular, the revival of the shock depends on the post-shock entropy and not the details of how this entropy is produced.

Given the location of the shock at a specific time, a progenitor model, and a prescription for the value of the entropy behind the shock, the trajectory of the shock can be calculated. Two variables which are commonly used as input parameters in nucleosynthetic models can be calculated. In piston models (Woosley & Weaver 1995), the outer surface of the iron core is artificially moved at a given velocity. To derive the velocity of the piston, we calculate the velocity of the post-shock material relative to the star as the shock leaves the iron core. In other nucleosynthetic models, the supernova shock is artificially created by adding energy to the surface of the iron core (Hashimoto, Nomoto, & Shigeyama 1990). Although this excess energy does not take into account the effects of pressure gradients, the energy added to the iron core is roughly the observed energy of a supernova of approximately  $1 \times 10^{51} \text{ ergs}$ .

To calculate the excess kinetic energy produced by a model we integrate the following equation

$$\frac{dE}{dt} = 4\pi r^2 \rho_1 v_1 \left( \frac{v_1^2}{2} - \frac{gm}{r^2} \right) \quad (2.14)$$

is integrated whenever the value  $dE$  is positive. In a realistic model, the post-shock entropy would vary with time. Here some simple prescriptions for the entropy are considered.

## 2.2 The stalled shock

The model described in the previous section can be used to look at the dynamics of a stalled supernova shock. To do this, one assumes that region behind the shock is in hydrostatic equilibrium. This corresponds to setting the velocity of the material behind the shock to zero in the reference frame of the

star.

Figure 2.1 gives the evolution of a stalled shock for a 15 solar mass model calculated by Woosley, Langer, and Weaver (1993). The shock is taken to be at 1.2 solar masses with a radius that depends on the time after onset of collapse. The shock is evolved with the condition that the velocity is zero behind the shock in the frame of the star.

There are several interesting aspects of figure 2.1. First of all, the accretion rate remains low, allowing the star to accrete matter for about a second before accreting the entire iron core. Second, none of the models assuming hydrostatic equilibrium explode. In order to have a successful explosion it is necessary to have the material behind the shock exceed escape velocity. A situation in which the velocity of the material is zero behind the shock relative to the star cannot explode. An explosion contradicts the condition for hydrostatic equilibrium.

## 2.3 The revived shock

The model can be used to calculate the conditions necessary for shock revival. To do so we assume that the shock has stalled at a certain location at a certain time after collapse. As an illustrative example the entropy behind the shock is taken to be constant after this time. Although it is possible to include more complicated entropy functions within this model, we choose the assumption of constant entropy, because this most clearly illustrates the relation between dynamics of our model to the entropy. In the actual supernova, the entropy will be determined by a combination of heating processes such as convection and neutrino heating and by cooling processes such as iron dissociation and

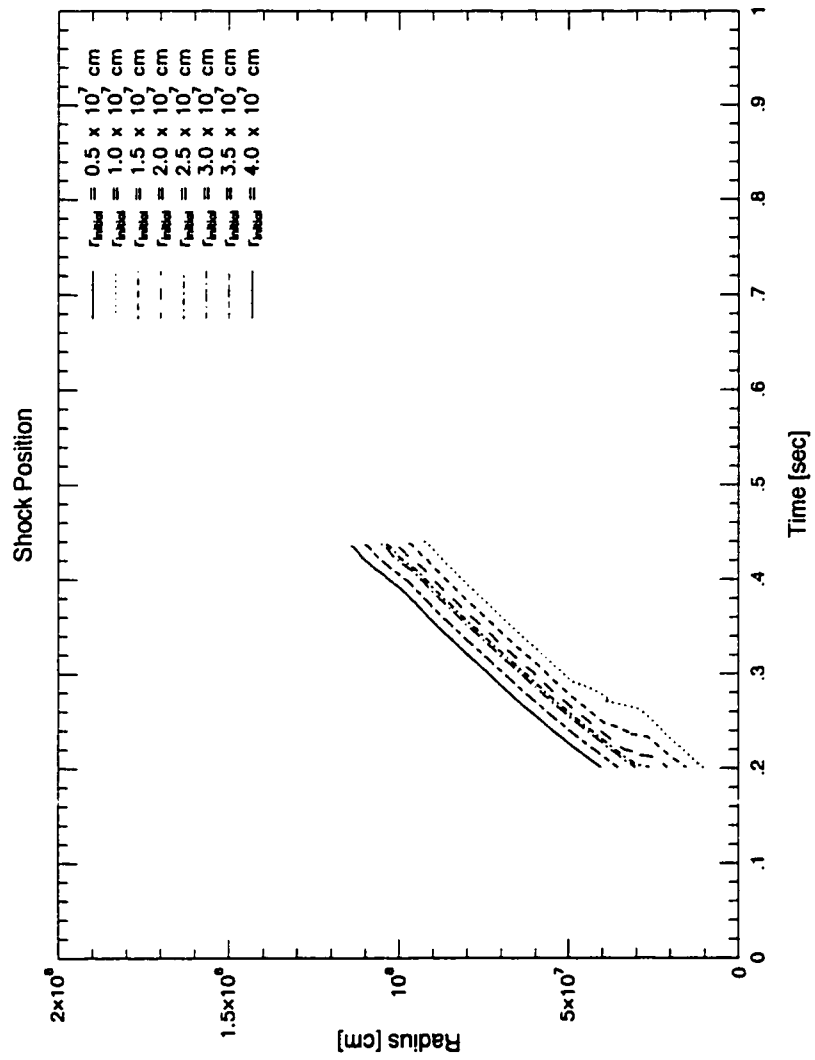


Figure 2.1: Time versus radius assuming hydrostatic equilibrium

neutrino losses.

In Figure 2.2, the trajectories of the shock are plotted assuming the shock is initially at a radius of  $3 \times 10^7$  cm and a mass location of 1.2 solar masses. The assumed constant entropy behind the shock is varied as a parameter. Figure 2.2 shows that there is a critical entropy necessary to revive the shock. As the entropy increases the shock strength also does.

Figure 2.3 presents the sum of the kinetic energy and potential energy as a function of different post shock entropy values and shock revival times for a shock starting at a 1.2 solar masses. As time passes, the becomes increasingly difficult to produce an explosion. Furthermore, there is a range of entropies and shock revival delay times which generate explosions with the kinetic energies in the observed range.

One significant feature of the model is that the trajectory of the shock is independent of the specific source of heating. The value of the entropy behind the shock may be caused by neutrino heating or by convection or by a combination of these mechanisms. These models provide a context by which to interpret recent calculations. For instance, Janka and Muller (1995) presented one and two dimensional models in which the neutrino flux at the base of the simulation was fixed at a prescribed value. For low neutrino fluxes, neither one or two dimensional models explode. For high neutrino fluxes, both explode. For intermediate neutrino fluxes, two dimensional models explode but one dimensional ones do not. Because the neutrino fluxes at the base of the simulation are fixed, these results cannot be because of increased neutrino fluxes due to convection beneath the neutrinosphere.

The various models can be interpreted in terms of the additional heat deposition provided by convection. For low values of neutrino flux, convective

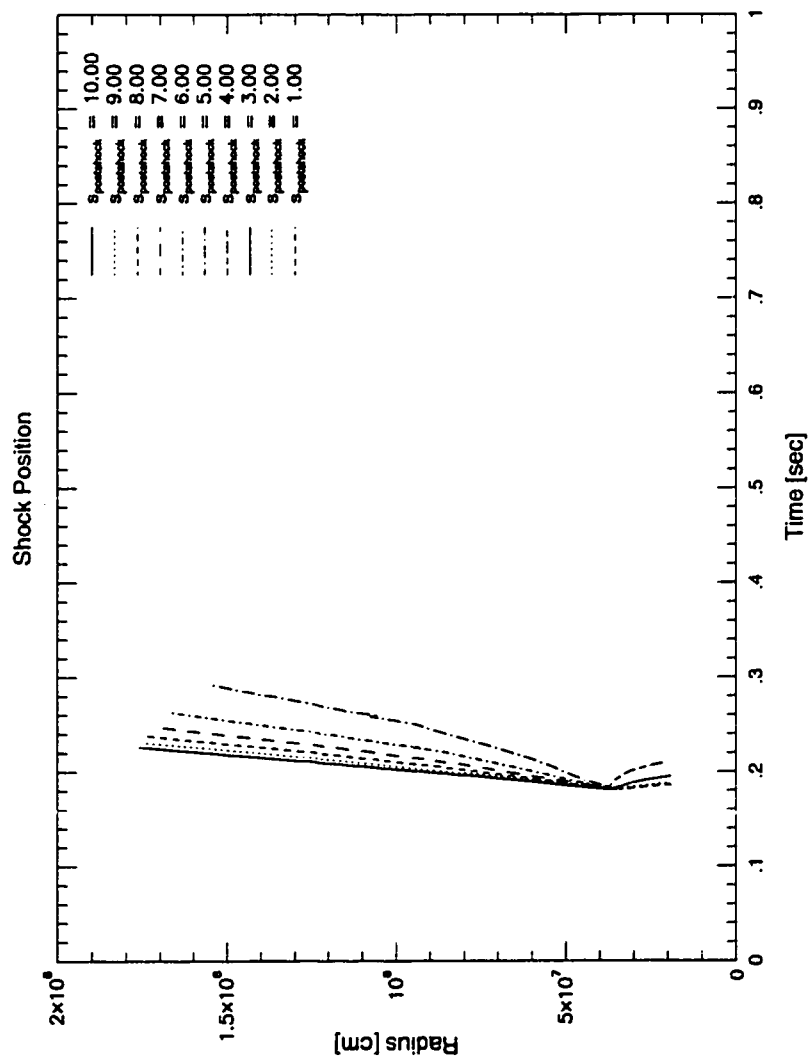


Figure 2.2: Time versus radius for given entropy

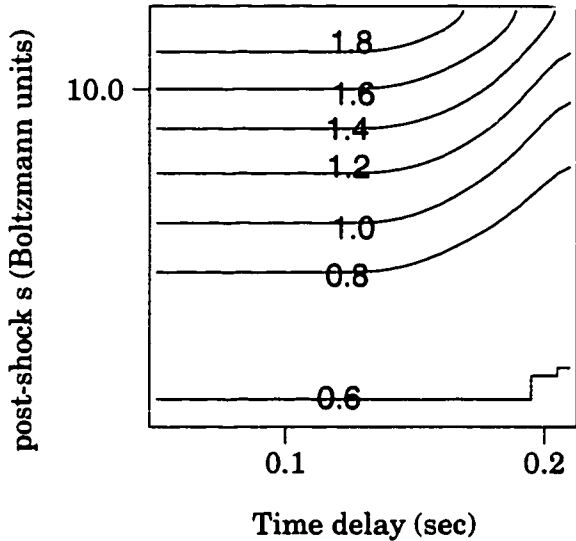


Figure 2.3: Energy versus time and entropy. Numbers in the plot are explosion energies in  $10^{51}$  ergs

heat transfer is unable to raise the entropy behind the shock to the level needed for an explosion. For high values, neutrino deposition alone is sufficient to provide the necessary post-shock entropy. For intermediate cases, the neutrino flux is insufficient to generate an explosion, but neutrino energy in combination with convective heat transfer can provide the necessary entropy directly behind the shock to produce an explosion.

Shigeyama (1995) and Burrows and Goshy (1993) express the criterion for a successful explosion in terms of a critical neutrino luminosity. In calculating the critical neutrino luminosity, Shigeyama concludes that it decreases with time. The present work suggests that if neutrino interaction is the only heating mechanism, that not only must the neutrino luminosity be high enough to heat the material behind the shock to a critical value, but that the timing of

the heating is important. As time passes, the velocity of the incoming material increases, thereby making it progressively harder to revive the shock.

In contrast to Shigeyama, we find that if the neutrino heating is delayed, the luminosity necessary to produce an explosion increases rather than decreases. The reason for this difference is that Shigeyama begins with the condition that the shock has stalled at a given time and calculates the neutrino flux necessary to revive the shock. In comparing two models which have stalled at different times, one is comparing two different models rather than one collapse model at different times.

The current results also disagree with conclusions of Bethe, Brown, and Cooperstein (1987: BBC). In that paper, the concept of "net ram" is used to calculate the effects of convection on the shock and to conclude that convection decreases the pressure behind the shock and hence the strength of the shock. The reason for this decrease in pressure is that the increase in entropy near the shock is accompanied by a decrease in entropy deeper in the supernova. This causes a decrease in pressure deep within the supernova, and the implicit condition of hydrostatic equilibrium in the "net ram" formulation means that this decrease in pressure is reflected in the pressure near the shock. In short, the flattening of the entropy gradient in a structure in hydrostatic equilibrium is predicted to decrease the pressure behind the shock. By contrast, the current results suggests that an increase in entropy will cause the shock to move more quickly with respect to the infalling material. In the strong shock limit, the ratio of the densities in front and behind the shock are determined only by the polytropic index  $\gamma$ ,

$$\frac{\rho_1}{\rho_2} = \frac{\gamma - 1}{\gamma + 1}. \quad (2.15)$$

Since  $\rho_1$  is fixed by the conditions in the material behind the shock,  $\rho_2$  is also a fixed quantity. Thus if the entropy  $s_2$  increases, the pressure behind the shock will increase, and thus the shock will grow stronger.

The reason for the differences between the present formulation and the net ram formulation is the assumption of hydrostatic equilibrium behind the shock in the net ram formulation. Although hydrostatic equilibrium is a good assumption for the conditions behind the shock while the shock is stalled, it is invalid once the shock has begun to revive and the velocities behind the shock are no longer zero. As we have noted earlier, assuming hydrostatic equilibrium will always result in a failed explosion and therefore hydrostatic equilibrium cannot hold if there is to be a successful explosion.

## 2.4 Conclusion

The shock in the iron core of a core collapse supernova is in a race against time. In order to have a successful explosion, the entropy behind the shock must be raised to a critical value before the core collapses. The method by which the entropy is raised to this critical value and sustained is irrelevant to the shock evolution and may be due to convection above the neutrinosphere, neutrino heating, or a combination of both.

Previous work on convection within Type II supernovae has focused on convection deep within the neutrinosphere increasing the neutrino flux in order to heat the outer layers near the shock. (Keil, Janka, & Mueller 1996). Our work suggests that convection above the neutrinosphere may provide an important contribution to a successful explosion by directly delivering entropy behind the shock as entropy gradients are flattened. Furthermore, because the

shock evolution is independent of the specifics of heating, the present analysis suggests that convection and neutrino heating complement each other. A larger convective energy flux will reduce the need for neutrino heating and vice versa. This finding is consistent with recent multi-dimensional calculations which have compared supernova dynamics with and without convection. (Janka & Mueller, 1996)

The present analysis suggests a means for relating the thermodynamic conditions in the early phases of the iron core collapse to the explosion energy. Only certain values of entropy behind the shock can produce explosions which are consistent with observations, and this allows one to constrain the possible conditions within the iron core collapse.

Finally this analysis may provide a clue as to the robustness of the supernova mechanism. One mystery with core collapse supernova is why their explosion energies appear to fall within a relatively small range despite the wide range of possible progenitors and the complicated physical processes. The physics behind the shock affects the energy of the supernova only to the extent to which it changes the entropy directly behind the shock. Because the physics within the core affects the energy of the shock through only one parameter, this somewhat decouples the energy of the shock from the detail of the core collapse physics.

Future one dimensional and multi-dimensional work can be done to explore the physics necessary to bring the entropy behind the shock wave to the critical value necessary for an explosion and to see how observational constraints further limit the physical conditions within the supernova.

# Chapter 3

## The convective model

Convection is a common phenomena in astrophysics. Despite this, there is no general theory of convection which would allow for the calculation of quantities such as energy and composition flux from first principles. Therefore, a number of heuristic formalisms have been devised to model convection.

### 3.1 Physical requirements

The convective formalism used to model Type II supernova should meet a number of requirements. First, because the core collapse is occurring on dynamic time scales, it is necessary for the convective formalism to be able to model the time dependent aspects of convection. Second, the convection formalism needs to be able to model phenomenon such as convective overshoot, which have been found in core collapse supernova (Keil, Janka, & Mueller 1996; Janka & Mueller 1994) Finally, the convective algorithm should be easy to include within an existing one dimensional supernova code. It should be noted that there may be tradeoffs between the final goal and the previous

ones. A convective formalism which attempts to capture the full complexity of convection may be difficult to incorporate within current one dimensional supernova codes.

One challenge in developing a numerical model of convection within the supernova core is the lack of observational and theoretical constraints on the nature of convection in the supernova core. Observationally, the conditions of the supernova core cannot be observed directly and must be inferred from the energy of the explosion, the nucleosynthetic yield of the supernova, and the spectra of the supernova. However, relating the observations of supernova to actual conditions within the supernova is difficult because there are still many uncertainties in how conditions in the supernova core relate to observations of the explosions.

There is a temptation to generate an extremely complex and sophisticated model of convection in the hopes that adding complexity will allow one to more accurately model the physical convection. However, the lack of constraints in this particular physical problem requires that one resist this temptation. Because of the fundamental uncertainties in the supernova problem, it is impossible to know whether adding complexity to the model actually brings the model closer to physical reality. Moreover, adding complexity to the model makes physical insight more difficult and increases both the computational resources necessary to calculate a model and the time necessary to numerically implement the model.

## 3.2 Review of convective algorithms

### 3.2.1 Standard mixing length theory

The model most widely used in one-dimensional simulations of astrophysical objects is mixing length theory. (Kippenhahn & Weigart 1994). Within mixing length theory, convection is modeled as a set of eddies of size  $l_m$  known as the mixing length, which rise a distance  $l_m$  before losing their separate identities and combining with the ambient medium. Using this model, expressions for the energy flux are derived in terms of the local gradients and values. The theory does not contain a means of deriving the size of the mixing length from first principles, but this length is generally taken to be the pressure scale height times a constant or

$$l_m = \alpha \frac{P}{\left| \frac{\partial P}{\partial r} \right|}. \quad (3.1)$$

Standard mixing length theory is the standard treatment of convection in stellar evolution models (Kippenhahn & Weigart 1994) . Two groups have used it in the context of core collapse (Wilson & Mayle 1988; Bruenn & Mezzacappa 1991; Bruenn & Mezzacappa 1994), the first finding that an explosion can be generated if there is salt-finer mixing, and the second finding that convection is a transient phenomena in the core collapse which only exists of a few tens of milliseconds.

Mixing length theory has some features which make it unsuitable for use as an algorithm in one dimensional core collapse calculations. First of all, standard mixing length theory does not include convective overshoot. This is especially a problem in supernovae, because the large negative entropy gradient generates large convective velocities which causes material to penetrate deeply

into stable layers. (Janka & Mueller 1995, 1996) Second, standard mixing length theory assumes instantaneous mixing and therefore does not include time dependence. In convection within stars on the main sequence, the time scales for evolution are the nuclear and thermal time scales which are typically on the order of at least tens of thousands of years. Hence they are much longer than the dynamic time scales which in the case of the sun is on the order of minutes. For these stars, the assumption of instantaneous mixing is therefore a good approximation. In cases such as Cepheid variables, the structure of the star changes on the same time scale as the convection and mixing length theory cannot be used. Instead, the models used in these situations is a topic of active research (Xiong, Cheng, & Deng 1997).

In the core collapse problem, convection occurs on the same time scales as the collapse, and hence the convection is not in steady state. Under these circumstances, mixing length theory is inappropriate and can give qualitatively incorrect results. In mixing length theory, the energy flux transfer is a increasing function of the entropy gradient. Therefore mixing length theory would predict that the convective energy flux is maximum at the beginning of the calculation and would decrease as the entropy gradient decreases. However, one would expect that the actual convective flux would be at a minimum at the start of the calculation. Although the entropy gradient is at a maximum, convective motions have not had an opportunity to manifest themselves. As time passes, the convective motions should be accelerated by the entropy gradient and the convective flux should increase. Furthermore, mixing length theory would predict that the convective motions would cease once the convective gradient disappears. This prediction contradicts the results of two dimensional simulations which indicate that convective motions continue, even after

the gradients which gave rise to those motions have been disappeared (Janka 1996).

### 3.2.2 Non-local mixing length theory

In another approach, often found in stellar models of high mass stars, mixing length theory is extended by including non-local quantities in order to include effects such as convective overshoot and semi-convection. (Langer 1986; Maeder 1975) Although, they can model aspects of convection which cannot be modeled by standard mixing length theory, the convective non-local formalisms used in high mass stellar evolution generally assume instantaneous mixing. This is possible since the evolutionary time scales of high mass stars are generally long in comparison to the convective time scales, and therefore the convection in high mass stars are usually in equilibrium. As a result, non-local mixing length models do not have the time dependence which is necessary for numerical supernova models.

### 3.2.3 Moment models

Another approach to convection has been to attempt to derive equations for the averaged hydrodynamic and thermodynamic quantities in a shell. In these models, equations are derived for the average velocity within a shell in terms of the second moments of the velocity. Equations for these second moments can be derived, but these contain the third moments. Equations for the third moments can be derived, but these contain fourth moments and so forth. Because equations for a given level of moments contain expressions for the next high level of moments, a closed set of equations cannot be written without making

additional assumptions about the behavior of the hydrodynamic equations. This problem is known as the “closure problem” and makes it impossible to obtain expressions for convective fluxes simply by calculating expanding the moments of hydrodynamic equations.

In a number of earlier works (Xiong 1991; Xiong 1984) the closure problem is managed by truncating the expansion of moments and including “closure hypotheses” for the behavior of the higher order moments. These models are primarily found within theoretical studies of convection (Grossman 1996; Grossman & Narayan 1993; Grossman, Narayan, & Arnett 1993) and in Cepheid variables, in which the goal is to predict the light curve of the star.

The chief problem with the moment models is their mathematical complexity (Grossman 1996). For example, typical moment models proposed by Canuto (1996, 1993, 1992) contain four or five coupled partial differential equations and dozens of terms. Not only does the complexity make them difficult to numerically difference, debug, and test but they also make it difficult to see the physical processes which the equations represent. Moreover, unlike the case of Cepheid variables, there is a lack of observational constraints within the supernova problem which can be used to test the correctness of the model.

This complexity may be necessary where the goal is to understand convection in detail or in situations such as Cepheid variables where observations are detailed enough to require an accurate model of convection in order to match the observations. However, in this dissertation, the goal is to produce an simple algorithm which reproduces the basic elements of convection in a one dimensional code. As a result, the complexity of moment models make them unsuitable for use in this dissertation.

### **3.2.4 Turbulent diffusion models**

Yet another class of convective models is typified by the work of Stellingwerf (1986) and Kuhfuss (1986) which has been proposed for application to Cepheid variables. In these models, convection is modeled in terms of the diffusion of small scale turbulent eddies. The physical picture used in these models is fundamentally different than the one used in this dissertation which views convection in terms of streams that are larger than the typical zone size.

The biggest difference between turbulent diffusion models and the present one is the functional nature of the advection term. Turbulent diffusion models represent transport in terms of the second derivative of the convective velocity with respect to radius while the model used in this dissertation represents transport as the first derivative of the velocity. The primary effect of these terms occurs at the edges of the convective zones. A turbulent diffusion model cause convection to expand at both the outer and inner edge of the convective zone. By contrast, the model used in this dissertation produces convection expanding only into the inner boundary. The latter behavior is what is recorded in numerical experiments such as those undertaken by Cattaneo et al. (1991) and Freytag, Ludwig, and Steffan. (1996).

### **3.2.5 Two-stream models**

Another class of models which has influenced the design of the convection model in this dissertation are the “two-stream convection models” which have been proposed in the literature to calculate the temperature structure of the solar convective zone. A number of two stream models have been proposed and are reviewed by Nordlund (1974). The general schema for this class of models

is to divide the material within a shell into an upstream and a downstream and then to then assume a model for the interaction between the streams, which then allows for the derivations of equations for temperature gradients.

### 3.3 Review of numerical work

Although the convection algorithm used in this dissertation is one dimensional, it was influenced by a number of multi-dimensional numerical simulations. One feature of these numerical experiments which has been a general feature of such simulations has been the asymmetry between updrafts and downdrafts. In general, the downward moving material becomes concentrated in high velocity plumes while the upward moving material expands and has a reduced velocity (Cataneo et al. 1991; Freytag et al. 1996) Although many of these models can be criticized for having unrealistic assumptions such as two-dimensionality or incompressibility, the pattern of slow-moving upflows and rapid moving downflows appears to be the case in solar convection and is what is thought to produce the granulation pattern on the solar photosphere (Spruit, Nordlund & Title 1990).

In addition, the convective model in this dissertation was heavily influenced by the numerical work of Freytag et al. (1996) who conducted numerical studies of convection in A-type stars and in white dwarfs. One important result of this work was the finding that mixing-length theory predicts incorrect profiles for convective flux in that it ignores the outward convective flux caused by convective overshoot that may exist in areas which are stable to convection. Furthermore, their work indicates that there is an exponential dependence between convective velocity and depth of penetration within the

overshoot region.

### 3.4 The convective model

The approach to convection used in this dissertation is inspired by these “two stream models.” Instead of deriving equations for the moments of the convection as is the case with moment models, the material within a shell is divided into an upstream and a downstream. The upstream defined as material which is moving faster than the average flow and the downstream defined as material which is moving slower than the average flow. Using heuristic physical principles, equations for the differences in hydrodynamic quantities between the upstream and the downstream are derived along with an equation which describes the area ratio between the upstream and the downstream flows. The resulting model is not intended to capture the full richness and complexity of convection, nor is the model intended to provide exact calculations for the value of convection quantities. Rather what is intended is a rough approximation of the actual convective flows, which crudely models some of the phenomena visible in two dimensional supernova models, and which allows for insight in the role of convection in Type II supernova.

In order to describe the model, it is necessary to define a system of notation for the material in the up and downstreams. Given a hydrodynamic variable  $a$ , an upstream average  $a_+$  is defined to be

$$\langle a \rangle_+ := \frac{\int_{v > \langle v \rangle} \rho a dA}{\int \rho dA}. \quad (3.2)$$

Similarly a downstream average  $a_-$  is defined by

$$\langle a \rangle_- := \frac{\int_{v < \langle v \rangle} \rho adA}{\int \rho dA} \quad (3.3)$$

where  $v$  is the velocity is a given fluid element and  $\langle v \rangle$  is the mean velocity within the shell.

The area fraction of the upstream and downstream are defined be the variables  $q_+$  and  $q_-$  respectively. From this definition we obtain the relationship

$$q_+ + q_- = 1 \quad (3.4)$$

Using the definition of the upstream and downstream quantities, the mean value for a hydrodynamic variable  $a$  can be shown to be

$$\langle a \rangle = q_+ \langle a \rangle_+ + q_- \langle a \rangle_- . \quad (3.5)$$

One can define the convective fluctuation of  $a$  to be the difference between upstream and the downstream averages,

$$a_{conv} = \langle a \rangle_+ - \langle a \rangle_-, \quad (3.6)$$

and primed quantities to be the difference between a quantity in a fluid element and the mean motion of a radial shell

$$a' = a - \langle a \rangle . \quad (3.7)$$

One then seeks to derive a closed set of formula for the mean hydrodynamic quantities and their respective convective fluctuations.

We begin with the Euler equations for hydrodynamic flow in Lagrangian coordinates which are

$$D_t \rho = -\rho \nabla \cdot v \quad (3.8)$$

$$D_t v = \frac{\nabla P}{\rho} - f \quad (3.9)$$

$$D_t(e + \omega) = \epsilon_{gen} - \nabla \cdot (\epsilon_{trans} + p v) \quad (3.10)$$

where  $\omega$  is the convective kinetic energy,  $\epsilon_{trans}$  includes any energy transport terms,  $\epsilon_{gen}$  includes energy generation terms, and  $f$  is the gravitational force on a fluid element. The derivative  $D_t$  is the substantial derivative in the frame of the individual fluid element,

$$D_t \equiv \partial_t + v \cdot \nabla. \quad (3.11)$$

From conservation of mass we obtain the relationship

$$q_+ v_+ = q_- v_-. \quad (3.12)$$

We take the anelastic approximation, which can be expressed as

$$\nabla(\langle \rho \rangle v') = 0 \quad (3.13)$$

and assumes that pressure is constant within a radial shell. This approximation is described in (Gough 1969) and is equivalent to asserting that pressure waves are not important. This approximation can be shown to be a reasonable one provided that the motions of the material are not on the order of the sound velocity. Using this approximation, the following equations are obtained for

momentum and energy

$$d_t \langle v \rangle = \frac{\nabla P}{\langle \rho \rangle} - \langle f \rangle \quad (3.14)$$

$$d_t \langle e \rangle = \langle \epsilon \rangle - \frac{p}{\langle \rho \rangle} - \left\langle \frac{1}{\rho} \nabla \cdot q \right\rangle - \frac{1}{\langle \rho \rangle} \nabla \cdot j_w \quad (3.15)$$

$$- d_t \omega + q_+ v_{conv} \nabla \cdot \omega - q_- v_{conv} \nabla \cdot \omega \quad (3.16)$$

where  $\omega$  is the kinetic energy of the convective motions,  $j_w$  is the enthalpy flux

$$j_w = \langle v' w' \rangle \quad (3.17)$$

$$= \langle v' s' \rangle \langle T \rangle \quad (3.18)$$

$$= v_{conv} s_{conv} \langle T \rangle \quad (3.19)$$

and where  $d_t$  is the substantial derivative with respect to the mean velocity within a shell,

$$d_t \equiv \partial_t + \langle v \rangle \cdot \nabla. \quad (3.20)$$

One should note that the derivative  $D_t$  defined earlier is not equivalent to the derivative  $d_t$ , because  $D_t$  is the derivative with respect to the local velocity while  $d_t$  is the derivative with respect to the average velocity within a radial shell.

These equations differ from the ones derived by Kuhfluss (1986) primarily by neglecting terms for a kinetic energy flux and a turbulent pressure. These differences arise from the assumption in the unaveraged energy equation that kinetic energy is small in comparison to the thermal energy of a fluid element.

### 3.4.1 The entropy and composition fluctuation equations

The equation for the mean energy includes a term containing the entropy fluctuations in a given radial shell. To calculate this quantity, a model for the creation and dissipation of these fluctuations must be derived. We first assume that the fluid element is adiabatic within the local reference frame.

$$D_t s = 0 \quad (3.21)$$

Expanding this equation in terms of the difference between the local values and the mean flow, we obtain the expressions

$$\partial_t \langle s \rangle + \partial_t s'_+ + \langle v \rangle \cdot \nabla \langle s \rangle + \langle v \rangle \cdot \nabla s'_+ + v'_+ \nabla \langle s \rangle + v'_+ \nabla s'_+ = 0 \quad (3.22)$$

$$\partial_t \langle s \rangle - \partial_t s'_- + \langle v \rangle \cdot \nabla \langle s \rangle - \langle v \rangle \cdot \nabla s'_- - v'_- \nabla \langle s \rangle - v'_- \nabla s'_- = 0 \quad (3.23)$$

Making the substitutions

$$v'_+ = (1 - q_+) v_{conv} \quad (3.24)$$

$$v'_- = q_+ v_{conv} \quad (3.25)$$

$$s'_+ = (1 - q_+) s_{conv} \quad (3.26)$$

$$s'_- = q_+ s_{conv} \quad (3.27)$$

and subtracting the two equations, we obtain an expression for  $s_{conv}$

$$d_t s_{conv} = -v_{conv} \nabla \langle s \rangle - q_+ v_{conv} \nabla q_+ s_{conv} - q_- v_{conv} \nabla q_- s_{conv} \quad (3.28)$$

Using the substitutions

$$q_+ + q_- = 1 \quad (3.29)$$

$$\nabla q_+ = -\nabla q_-, \quad (3.30)$$

this expression can be simplified to

$$d_t s_{conv} = -v_{conv} \nabla \langle s \rangle + (1 - 2q_+) v_{conv} \nabla s_{conv} + v_{conv} s_{conv} \nabla q_+ \quad (3.31)$$

As written this equation assumes no damping, and therefore produces the result that the convective entropy fluctuations grow without bound. In the actual star, there are two processes which would damp the growth of the convective fluctuations. The first is the mixing of material between stream and occurs both in the stable and unstable regions. The second occurs only within regions of the star which are convectively stable and consists of buoyancy forces causing the entropy and composition fluctuations to become uncorrelated with the velocity fluctuations.

The first damping process can be modeled assuming that the fluctuations in the entropy are damped over a length scale  $l_m$  equal to a constant  $\alpha_{ml}$  times the pressure scale height. The second can be modeled assuming that the damping occurs over a time scale proportional to the inverse Brunt-Vasala timescale, which is the oscillation period of a perturbed gas element. The constant in this case is designated  $\alpha_{bv}$ .

With these assumptions, the equation for the entropy fluctuations within a shell is given as

$$\begin{aligned} d_t s_{conv} = & -v_{conv} \nabla \langle s \rangle + (1 - 2q_+) v_{conv} \nabla s_{conv} \\ & + v_{conv} s_{conv} \nabla q_+ - l_m v_{conv} s_{conv} - \alpha_{bv} s_{conv} \tau_{bv} \end{aligned} \quad (3.32)$$

where

$$l_m = \alpha_{ml} P \frac{\partial r}{\partial P}. \quad (3.33)$$

and where

$$\tau_{bv} = \left( \frac{g_{eff}}{\gamma} \frac{\partial(\ln \rho - \ln p)}{\partial r} \right) \quad (3.34)$$

where  $g_{eff}$  is the effective gravitational force and  $\gamma$  is the polytropic index

Each term in the resulting equation can be interpreted as signifying a physical process. The first term represents the advection of the mean value of the entropy by the velocity differences in the upstream and downstream. The second and third terms represent the advection of the entropy fluctuations by the velocity differences. The fourth and fifth terms represent the damping of the entropy fluctuations by mixing between streams and by buoyancy forces where the entropy gradient is stable.

The derivation for the entropy fluctuation equation can also be used for calculating composition fluctuations. One begins by taking the local composition to be unaffected by convection. In other words,

$$\nabla Y_e = 0. \quad (3.35)$$

Then by a calculation identical to that of the entropy fluctuation, one obtains the equation

$$d_t Y_{e,conv} = -v_{conv} \nabla \langle Y_e \rangle + (1 - 2q_+) v_{conv} \nabla Y_{e,conv} \\ + v_{conv} Y_{e,conv} \nabla q_+ - l_m v_{conv} Y_{e,conv} - \alpha_{bv} Y_{e,conv} \tau_{bv} \quad (3.36)$$

### 3.4.2 The velocity fluctuation equation

In order to derive the velocity fluctuation equation, one begins with the Euler momentum equation for a fluid element.

$$d_t \langle v \rangle = \frac{\nabla P}{\langle \rho \rangle} - \langle f \rangle. \quad (3.37)$$

To derive an equation for the velocity fluctuations in a shell, one may begin by subtracting the velocities in the upstream from those in the down-

stream. Ignoring damping terms at this point, one obtains the equation

$$\begin{aligned} d_t v_{conv} = & -v_{conv} \nabla \langle v \rangle - (1 - 2q_+) v_{conv} \nabla v_{conv} \\ & + v_{conv}^2 \nabla q_+ + \nabla P \left( \frac{1}{\rho_+} - \frac{1}{\rho_-} \right). \end{aligned} \quad (3.38)$$

This assumes that the gravitational field is spherically symmetric so that the forces in the up and down stream are constant, thereby cancelling the force terms when the equation for the upstream and downstream are subtracted from each other. It is also assumed, in accordance with the anelastic approximation, that the pressure within a radial shell reaches equilibrium quickly enough so that it is identical within the up and down streams and can therefore be represented by a single value  $P$ .

The final term in the equation represents the buoyancy forces on the material within a stream. This term can be simplified by taking a first order expansion around the mean density, this allows one to substitute the final term in equation 3.38 with

$$\frac{\rho_{conv}}{\langle \rho \rangle^2} \nabla P. \quad (3.39)$$

The effect of this buoyancy force term is fundamentally different between the convectively unstable region and in the convectively stable region. In the convectively unstable region, the buoyancy forces cause the material within the streams to be accelerated and the velocity fluctuations within a shell to increase. In the convectively stable regions, the buoyancy forces cause the fluid elements to oscillate instead of causing increasing large velocity fluctuations. Unlike the convectively unstable case, the buoyancy forces in the convectively stable case do not cause an increase in velocity fluctuations. To take this effect into account, the buoyancy driving term is set to zero when the region is convectively stable.

As with the entropy and composition fluctuation equations, it is necessary to introduce damping terms in order to prevent the calculated velocity fluctuations from increasing without bound. Likewise, there are two damping processes to take into account, the mixing of the streams and the equilibration of the material in convectively stable regions.

To take into account the mixing between streams, we introduce a term

$$l_m v_{conv}^2, \quad (3.40)$$

where  $l_m$  is the mixing length and as defined identically as the other fluctuation equations.

Combining these terms we can write the velocity fluctuation equation as

$$d_t v_{conv} = \frac{\rho_{conv} \nabla P}{\langle \rho \rangle^2} - \frac{v_{conv}^2}{l_m} + (1 - 2q_+) v_{conv} \nabla v_{conv} \quad (3.41)$$

where  $\rho_{conv}$  is calculated to be

$$\rho_{conv} = \frac{\partial \rho}{\partial s} s_{conv} + \frac{\partial \rho}{\partial Y_e} Y_e \text{ conv} \quad (3.42)$$

when the layer is convectively unstable and 0 when the layer is convectively stable.

### 3.4.3 Asymmetry parameter

As written, the equations are not closed because they require knowledge of  $q_-$  which is the area fraction of a shell which is covered by the downstream. In the physical supernova, this quantity is determined in a balance between processes that increase the area of the stream and those that decrease it. The area of the stream is increased by entrainment of material from the slower

moving and hence larger stream into the faster moving and hence smaller stream. Another process that affects the area of a stream is the expansion or contraction of a stream as it moves between layers and responds to pressure changes by expanding or contracting.

Although it is possible to derive another differential equation to describe the effects of these processes, this equation would add to the complexities of the model and would make it more difficult to gain physical insight into the dynamics of the model. Therefore instead of constructing another differential equation to calculate the asymmetry between the streams, it was decided to set the value of  $q_-$  to be a constant value which would be determined from examining numerical simulations. The value of the parameter to which  $q_-$  was set is designated  $\alpha_{asym}$ .

### 3.4.4 Coupling with the neutrinos

The interaction between neutrinos and matter is very complex, and a proper treatment of the effects of convection on neutrinos is beyond the scope of this dissertation. In order to observe the effects of convection on neutrino transfer, we take two extreme approximations in order to bracket the possible effects. One approximation is to assume that the neutrino field remains unaffected by the convection. This is likely to produce an underestimate of the neutrino flux in that it does not take into account the dredging up of neutrinos from within the neutrinosphere to the area of free streaming. The other approximation is to assume that all of the neutrinos are advected by the convection. This is likely to produce an extreme overestimate of the neutrino flux in that it ignores the fact that the outer layers of the core collapse are transparent to

neutrinos.

The equation for the assumption of complete convective advection of neutrinos can be written as

$$\left( \frac{\partial Y_\epsilon}{\partial t} \right)_{conv} = v_{conv} \frac{\partial Y_\epsilon}{\partial r}. \quad (3.43)$$

where  $v_{conv}$  is the convective velocity and  $Y_\epsilon$  is the neutrino concentration at a given energy. This term is inserted into the non-convective neutrino transport equations. This expression contains only  $v_{conv}$  and not the mean velocity  $\langle v \rangle$  because this expression only takes into account transport of neutrinos by convection between mass zones. The effect of the mean velocity on the neutrinos is taken into account by the non-convective portions neutrino transport equation.

The equation corresponding to no advection can be written as

$$\left( \frac{\partial Y_\epsilon}{\partial t} \right)_{conv} = 0. \quad (3.44)$$

### 3.4.5 Energy conservation

Kinetic energy was conserved by assuming that the convection was isotropic. Therefore the equation for the main energy equation was modified by adding the term

$$\left( \frac{\partial E}{\partial t} \right) = -\frac{3}{2} \frac{\partial v_{conv}^2}{\partial t}. \quad (3.45)$$

### 3.4.6 Braking parameter

As written, the convection does not affect the average velocity of the material. It has, however, been suggested (Burrows, Fryxell et al 1995) that convection

can generate an explosion by braking the infalling material so that it has more time to be heated in the neutrino heating region. In order to model this process, albeit at a crude level, it is possible to add a term to the average velocity equation to reflect the braking action of convection. From dimensional grounds, this braking term is

$$-\alpha_{brake} \frac{v_{conv}}{l_m} v \quad (3.46)$$

where  $l_m$  is the mixing length which has been defined earlier.

### 3.4.7 Turbulent pressure

Another aspect of convection which may affect the dynamics of the explosion is turbulent pressure. From dimensional grounds, a expression for the turbulent pressure may be written as

$$P_{turb} = \alpha_{turb} \rho v_{conv}^2 \quad (3.47)$$

where  $\alpha_{turb}$  is a dimensionless parameter.

### 3.4.8 Boundary conditions and initial perturbations

This convective formulation requires an initial perturbation as well as both outer and inner boundary condition. The need for a initial perturbation arises from the fact that zero is an unstable fixed point for the convective equations. If all of the convective quantities are set to zero, the right hand side of the convective equations all become zero and the convective quantities will not move from this value in the course of the calculation. they will remain at that value throughout the entire calculation. However a slight deviation in the

values of the convective variables from zero will cause the convective quantities to grow.

Care needs to be taken in treating the interaction between the convective algorithm and the shock. Without any special treatment, the algorithm will treat the large negative entropy drop associated with the shock as the driving force for convection and will attempt to convect material through the shock. To prevent this unphysical occurrence, the convective algorithm is restricted to the region behind the shock. This restriction requires a boundary condition at the location of the shock.

Both of these problems can be solved by setting the value of the convective velocity at the shock to be a small fraction of the sound speed at that radius. In other words

$$v_{\text{shock}} = \alpha_{\text{perb}} \langle v \rangle_{\text{shock}}. \quad (3.48)$$

An inner boundary condition needs to be set when convection reaches the center of the proto-neutron star. At the center all velocities reach zero, and therefore the inner boundary condition can be set to be

$$v_{\text{conv}}(0) = 0. \quad (3.49)$$

parameter name	description	standard value
$\alpha_{ml}$	mixing length dissipation factor	1.0
$\alpha_{bv}$	strength of dissipation in stable regions	1.0
$\alpha_{asym}$	area fraction of matter in downstream	0.1
$\alpha_{pert}$	perturbation value to set up instabilities	0.1
$\alpha_{bra}$	convective braking parameter	0.0
$\alpha_{turb}$	turbulent pressure parameter	0.0

Table 3.1: Parameters in the convective model

### 3.4.9 Summary of equations and parameters

Bringing everything together, the convective model used in this dissertation can be written as the following differential equations

$$d_t v_{conv} = \frac{\rho_{conv} \nabla P}{(\rho)^2} - \frac{v_{conv}^2}{l_m} + (1 - 2q_+) v_{conv} \nabla v_{conv} \quad (3.50)$$

$$d_t s_{conv} = -v_{conv} \nabla \langle s \rangle + (1 - 2q_+) v_{conv} \nabla s_{conv} \quad (3.51)$$

$$- l_m v_{conv} s_{conv} - \alpha_{bv} s_{conv} \tau_{bv}$$

$$d_t Y_{e,conv} = -v_{conv} \nabla \langle s \rangle + (1 - 2q_+) v_{conv} \nabla Y_{e,conv} \\ - l_m v_{conv} Y_{e,conv} - \alpha_{bv} Y_{e,conv} \tau_{bv} \quad (3.52)$$

The parameters for these equations along with the “standard values” used in this investigation are listed in Table 3.1. In the standard parameter set, convective braking is assumed not to occur, and turbulent pressure is not considered to be significant. In addition, the asymmetry parameter  $\alpha_{asym}$  is set to 0.1 in order to model the download plumes which have been observed in numerical models of convection.

### 3.5 Analytic limits

Insight into the structure of these equations can be obtained by observing their behavior in certain limits. First, the convective velocity  $v_{conv}$  contains an unstable critical point to zero. If all of the convective values are set at zero they will remain at zero, but any deviation from zero will cause the  $v_{conv}$  to move away from zero.

In the limit of steady state convection within a region of constant entropy gradient, the velocity fluctuation reduces to

$$v_{conv} = \frac{(l\beta\nabla P s_{conv})^{1/2}}{\rho} \quad (3.53)$$

$$s_{conv} = l\nabla S \quad (3.54)$$

where  $\beta$  is the coefficient of expansion with constant entropy.

This produces a flux of

$$F_c = \rho T v_{conv} s_{conv} \quad (3.55)$$

$$= T l^2 (\beta \nabla P)^{1/2} (\nabla s)^{3/2}. \quad (3.56)$$

This convective flux is functionally identical to the expression in standard mixing length theory. An expression for the convective flux in standard mixing length theory (Kippenhahn and Weigart 1991) is

$$F_c = \rho c_p T \sqrt{g\delta} \frac{l_m^2}{4\sqrt{2}} H_P^{-3/2} (\nabla - \nabla_e)^{3/2} \quad (3.57)$$

where  $c_p$  is the heat capacity at constant pressure,  $g$  is the local gravitational value,  $H_P$  is the pressure scale height and the remaining variables are defined

to be

$$\delta = - \left( \frac{\partial \ln \rho}{\partial \ln T} \right)_P \quad (3.58)$$

$$\nabla = \left( \frac{\partial \ln T}{\partial \ln P} \right) = \frac{H_p}{T} \left( \frac{\partial T}{\partial r} \right) \quad (3.59)$$

$$\nabla_e = \left( \frac{\partial \ln T}{\partial \ln P} \right)_e = \frac{H_p}{T} \left( \frac{\partial T}{\partial r} \right)_e. \quad (3.60)$$

Making the appropriate substitutions, the following expression for the convective flux under mixing length theory is obtained

$$F_c = \frac{1}{2\sqrt{2}} T l^2 (\beta \nabla P)^{1/2} (\nabla s)^{3/2}. \quad (3.61)$$

The equation for the convective flux in standard mixing length theory is identical in form to that of the current convective theory. The only difference is a scaling constant.

Another analytic limit is the limit of steady state convective overshoot. In this limit, the equation for the velocity in an overshoot region is

$$v_{conv} \nabla v_{conv} = \frac{v_{conv}}{l_m}. \quad (3.62)$$

The solution for this equation is an exponential decrease on a length scale  $l_m$  which is consistent with the numerical findings of Freytag et al. (1996).

## 3.6 Extensions to the model

The model presented thus far assumes that the material is advected adiabatically between radial shells. It therefore lacks the capacity to represent salt-finger driven convection, which is the result of thermal transfers. It also lacks the ability to take into account radiative effects. Both of these pieces of physics can be added to the code.

### 3.6.1 Radiative damping extensions

One element that is missing from this convective algorithm is radiative transfer between the upstream and downstream. In the actual proto-neutron star, the different streams would transfer heat and composition radiatively through neutrinos, and this will tend to damp out temperature and composition fluctuations. It has been suggested that this damping may prevent convection from developing altogether. (Bruenn and Dineva 1996)

Radiative damping can be added to this convective model using the “neutrino response functions” as defined by Bruenn and Dineva. Using a one dimensional code, they calculate how neutrino diffusion eliminates perturbations in entropy and composition. Their equations are

$$\dot{\theta}_s = \Sigma_s \theta_s + \Sigma_{Y_e} \theta_{Y_e} - \frac{d\bar{s}}{dz} \dot{z}, \quad (3.63)$$

$$\dot{\theta}_{Y_e} = Y_s \theta_s + Y_{Y_e} \theta_{Y_e} - \frac{d\bar{s}}{dz} \dot{z}, \quad (3.64)$$

$$\rho \ddot{z} = -g \left( \frac{\partial \rho}{\partial s} \right) \theta_s - g \left( \frac{\partial \rho}{\partial Y_e} \right) \theta_{Y_e} \quad (3.65)$$

In calculating the response functions, Bruenn and Dineva conclude that salt-finger does not occur within the supernova core, because in contrast to the terrestrial examples of salt-finger mixing, in the supernova core, composition diffusion occurs more rapidly than thermal diffusion. As a result of this, the gradient in the center of the supernova is stable to salt-finger mixing rather than being unstable.

Once these convective response functions are calculated, the effects of radiative transfer between upstream and downstream can easily be incorporated into the formalism used in this dissertation. Since the response functions express how quickly fluctuations in density and composition are damped, the

radiative transfer of composition between the upstream and the downstream can be written as

$$\left. \frac{\partial s}{\partial t} \right)_{rad} = \Sigma_s s_{conv} + \Sigma_{Y_e} Y_{e,conv}, \quad (3.66)$$

$$\left. \frac{\partial Y_e}{\partial t} \right)_{rad} = Y_s s_{conv} + Y_{Y_e} Y_{e,conv}. \quad (3.67)$$

The buoyancy term in the formalism can be written as

$$\rho_{conv} = \frac{\partial \rho}{\partial s} s_{conv} + \frac{\partial \rho}{\partial Y_e} Y_{e,conv}. \quad (3.68)$$

Unfortunately, the supernova code which was used for the calculations did not easily allow for the calculations of the neutrino response functions, and to add this functionality to the code was beyond the scope of the current work.

# **Chapter 4**

## **Numerical implementation**

### **4.1 Numerical implementation**

One of the most important considerations in designing the convection model is that it be possible to add this model to an existing one dimensional code with a minimum of programming. This chapter describes the implementation of the non-convective code and then describes the convective additions that were added to it.

### **4.2 The non-convective implementation**

The code used in this dissertation was originally written by Itamar Lichtenstadt of the Hebrew University of Jerusalem. A version of the code was described in Myra et al. (1987) although a number of major modifications have been made to the code.

### 4.2.1 Hydrodynamics

The hydrodynamic portions of the code were written using an implicit Lagrangian formalism. In these models, Newtonian gravity was assumed and general relativity was ignored. The effects of general relativity on supernova are unclear (De Nisco, Bruenn, & Mezzacappa 1998), but were ignored in order to reduce complexity in developing the convective model.

The momentum, mass, and energy equations for the matter component are

$$d_t v = -4\pi r^2 \frac{\partial P_M}{\partial m} - G \frac{m}{r^2} - 4\pi \frac{\partial}{\partial m} (r^2 Q) + (d_t v)_v, \quad (4.1)$$

$$\frac{\partial r}{\partial m} = \frac{1}{4\pi r^2 \rho}, \quad (4.2)$$

$$d_t E_M = \frac{P_M}{\rho^2} d_t \rho - 4\pi r^2 Q \frac{\partial v}{\partial m} + (d_t E_M)_v. \quad (4.3)$$

where  $m$  is the mass interior to radius  $r$ , and  $E_M$ ,  $P_M$ ,  $\rho$ , and  $v$  are the specific energy, specific pressure, density and velocity. The matter-neutrino interactions are represented by the term  $(d_t v)_v$  and  $(d_t E_M)_v$ . The term  $Q$  represents the artificial viscosity needed in order to model the shock in a numerically stable fashion. The form of  $Q$  is given in Lichtenstadt, Sack, and Bludman (1980) and is a standard Ritchmeyer's viscosity in which

$$\begin{cases} Q_j = k^2 \rho_j (v_{j+\frac{1}{2}} - v_{j-\frac{1}{2}})^2 & \text{if } \partial_r v < 0, \partial_t \rho > 0 \\ Q_j = 0 & \text{otherwise} \end{cases} \quad (4.4)$$

where  $k$  is a constant which roughly corresponds to the number of zones over which a shock is to be spread. In the current models,  $k^2$  was fixed at the value 1.2.

The first two hydrodynamic equations were solved explicitly and the

results of that calculation was used to simultaneously solve  $E_M$  and  $P_M$  iteratively for the non-convective and non-neutrino terms of that equation. The effects of neutrino and convective interactions were then added to the resulting value for the energy and the pressure recalculated using the equation of state.

There were several limits on the size of the time step. The first is the Courant time condition which requires that the time step be less than the sound crossing time across a single zone to guarantee numerical stability. To insure that this condition was met, the size of the time step is limited to a fraction of the Courant time. Another limit to the size of the time step is that the energy and composition changes due to neutrino and convective interactions are limited to a fraction (typically on the order of  $10^{-2}$  or  $10^{-3}$ ) of the original energy and composition. This is done so that the hydrodynamic portions of the code were able to react to changes in energy due to convection or neutrino interactions.

The size of a single time step varied from  $10^{-5}$  seconds and  $10^{-8}$  seconds. The shortest time steps were to be found immediately after bounce occurred and the shock wave began to propagate outward. The reason for this is the large changes in composition and energy as unshocked material passes through the shock.

There is provision in the code for causing a region that had exceeded a certain density to be assumed to be in equilibrium both hydrodynamically and in terms of neutrino interactions. This feature of the code can save a considerable amount of computer time by avoiding calculation of the innermost parts of the proto-neutron star, where the Courant times are smallest.

The model only calculated the behavior of the innermost 1.5 solar masses of the star, since the equation of state assumed that material was

in nuclear statistical equilibrium, and therefore would have yielded incorrect results for the behavior of the neutron star in the silicon shells and shells exterior to that. The outer boundary condition was that of constant pressure. The pressure used was the pressure at an outer boundary radius in the progenitor model so that the velocity of the outer boundary would be zero at the start of the calculation.

## 4.3 Neutrino transport algorithm

### 4.3.1 Multi-group flux limited diffusion

The neutrino transport in the code was modeled using a multi-group flux limited (MGFLD) scheme. In this scheme neutrinos are divided into different energy groups and the evolution of each energy group is calculated using a diffusion equation.

The transport equation used for neutrino diffusion was derived by Castor (1972) and by Mihalas, Weaver, and Sanderson (1982) and is

$$\rho D_t \left( \frac{u_\nu}{\rho} \right) = (d_t u_\nu)_M - 4\pi\rho \frac{\partial}{\partial m} (r^2 j_\nu) - \epsilon_\nu \frac{\partial}{\partial \epsilon_\nu} \left[ \frac{v}{r} (3p_\nu - u_\nu) + \frac{1}{\rho} D_t \rho p_\nu \right] \quad (4.5)$$

where  $j_\nu$  is the energy flux.

In physical terms, equation 4.5 can be interpreted as equating the change in the number of neutrinos as the sum of three physical processes. The first term on the right hand side of the equation represents interaction between matter and neutrinos and incorporates all neutrino emission and absorption processes in addition to inelastic scattering processes, which redistribute neu-

trinos from energy zone to energy zone. The second term on the right hand side of the equation represents the diffusion of neutrinos outward from mass shell to mass shell. The final term on the right hand side of the equation represents the effects of Doppler shifts in redistributing neutrinos from energy group to energy group.

### The flux limiter

In the transport equation, transport of neutrinos between different physical regions is represented by a term containing the energy flux  $j_\nu$ . In order to solve the transport equation, an expression must be found for this value. There are simple expressions for this quantity in the optically thick limit where the angular distribution of radiation is almost isotropic and on the optically thin limit where the neutrino radiation is free streaming and therefore traveling outward at the speed of light. Unfortunately, the supernova problem involves regions in which both limits are valid and an intermediate region in which neither is.

The MGFLD approximation deals with this situation by first assuming that the flux follows a diffusing relationship given by

$$j_\nu = -D \nabla u_\nu. \quad (4.6)$$

This expression can be derived from a first order expansion of the full radiative equations when the radiation field is almost isotropic (Bruenn 1986), and is only valid in that limit. In the free streaming limit, the diffusion relationship gives incorrect results and results in fluxes corresponding to neutrinos moving faster than the speed of light.

To avoid this unphysical result, a flux limiter is necessary to limit the

calculated fluxes to below  $cu_\nu$ . The flux limiter that is used in this particular calculation is that by Levermore and Pomraning (1981) in which the dimensionless diffusion coefficient  $d = D\sigma/c$  is set to be

$$D = \frac{1}{\omega R} \left( \coth R - \frac{1}{R} \right) \approx \frac{1}{\omega} \left( \frac{2+R}{6+3R+R^2} \right), \quad (4.7)$$

where  $\omega$  is the effective albedo and is given by

$$\omega = \frac{\sigma^* ab + \sigma_s u_\nu}{\sigma u_\nu} \quad (4.8)$$

where  $b$  is the Fermi-Dirac energy distribution function and

$$R = -\frac{\nabla u_\nu}{\sigma \omega u_\nu}. \quad (4.9)$$

The variables  $\sigma_s$  and  $\sigma_a^*$  represent the scattering and absorption cross sections with the asterisk indicating that stimulated absorption is included. The Eddington factor is calculated to be

$$\chi \equiv \frac{p_\nu}{u_\nu} = \coth R \left( \coth R - \frac{1}{R} \right). \quad (4.10)$$

These expressions produce the correct limits

$$\begin{cases} D \rightarrow \frac{1}{3}, \chi \rightarrow \frac{1}{3} & R \rightarrow 1 \\ D \rightarrow \frac{1}{\sigma} \frac{u_\nu}{|\nabla u_\nu|}, \chi \rightarrow 1 & R \rightarrow \infty \end{cases} \quad (4.11)$$

where the former is the free streaming limit and the latter is the diffusive limit.

Defining  $y$  as the neutrino concentration per baryon, and using the expression

$$y \equiv \frac{u_\nu}{\epsilon_\nu \rho N_A} \quad (4.12)$$

where  $N_A$  is Avogadro's number, one obtains the expression

$$\frac{Dy}{Dt} + \frac{\partial Z}{\partial m} + \frac{\partial}{\partial \epsilon_\nu} \left[ -\epsilon_\nu \left( P_2 \frac{\partial v}{\partial r} + Q_2 \frac{1}{\rho} \frac{D\rho}{Dt} \right) y \right] = \left( \frac{Dy}{Dt} \right)_M \quad (4.13)$$

where the spatial current  $Z$  is

$$Z \equiv -4\pi r^2 D \frac{\partial(y\rho)}{\partial r} \quad (4.14)$$

and

$$P_2 = \frac{3\chi - 1}{2} \quad (4.15)$$

$$Q_2 = \frac{\chi - 1}{2}. \quad (4.16)$$

### 4.3.2 Neutrino matter coupling

The neutrino-matter interactions are introduced in the hydrodynamic equations by the following equations

$$(d_t y)_\nu = -4\pi r^2 \frac{\partial P_\nu}{m} - \frac{N_A}{r} \int_0^\infty (3\chi - 1) y \epsilon_\nu d\epsilon_\nu + (d_t y)_{\nu,conv} \quad (4.17)$$

$$(d_t E_M)_\nu = -N_A \int_0^\infty (d_t y) \epsilon_\nu d\epsilon_\nu \quad (4.18)$$

where  $y$  is the number of neutrinos per unit volume and unit energy. The term  $(d_t y)_{\nu,conv}$  represents the effects of neutrino emission and absorption in addition to the effects of convection on neutrino concentration. This term can be written as

$$(d_t y)_{\nu,conv}(\omega) = (d_t)_{conv} + \sum_{\text{all processes}} j(\omega) - \frac{cy}{\lambda(\omega)} \quad (4.19)$$

where  $(d_t)_{conv}$  contains the effects of convection on neutrino concentration,  $j(\omega)$  is the neutrino emission rate, and  $1/\lambda\omega$  is the absorption cross section.

All six types of neutrinos were modeled in the code. Because mu and tau neutrinos and anti-neutrinos have almost identical cross-sections, they can be all be calculated using one set of neutrino groups. This results in three sets of neutrino groups, one for electron neutrinos, electron anti-neutrinos, and a combined group contained the remaining flavors of neutrinos.

### **Neutrino production and absorption**

The neutrino production and absorption processes in this code were based on cross sections calculated by Bruenn (1985) instead of the rates described in Myra et al. (1987). The production and absorption processes included in the models calculated in this dissertation were

- electron neutrino absorption on neutrons ( $\nu_e + n \Rightarrow e + p$ )
- electron anti-neutrino absorption on protons ( $\bar{\nu}_e + p \Rightarrow e + n$ )
- electron neutrino absorption on nuclei ( $\nu_e + A' \Rightarrow A + e$ )
- electron, mu, and tau neutrino production and absorption from pair production

The rate used for electron neutrino interactions with nucleons was

$$\frac{1}{\lambda(\omega)} = \frac{G^2}{\pi} n_n (g_\nu^2 + 3g_A^2) [1 - F_e(\omega + Q)] (\omega + Q)^2 \left[ 1 - \frac{M_e^2}{(\omega_Q)^2} \right] \quad (4.20)$$

$$j(\omega) = \frac{G^2}{\pi} n_p F_e(\omega + Q) (\omega + Q)^2 \left[ 1 - \frac{M_e^2}{(\omega_Q)^2} \right] \quad (4.21)$$

where  $G^2$  is the fermi constant with the value

$$G^2 = 5.18 \times 10^{-44} MeV^{-2} cm^2, \quad (4.22)$$

$Q$  is the difference in mass between neutrons and protons

$$Q = M_n - M_p = 1.2933 \text{ MeV}. \quad (4.23)$$

The rates used differ from the rates described in Bruenn (1985) in that nucleon degeneracy is not taken into account.

The rates for neutrino-nuclei absorption is

$$\frac{1}{\lambda(\omega)} = \frac{G^2}{\pi} n_A \exp [\beta(\mu_n - \mu_p - Q')] g_A^2 \frac{2}{7} N_p(Z) N_n(N) [1 - F_e(\omega + Q')] (\omega + Q')^2 \left[ 1 - \frac{M_e^2}{(\omega + Q')^2} \right] \quad (4.24)$$

$$j(\omega) = \frac{G^2}{\pi} n_A \frac{2}{7} N_p(Z) N_n(N) F_e(\omega + Q') (\omega + Q')^2 \left[ 1 - \frac{M_e^2}{(\omega + Q')^2} \right] \quad (4.25)$$

where

$$Q' = \mu_n - \mu_p + \Delta \quad (4.26)$$

and

$$N_p(Z) = \begin{cases} 0 & Z < 20 \\ Z - 20 & 20 < Z < 28 \\ 8 & Z > 28 \end{cases} \quad (4.27)$$

$$N_n(N) = \begin{cases} 6 & N < 34 \\ 40 - N & 34 < N < 40 \\ 0 & N > 40 \end{cases} \quad (4.28)$$

The rates for anti-neutrino absorption on nucleons was

$$\frac{1}{\lambda(\omega)} = \frac{G^2}{\pi} n_n (g_v^2 + 3g_A^2) [1 - F_{e+}(\omega - Q)] (\omega - Q)^2 \left[ 1 - \frac{M_e^2}{(\omega - Q)^2} \right] \theta(\omega - Q - M_e) \quad (4.29)$$

$$j(\omega) = \frac{G^2}{\pi} n_p F_{e+} (\omega - Q) (\omega - Q)^2 \left[ 1 - \frac{M_e^2}{(\omega - Q)^2} \right] \theta(\omega - Q - M_e) \quad (4.30)$$

Although this equation results in the correct analytic expressions for the emission and absorption coefficients, the numerical method used in Myra et al. (1987) of first calculating the emission coefficients and then using the Kirchoff's law relationship between the emission and absorption coefficients to calculate absorptions proved to be highly unsatisfactory and lead to incorrect numerical results.

The difficulty lies in the Fermi function

$$F_i(E_i) = \frac{1}{1 + \exp \beta(E_i - \mu_i)} \quad (4.31)$$

which is found in the expression for the emission rates. This function has the limits

$$\begin{cases} 1 & F_i \rightarrow -\infty, \\ 0 & F_i \rightarrow \infty. \end{cases} \quad (4.32)$$

In multiplying this term by the factor in Kirchoff's laws, the function

$$F_i(E_i)' = \frac{\exp \beta(E_i - \mu_i)}{1 + \exp \beta(E_i - \mu_i)} = 1 - F_i E_i \quad (4.33)$$

is calculated. This function has the limits

$$\begin{cases} 0 & F_i \rightarrow -\infty, \\ 1 & F_i \rightarrow \infty. \end{cases} \quad (4.34)$$

In calculating the absorption coefficients from the emission coefficients in the limits of large  $E_i$ , one is multiplying a very large number by a very small number. Numerical errors in the calculation of the exponentials were found to create results that were far from the proper limits.

The production and absorption rates for pair production are based on the rates in Bruenn (1985). Unlike that calculation, the current model assuming isotropic production and absorption and does not take into account angle dependencies. The result of this is that only the zero-order Legendre terms of the pair production equation were calculated and used, in contrast to the Bruenn treatment in which the effects of the first-order Legendre terms were calculated and included in the transport equation. The equations used in the current treatment were

$$\frac{1}{\lambda(\omega, \omega')} = \frac{G^2}{\pi} \int_0^{\omega+\omega^+} dE_e \{F_e(E_e)F_{e+}(\omega + \omega' - E_e)\} \phi_0 \quad (4.35)$$

$$j(\omega, \omega') = \frac{G^2}{\pi} \int_0^{\omega+\omega^+} dE_e \{[1 - F_e(E_e)][1 - F_{e+}(\omega + \omega' - E_e)]\} \phi_0 \quad (4.36)$$

where

$$\phi_0(\omega, \omega', E_e) = c_1 J_0^I(\omega, \omega', E_e) + c_2 J_0^{II}(\omega, \omega', E_e). \quad (4.37)$$

$$\begin{aligned} J_0^{II}(\omega', \omega, E_e) &= J_0^I(\omega, \omega', E_e) = \frac{1}{\omega\omega'} \{ [\theta(\omega - E_e)\theta(\omega' - \omega) \\ &\quad + \theta(\omega' - E_e)\theta(\omega - \omega')]a_0(\omega, \omega', E_e) \\ &\quad + [\theta(E_e - \omega)\theta(\omega - \omega')] \\ &\quad + \theta(E_e - \omega')\theta(\omega' - \omega')]b_0(\omega, \omega', E_e) \\ &\quad + \theta(E_e - \omega)\theta(\omega' - E_e)c_0(\omega, \omega', E_e) \\ &\quad + \theta(E_e - \omega')\theta(\omega - E_e)d_0(\omega, \omega', E_e) \} \end{aligned} \quad (4.38)$$

where

$$a_0(\omega, \omega', E_e) = \frac{1}{\omega\omega'} \left[ \frac{4}{15}E_e^5 - \frac{4}{3}E_e^4\omega' + \frac{8}{3}E_e^3e\omega'^2 \right] \quad (4.39)$$

$$\begin{aligned} b_0(\omega, \omega', E_e) = & \frac{1}{\omega\omega'} \left[ -a_0(\omega, \omega', E_e) + \frac{8}{3}E_e^2(\omega^3 + \omega'^3) \right. \\ & - \frac{4}{3}E_e(\omega + \omega')^2(\omega'^2 - 2\omega\omega' + 3\omega^2) \\ & \left. + \frac{4}{15}(\omega + \omega')^3(\omega'^2 - 3\omega\omega' + 6\omega^2) \right] \end{aligned} \quad (4.40)$$

$$\begin{aligned} c_0(\omega, \omega', E_e) = & \frac{\omega^2}{\omega'} \left[ \frac{8}{3}\omega'^2 + 4\omega\omega' + \frac{8}{5}\omega'^2 \right] \\ & - E_e \left[ \frac{16}{3}\omega^2 + 4\frac{\omega^3}{\omega'} \right] + \frac{8}{3}E_e^2\frac{\omega^2}{\omega'} \end{aligned} \quad (4.41)$$

$$d_0(\omega, \omega', E_e) = \frac{4}{15}\frac{\omega'^4}{\omega} - \frac{4}{3}\frac{\omega'^3}{\omega} + \frac{8}{3}\frac{\omega'^2}{\omega}E_e^2 \quad (4.42)$$

and

$$\begin{cases} c_1 = (C_V + C_A)^2, c_2 = (C_V - C_A)^2 & \nu_e \\ c_1 = (C_V - C_A)^2, c_2 = (C_V + C_A)^2 & \bar{\nu}_e \\ c_1 = (C_V + C_A - 2)^2, c_2 = (C_V - C_A)^2 & \nu_\mu, \nu_\tau \\ c_1 = (C_V - C_A)^2, c_2 = (C_V + C_A - 2)^2 & \bar{\nu}_\mu, \bar{\nu}_\tau \end{cases} \quad (4.43)$$

## Neutrino scattering

There are two scattering processes included in the supernova code, neutrino-nucleon scattering and neutrino-electron scattering. Because of the large mass of the nucleons, this neutrino process is largely energetically conservative. By contrast, neutrino-electron scattering is largely non-conservative and tends to thermalize the neutrino spectrum. This process is likely to increase the neutrino flux and the rate of leptonization by causing high energy neutrinos to scatter into lower energies which have longer mean free paths. In addition,

there are two secondary effects that potentially help the explosion. First, the neutrino heating caused by the extra neutrinos increases the concentration of free protons and therefore the rate of electron capture and neutrino production. Second, when high energy neutrinos are scattered into lower energy, they provide an open neutrino state which can be filled by further electron captures.

The equation used for coherent nuclear scattering is identical to that used in Myra (1987), which corrects a mistake in the derivation by Bruenn (1985). The cross sections for neutron  $\sigma_n$ , protons  $\sigma_p$ , and heavy nuclei  $\sigma_h$  are

$$\sigma_n = \frac{\sigma_0}{4} \left( \frac{\epsilon_\nu}{m_e c^2} \right)^2 n_n \quad (4.44)$$

$$\sigma_p = \frac{\sigma_0}{4} \left( \frac{\epsilon_\nu}{m_e c^2} \right)^2 \left( 1 - \frac{4}{3} \sin^2 \theta_W + \frac{8}{3} \sin^4 \theta_W \right) n_p \quad (4.45)$$

$$\sigma_h = \frac{2}{3} \frac{\sigma_0}{4} \left( \frac{\epsilon_\nu}{m_e c^2} \right)^2 \left[ A C_{v0} + \frac{1}{2} (Z - N) C_{v1} \right]^2 n_H \quad (4.46)$$

where  $n_n$ ,  $n_p$ , and  $n_H$  are the number densities for neutrons, protons, and heavy nuclei respectively,  $\sigma_0$  is defined to be  $4G^2 m_e \hbar^2 / \pi c^2 = 1.76 \times 10^{-44} \text{ cm}^2$ ,  $\theta_W$  is the Weinberg angle, A, Z, and N are the mass, charge, and nuclear numbers, and  $C_{v0} = -\sin^2 \theta_W$  and  $C_{v1} = 1 - 2 \sin^2 \theta_W$  are the isoscalar and isovector coupling constants. Nuclear size effects and scattering off alpha particles are ignored.

The inelasticity of neutrino-electron scatter makes it difficult to model. Unlike elastic scattering, absorption, or emission processes, inelastic neutrino electron scatter couples each energy group with all of the other energy groups. To calculate this process in detail would be time-consuming. Rather, a Fokker-Planck approximation similar to the one introduced by Bowers and Wilson (1982) was used. In this approximation, only the interactions between a neu-

trino group and the neighboring groups are computed.

$$\sigma_{NES} = \frac{R}{c}(1 - f_\nu)\epsilon_\nu \left( \frac{1}{6T + 3/2\mu_e + \epsilon_\nu} \right) \text{cm}^{-1} \quad (4.47)$$

where  $R$  is the neutrino equilibration rate and is set to be

$$frac{Rn_e c}{} = \begin{cases} 4.47\sigma_0\epsilon_\nu T & T > \mu_e \\ 1.12\sigma_0\epsilon_\nu\mu_e & T < \mu_e < \epsilon_\nu \\ 0.86\sigma_0\frac{\epsilon_\nu T}{\mu_e} \left( 1 + 0.258\frac{\epsilon_\nu^2}{T} \right) \left( 1 + 11.6\frac{T}{\epsilon_\nu} \right) & R, \epsilon_\nu < \mu_e \end{cases} \quad (4.48)$$

## 4.4 Neutrino differencing algorithm

The algorithm is based on that used by Myra et al. (1987) and was also fully-implicit in energy space and semi-implicit in physical space but differed from the original in that the new algorithm modeled the advective term using a donor cell approximation. In describing the algorithm,  $A$  and  $B$  superscripts are the outdated and updated quantities, and  $j, m$  subscript refers to the  $j$ -th spatial zone and the  $m$ -th energy zone.

The difference equation to be solved is

$$\frac{y^B - y^A}{\Delta t} = h_{dif} + h_{abs-emis} + h_{NES} + h_{advect} \quad (4.49)$$

where and  $h_{dif}$ ,  $h_{advect}$ ,  $h_{abs-emis}$ ,  $h_{NES}$  are the terms that model the diffusion, absorption/emission, NES, and advection terms.

The diffusion term  $h_{dif}$  calculated from the incoming and outgoing currents as

$$h_{dif} \equiv \frac{Z_{j+1/2,m} - Z_{j-1/2,m}}{\Delta m_{j,m}} \quad (4.50)$$

where  $\Delta m_{j,m}$  is the mass size of the  $j$ -th zone and  $Z_{j+1/2,m}$  is the current between zones  $j$  and  $j + 1$  which is calculated to be

$$Z_{j+1/2,m} \equiv -4\pi r_{j+1/2}^2 D_{j,m} \frac{y^A \rho^A - y^B \rho^B}{\Delta r_j}. \quad (4.51)$$

The combination of both outdated and updated quantities in the current makes the difference equation semi-implicitly.

The emission and absorption terms are modeled by

$$h_{abs-emis} \equiv S_{j,m} \left( 1 - \frac{\rho^B y^B}{a \epsilon_\nu^2} \right) - \Gamma y^B \quad (4.52)$$

and

$$h_{NES} \equiv \Gamma_{j-1,m} y_{j-1}^B + \Gamma_{j+1,m} y_{j+1}^B - \Gamma_{j+1,m} y_{j-1}^B - \Gamma_{j+1,m} y_{j+1}^B \quad (4.53)$$

In discussing the advective term, we define the advective velocity  $v_{advect}$

$$v_{advect} \equiv -\epsilon_\nu \left( P_2 \frac{\partial v}{\partial r} + Q_2 \frac{1}{\rho} \frac{D\rho}{Dt} \right) \quad (4.54)$$

The algorithm used to difference this equation is different than the one described in Myra et al. (1987). The original algorithm was fully-implicit in energy space and semi-implicitly in physical space and was found to cause numerical instabilities in the next to lowest neutrino energy group. The cause of this instability was found to be due to the approximation

$$h_{advect} \equiv v_{advect} \frac{y_{j+1,m} - y_{j-1,m}}{\Delta \epsilon} \quad (4.55)$$

which caused the value of the neutrino concentration to be calculated as negative under some conditions. Once one neutrino group had a negative concentration, the original algorithm would cause this result to be propagated outward resulting in a “streak” in the tables of neutrino concentration.

After much effort, the following expression was found to give satisfactory numerical results

$$h_{advection} \equiv \begin{cases} v_{advection} \frac{y_{j+1,m} - y_{j,m}}{\Delta \epsilon} & v_{advection} > 0 \\ v_{advection} \frac{y_{j,m} - y_{j-1,m}}{\Delta \epsilon} & v_{advection} < 0 \end{cases}. \quad (4.56)$$

This approximation is known as the “donor cell” approximation. This algorithm proves to be more numerically well-behaved in that it did not evidence the negative neutrino concentration problem present in the original algorithm.

After combining the terms and engaging in much algebra, the difference equation is brought into the form

$$-A_{j,m-1}y_{j,m-1} + B_{j,m}y_{j,m} - C_{j,m+1}y_{j,m+1} - D_{j,m} = 0 \quad (4.57)$$

which is then solved fully-implicitly. Because the equation is non-linear, several iterations are made in which the coefficients are updated with the new values of the neutrino concentration. The solution is considered to have converged with the solutions do not change more than one part in  $10^5$ . If the equation does not converge, the time step is halved and the hydrodynamic values within the equation are calculated from interpolated values.

## Numerical zoning

The hydrodynamic equations were solved numerically. A typical initial model used 180 zones which modeled the interior 1.5 solar masses of the star. The model was limited to this region because the equation of state had not been extended to calculate the behavior of material outside of the iron core. The initial zoning placed 40% of the zones in the interior 0.8 solar masses, 40% in the 0.6 solar masses exterior to that, and 20% in the remainder of the simulation. This zoning was chosen after extensive trial and error and was intended

to maximize resolution of the region of shock formation during bounce. A smoothing function was used to insure that the size of the zones were smoothly varying throughout the simulation.

A Lagrangian rather than an Eulerian formulation is most natural for the infall phase of the supernova problem, during which the collapse causes the radii of material to decrease rapidly. However, a Lagrangian formulation becomes more problematic during the expansion phase of the supernova problem. For accurate results, it is necessary to have fine zoning of the material near the shock so that both shock propagation and neutrino heating behind the shock can be accurately modeled. However, once material has fallen through the shock and reached hydrostatic equilibrium, fine zoning is not necessary to model the supernova and is merely a waste of computational resources. The need for adequate zoning is particularly difficult in the case of core collapse models, because as the shock propagates outward, the requirements for the fineness of the zones for a given mass shell changes, requiring finer zones when a mass shell is near the shock and coarser zoning when the mass shell has settled into hydrostatic equilibrium.

The solution to this dilemma is to rezone the model as the shock propagates outward, insuring that fine zones are found in the neighborhood of the shock while coarse zones are placed where there is little dynamic activity. However, rezoning must be done very carefully to avoid unphysical results. The first attempts made at rezoning involved calculating a completely new grid and then redistributing the material within the model from the old grid into the new grid. This proved to be extremely unsuccessful as it resulted in large and unphysical explosions which occurred within milliseconds after the model was rezoned. In the numerical models, the shock is in a quasi-static

equilibrium between the pressure of the material behind the shock and the ram pressure of the infalling material. When the model was rezoned these pressures behind and in front of the shock became unbalanced leading to a rapid and unphysical explosion.

Following a suggestion by Steve Bruenn, a rezoning algorithm was adopted which deals with the problem of rezoning by making small changes to the gridding at each time step. Instead of rezoning by imposing a completely new grid on our model, the zones of the model are examined at each time step to see which zones can be merged and which zones can be split. Because this method preserves most of the original zoning and because rezoning affects only a few zones at each time step, unphysical results which are the result of unbalancing global quantities can be avoided. Nevertheless, a proper rezoning algorithm required the satisfaction of a large number of criteria and a great deal of effort and numerical experimentation was necessary in order to develop a functional rezoning algorithm.

In order to minimize the numerical effects caused by rezoning, a number of conditions must be satisfied by a region before it can be rezoned. First, there is no rezoning in the infall phase of the collapse. Second, there is no rezoning in regions with high artificial viscosity. Regions of high artificial viscosity generally signify that the shock is nearby and therefore that rezoning may unphysically change the characteristics of the shock. Third, the innermost and outermost zones are not rezoned, thereby preventing any numerical effects which may be due to changing boundary conditions. In order to prevent numerical errors from the continual splitting and combining of zones, only zones in front of the shock were split and only zones behind the shock were combined.

The final rezoning algorithm involved the calculation of a characteristic length  $\Delta r_{char}$ . For the zones in front of the shock, a new zone was inserted between two older zones when the difference in density between zones exceeded 0.2 times the density of the inner zone or when the size of the two zones exceeded  $\Delta r_{char}$ . For zones interior to the shock, two zones were combined when the difference in pressure between two zones was less than 0.05 times the pressure of the inner zone, when the velocity difference between the two zones was less than  $5 \times 10^7 \text{ cm sec}^{-1}$ , and when the combined zone was less than  $\Delta r_{char}$ . The pressure criterion for zone merging was particularly important since it was found that when pressure was not taken into account, combining zones produced large motions in regions which were expected to have been in hydrodynamic equilibrium.

The effect of the zone splitting and merging was to cause the zones to approach the radial size of the characteristic length  $\Delta r_{char}$ . It was found that the expression for  $\Delta r_{char}$  needed to satisfy several criteria. First,  $\Delta r_{char}$  needed to be sufficiently small near the shock so that the width of the simulated shock is much smaller than the scale heights of all of the pre-shock and post-shock variables in the simulation. This is so that the shock appears as a discontinuity in the simulation. Second, it was found that sudden changes in zone size between adjacent zones created numerical instabilities. Hence it was found necessary to define  $\Delta r_{char}$  so as to avoid sudden changes in zone size between zones. Finally, a minimum size restriction was put on the zones to avoid excessively small sound crossing times, which would then produce small time steps in the simulation.

After much trial and error, satisfactory results were obtained when the

expression which was used for  $\Delta r_{char}$  was

$$\Delta r_{char} = \max(\min(\Delta r_1, \Delta r_2), \Delta r_3) \quad (4.58)$$

where

$$\Delta r_1 = 1 \times 10^5 \text{ cm} + 1.9 \times 10^6 \text{ cm} \left( \frac{j - j_{shock}}{20} \right)^2 \quad (4.59)$$

$$\Delta r_2 = 3 \times 10^5 \text{ cm} + 2.7 \times 10^6 \text{ cm} \left( \frac{r - r_{shock}}{2 \times 10^7} \right)^2 \quad (4.60)$$

$$\Delta r_3 = 2 \times 10^6 \text{ sec} \times c_s \quad (4.61)$$

where  $j$  and  $j_{shock}$  are the local zone number and the zone number of the shock,  $r$  and  $r_{shock}$  are the local radius and the radius of the shock, and  $c_s$  is the local sound speed.

The parameter  $\Delta r_1$  relates the characteristic length to the number of zones away from the shock, while  $\Delta r_2$  relates the characteristic length to the distance away from the shock, and  $\Delta r_3$  relates the characteristic length to the local sound speed. It was found that it was necessary to use all three expressions in calculating the characteristic length. Using  $\Delta r_1$  alone proved unsatisfactory in that this criterion would not split a large zone in front of the shock, and hence when this criterion was used alone, it resulted in unsatisfactorily large zones, making it impossible to adequately resolve the shock. By expressing the characteristic length as a function of zone location, it was possible to insure small zones near the shock. However, this criterion used alone also proved unsatisfactory. While the equation for  $\Delta r_2$  insured a large number of small zones near the shock, the criterion did not place strong limits on the size of the zones below the shock. The large zones which resulted presented two numerical difficulties. The first difficulty was that there was insufficient

resolution in the region below the shock. The second difficulty was that the presence of large zones immediately adjacent to small ones caused numerical instabilities. Finally, without an equation which related the characteristic length with the Courant sound speed, it was found that the algorithm would cause the model to produce excessively small zones behind the shock which would cause excessively small time steps in the model.

In the current model, the three criteria were thus combined, and this insured small zones near the shock gradually merging into larger, but still small, zones interior to the shock. The typical size of a zone near the shock was  $1 \times 10^5$  cm gradually increasing to  $5 \times 10^5$  cm further behind the shock.

## 4.5 Switch on criterion

There was also some subtlety in the criterion for switching on the adaptive algorithm. It was desirable to turn on zone splitting as soon after bounce as possible in order to insure that the shock is adequately resolved. At the same time, it was desirable not to immediately merge zones after bounce so that the inner core could settle down to equilibrium without the numerical disturbances caused by rezoning. To deal with these conflicting requirements, separate switch on criteria for splitting zones and merging zones were imposed. Zone splitting was switched on when the shock moved past  $6 \times 10^6$  cm, and zone merging was switched on when the shock moved past  $8 \times 10^6$  cm.

## 4.6 Splitting algorithm

The algorithm for splitting a zone involved creating a third zone at the boundary of two old zones. The inner and outer boundaries of the new zone was calculated to be

$$r_{in} = r_j - \frac{1}{3}(r_j - r_{j-1}) \quad (4.62)$$

$$r_{out} = r_j - \frac{1}{3}(r_{j+1} + r_j) \quad (4.63)$$

where  $r_j$  is the boundary at which the new zone is to be created,  $r_{in}$  is the inner boundary of the new zone and  $r_{out}$  is the outer boundary of the new zones. The values of the hydrodynamic quantities, which are models at the shell edges, are interpolated and calculated to be

$$a_{in} = r_j - \frac{1}{3}(a_j - a_{j-1}) \quad (4.64)$$

$$a_{out} = r_j - \frac{1}{3}(a_{j+1} + a_j) \quad (4.65)$$

where  $a$  is a generic hydrodynamic quantity.

The extensive thermodynamic quantities were calculated by adding the contribution from the old shells into the new shell. From the radii calculated above, the volume and mass contributions to the new shell from the old shell are calculated to be

$$V_A = \frac{4\pi}{3}(r_j^3 - r_{in}^3) \quad (4.66)$$

$$V_B = \frac{4\pi}{3}(r_{out}^3 - r_j^3) \quad (4.67)$$

$$M_A = \rho_{j-\frac{1}{2}} V_A \quad (4.68)$$

$$N_B = \rho_{j+\frac{1}{2}} V_B. \quad (4.69)$$

where  $V_A$  and  $V_B$  are the volume contributions of the interior and exterior shells and  $M_A$  and  $M_B$  are the mass contributions. The density  $\rho$ , energy  $e$  and  $Y_e$  of the new shell were then calculated to be

$$\rho = \frac{M_A + M_B}{V_A + V_B} \quad (4.70)$$

$$e = \rho_{j-\frac{1}{2}} M_A + \rho_{j+\frac{1}{2}} M_B \quad (4.71)$$

$$Y_e = Y_{e,j-\frac{1}{2}} M_A + Y_{e,j+\frac{1}{2}} M_B, \quad (4.72)$$

and using these values, all of the remaining thermodynamic values were calculated using the equation of state.

Similarly the neutrino concentrations were calculated to be

$$y = y_{j-\frac{1}{2}} V_A + y_{j+\frac{1}{2}} V_B. \quad (4.73)$$

## 4.7 Merging algorithm

The criteria for merging zones  $j$  and  $j+1$  are

$$\begin{cases} |\rho_{j+1} - \rho_j| \leq c_\rho \rho_j \\ |e_{j+1} - e_j| \leq c_e e_j \\ |v_{j+\frac{1}{2}}| \leq c_{vel} \end{cases} \quad (4.74)$$

where  $\rho_j$  and  $e_j$  are the density and energy for shell  $j$ . If the criteria for merging zones are satisfied, the total mass  $M$ , energy  $E$ , and electron concentration  $Y_E$  for shells  $j$  and  $j+1$  are calculated,

$$M = \frac{4\pi}{3} \rho_j \left( r_{j+\frac{1}{2}}^3 - r_{j-\frac{1}{2}}^3 \right) + \rho_{j+1} \left( r_{j+\frac{3}{2}}^3 - r_{j-\frac{1}{2}}^3 \right) \quad (4.75)$$

$$E = \frac{4\pi}{3} e_j \left( r_{j+\frac{1}{2}}^3 - r_{j-\frac{1}{2}}^3 \right) + e_{j+1} \left( r_{j+\frac{3}{2}}^3 - r_{j-\frac{1}{2}}^3 \right) \quad (4.76)$$

$$Y_E = \frac{4\pi}{3} Y_{ej} \left( r_{j+\frac{1}{2}}^3 - r_{j-\frac{1}{2}}^3 \right) + Y_{ej+1} \left( r_{j+\frac{3}{2}}^3 - r_{j-\frac{1}{2}}^3 \right). \quad (4.77)$$

We then calculate the total volume of the merged zone  $V$ :

$$V = \frac{4\pi}{3} \left( r_{j+\frac{3}{2}}^3 - r_{j-\frac{1}{2}}^3 \right). \quad (4.78)$$

Using these quantities, we can calculate the mass density  $\rho_M$ , energy density  $e_M$ , and electron fraction  $Y_{eM}$  of the merged zone,

$$\rho_M = \frac{M}{V} \quad (4.79)$$

$$e_M = \frac{E}{V} \quad (4.80)$$

$$Y_{eM} = \frac{Y_E}{V} \quad (4.81)$$

## 4.8 Computational hardware

The hardware used to run the production models in this dissertation was a CRAY T3E supercomputer at the Texas Advanced Computing Facility. The code was written portably in Fortran 90, and test runs were successfully performed on a DEC Alpha, a Sparcstation 5, a Silicon Graphics Indy. A test run was also performed on a Cray J90. Although the code complied and executed successfully on the J90, the non-vectorized nature of the code drastically limited performance on that platform. Despite efforts to restructure the code to optimize performance in the J90 vector processor, the code still ran approximately two to three times slower than on a Sparcstation 5.

Unlike the J90 platform, the CRAY T3E platform was particularly suited to run supernova models using this current code. The T3E consists of up to 64 DEC Alpha chips in parallel. Because, each chip is a scalar processor which can be programmed to run independently of the others, it was therefore possible to program the simulation to run with different initial pa-

rameters on each CPU. As a result, it was possible to run many supernova models in parallel on the T3E.

## 4.9 Computational tests

In order to insure the correctness of the code, both the hydrodynamics and neutrino algorithms were subjected to a number of test problems and self-consistency checks, a number of which where inspired by Bruenn (1985).

**Global energy conservation** Within the code there are a number of processes which exchange energy between thermal, neutrino, and kinetic forms, and which radiate energy from the model. It was found that the code conserved energy within 50% of the initial total energy of  $4 \times 10^{50}$  ergs. This energy conservation provided a strong test of the code in light of the fact that the terms within the energy conservation equation were on the order of  $10^{53}$  ergs.

**Global lepton conservation** A check was also made for global lepton conservation. It was found that the sum of leptons remained within 1% of the original value.

**Adiabatic flow** In the absence of shocks and heat transfer processes, the entropy of a region should remain constant. This condition can be verified by examining the entropy profiles of the entire model during infall and the center 0.1 solar mass region throughout the entire calculation. It was found that the during the first 200 milliseconds of the calculation, that the entropy did not vary by more than 1% and the entropy of the center did not vary by more

than 1% throughout an entire calculation. This adiabaticity is particularly significant because of the large velocity changes that are encountered by the material under analysis and the fact that adiabaticity is not explicitly included in the calculation of the code.

**Sedov Blast Wave** In order to test the correctness of the shock propagation and the adaptive meshing scheme, a test calculation was performed to simulate a Sedov blast wave. In this calculation a model consisting of a homogeneous sphere was prepared. This sphere contained a density of  $10^5 \text{ gm/cm}^3$ , a temperature of  $10^9 \text{ K}$ , and a  $Y_e$  of 0.5. Once this sphere was prepared, a total of  $1 \times 10^{53}$  ergs of energy was injected into the interior 0.1 solar masses of the model. To prevent instabilities at the boundary of the injection region, the energy was added according to the formula

$$e = \frac{2E}{M_0} \left(1 - \frac{m}{M_0}\right) \quad (4.82)$$

where  $e$  is the energy per unit mass that was injected into a zone,  $m$  was the mass interior to the zone,  $E$  was the total energy to be injected, and  $M_0$  was the mass enclosed by the injection zone. The density (figure 4.1) and pressure (figure 4.2) profiles were then plotted. After an initial transient phase, the profiles were found to be in agreement with the profiles expected for a Sedov blast wave. This agreement is particularly significant as during the transient phase, there were spikes of less than  $1 \times 10^8$  cm in width whose density and pressures quantities were two to three orders of magnitude larger than the background (figures 4.4 and 4.5). The adaptive mesh scheme placed large numbers of zones in these regions, and successfully allowed the profiles to relax to those expected in Sedov blast waves. The shock radial propagation

was examined and found to be consistent with the  $t^{2/5}$  dependence expected in Sedov blast waves. This agreement can be illustrated as the linear relationship between time and radius $^{5/2}$  (figure 4.3).

**Rate Equations** To insure the accuracy of the neutrino rates, the rates were plotted and compared with those used in Bruenn (1985). Several differences were noted. First, the rates in this study include the corrections of Myra et al. (1987) which boost the neutrino-nuclei scattering rates by a factor of three. Second, to reduce computational time, the pair production rates of the electron neutrinos and anti-neutrinos were calculated to be averaged values rather than separate ones. Finally, neutrino-nuclei interactions were found to be suppressed in the first test case in the current models while they still exist in those of Bruenn. The reason for this difference was due to different equations of state. The equation of state in the current model produced nuclei which were more neutron-rich than in the Bruenn case and this served to suppress neutrino-nuclei interactions.

**Neutrino transport with scattering** To test the neutrino scattering properties of the code, an isotropic model was prepared with density  $1 \times 10^{12} g/cm^3$  and radius  $5 \times 10^9$  cm. This model was divided at a radius of  $1 \times 10^8$  cm into a production zone and a radiation zone. Within the production zone, the emission and absorption rates were set to their natural values, while in the radiation zone, neutrino emission and absorption were suppressed. At the beginning of the simulation the scattering depth for both the production zone and the radiation zone was set to  $10^5$  cm. At 0.2 seconds into the simulation, scattering was turned off in the scattering zone. The evolution of the system

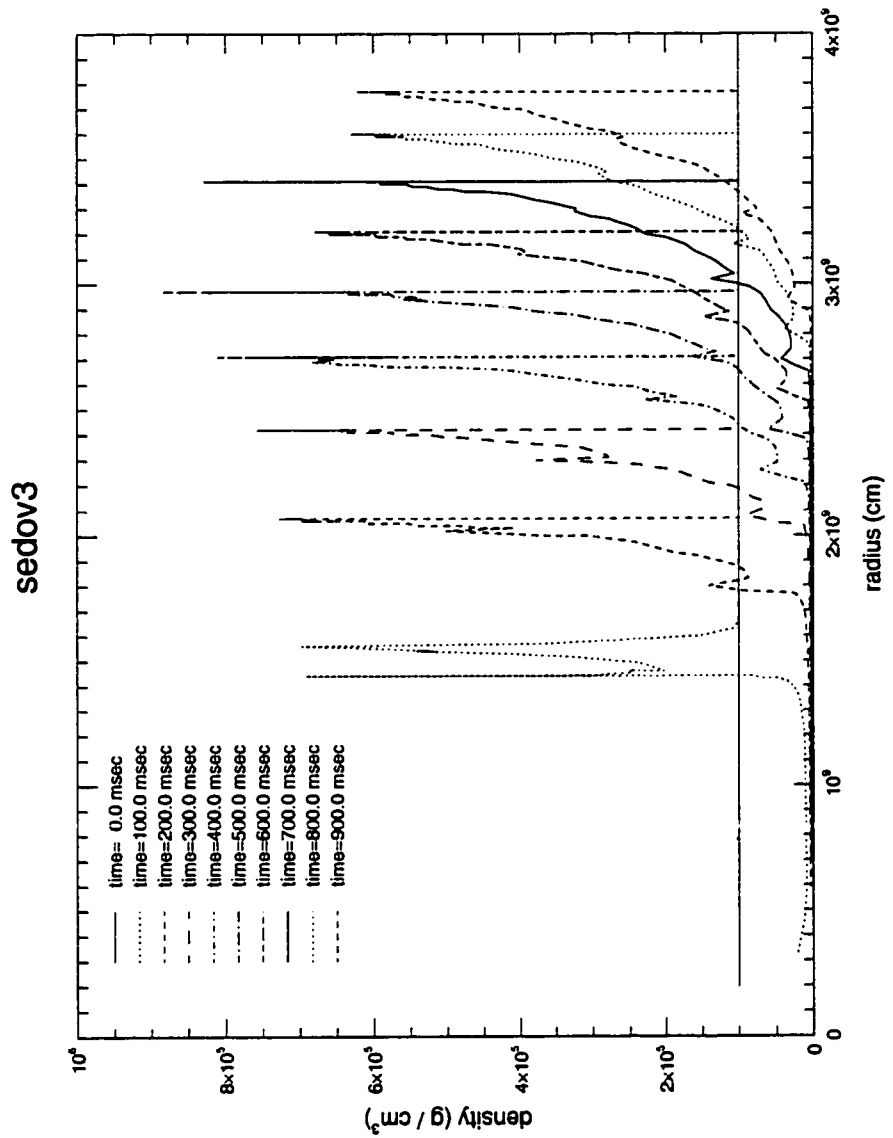


Figure 4.1: Sedov blast wave density evolution

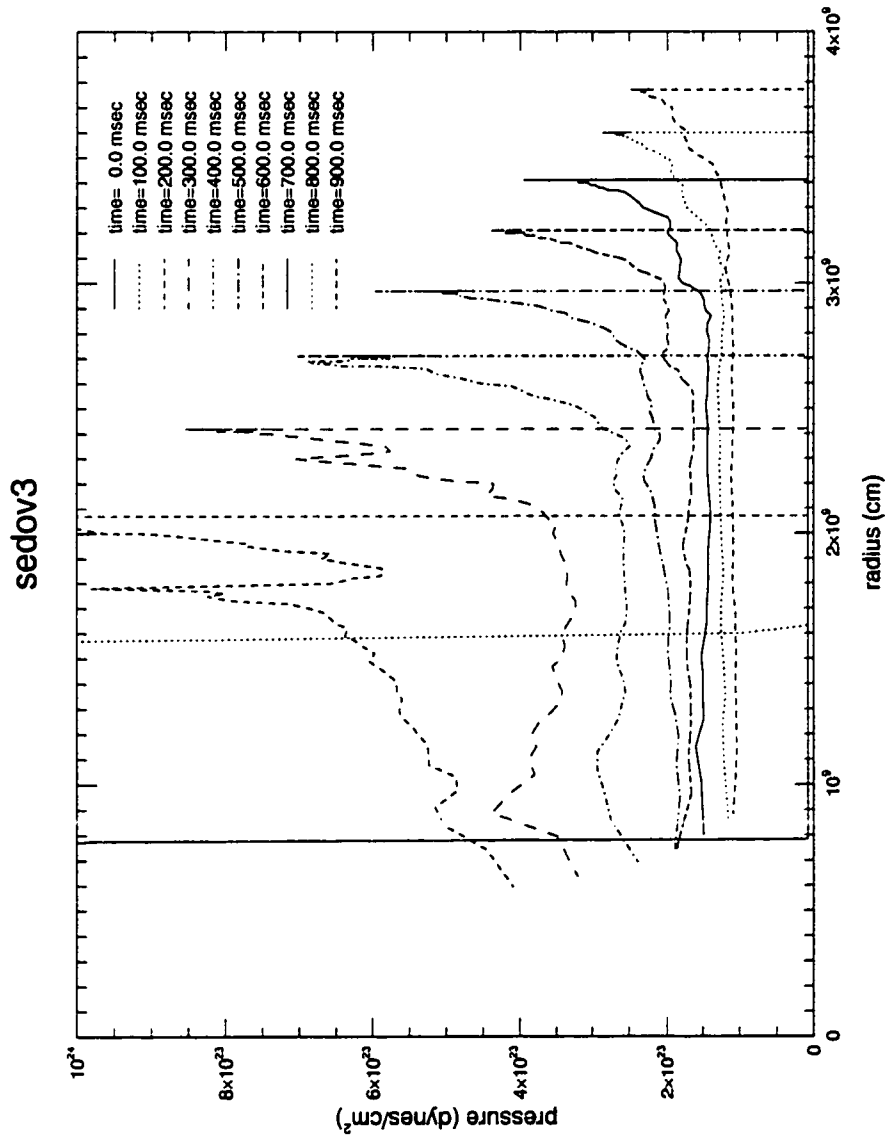


Figure 4.2: Sedov blast wave pressure evolution

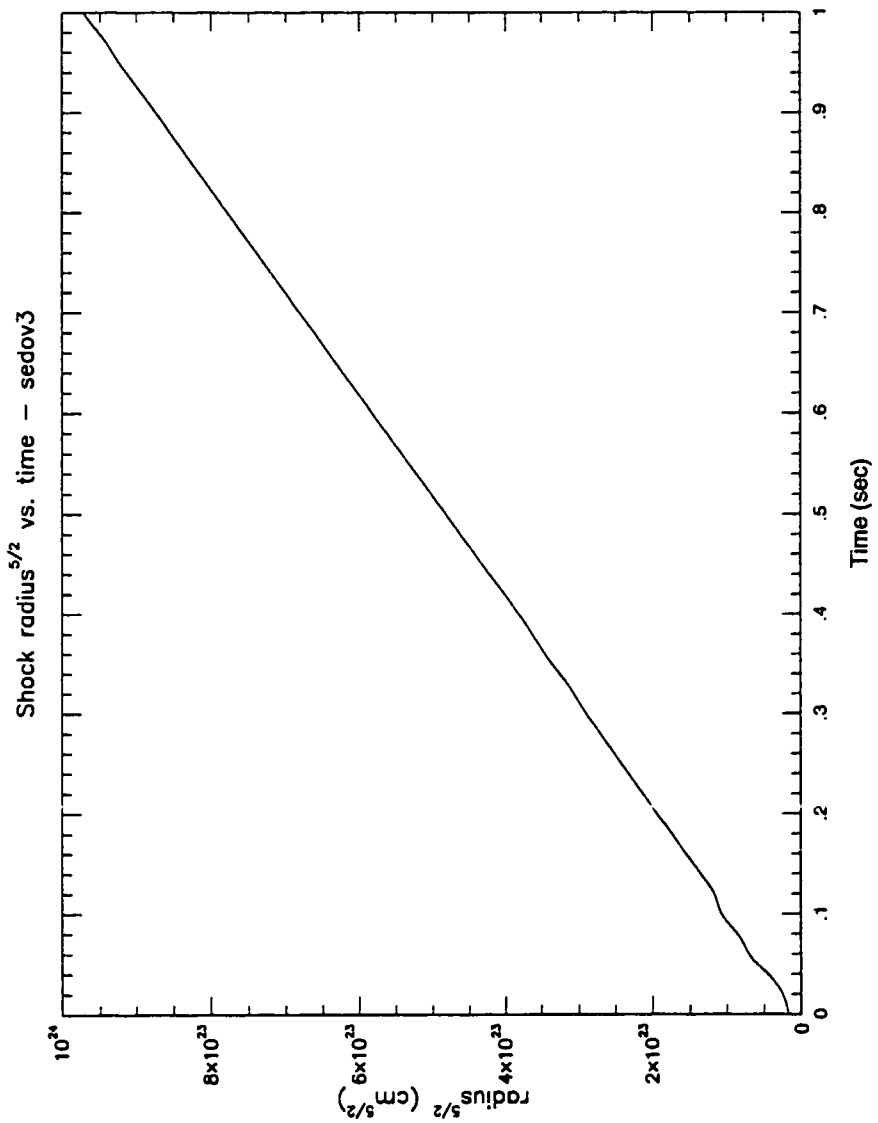


Figure 4.3: Sedov blast wave radius<sup>5/2</sup> versus time evolution

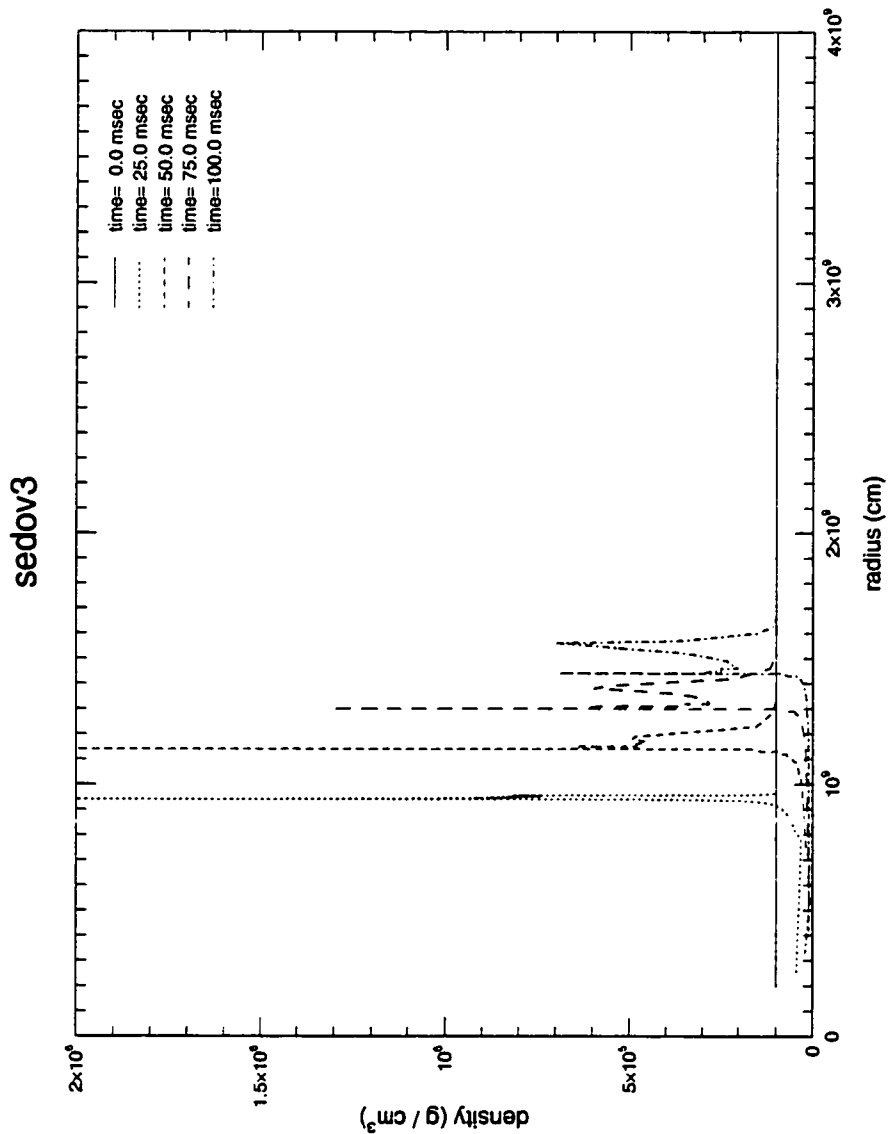


Figure 4.4: Sedov blast wave density transient evolution

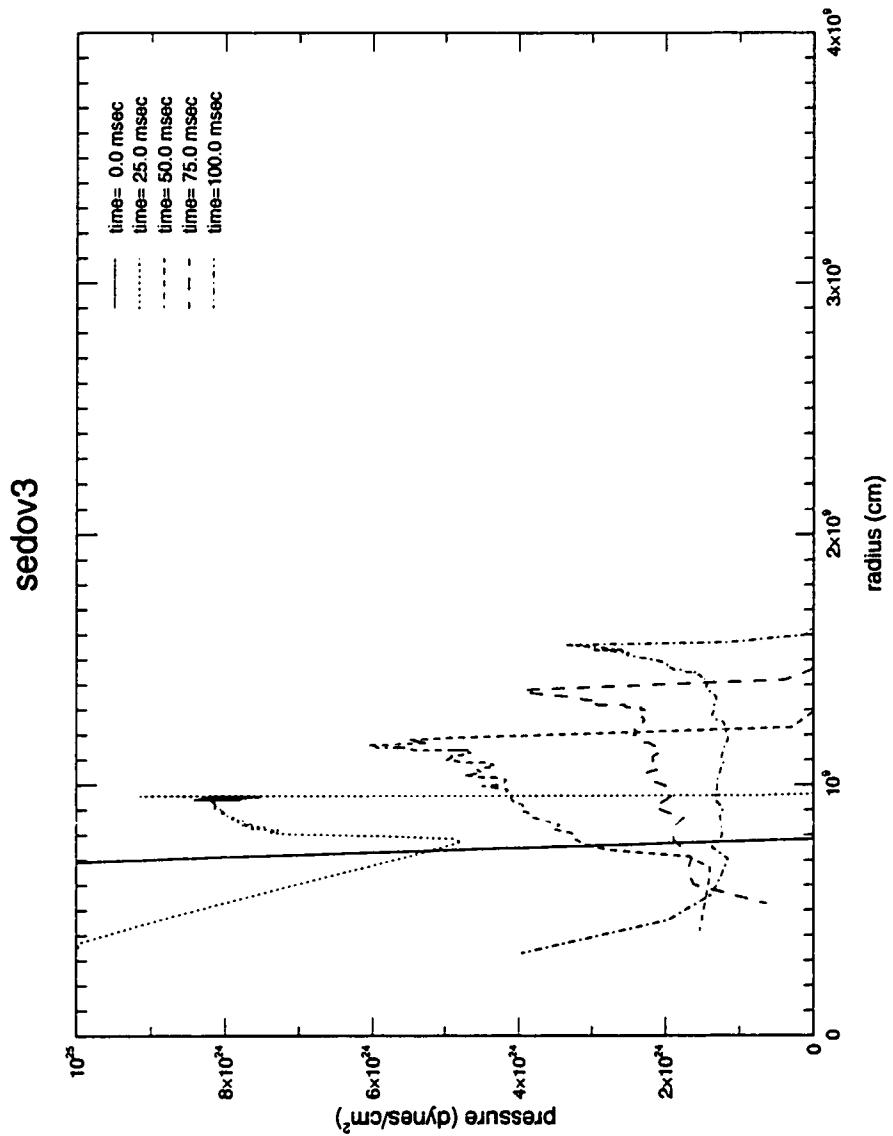


Figure 4.5: Sedov blast wave pressure transient evolution

after the scattering was turned off in the radiation zone is illustrated in figure 4.6. This test produces a neutrino front that moves forward at the speed of light, and illustrates the ability of the code to preserve the shape of a neutrino radiation front.

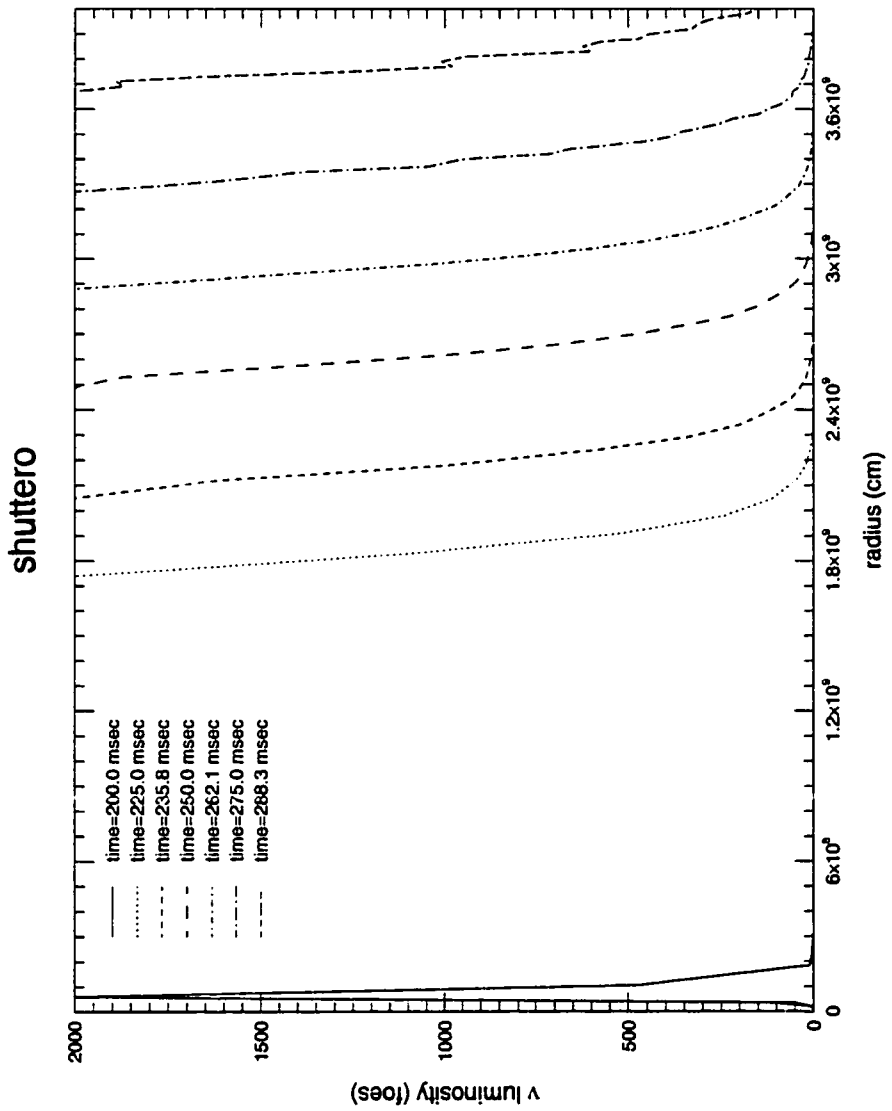


Figure 4.6: Neutrino propagation test

# Chapter 5

## Results and discussion

### 5.1 Model runs

Table 5.1 lists the models which were run. The model *ntest1* did not include neutrino transport and was intended to test the hydrodynamics of the code and to insure that an explosion was possible without neutrino losses taken into account. Because convection requires neutrino losses to create the initial negative entropy gradient, no models without neutrino losses but with convection were computed.

The models *test3* and *test3c* were run with electron neutrinos only. The *test3* model did not contain convection while *test3c* contained convection with the standard convection parameters, as defined in the previous chapter (asymmetry parameter =0.1, all other parameter=1.0, no salt finger mixing). Although physically unrealistic, these models were intended to calculate the impact on different neutrino heating assumptions on the behavior of the model.

The models *tau3* contained all neutrino species. Model *tau3* omitted

model name	$\nu$ -types	convection
ntest1	none	none
test3	$\nu_e$	none
test3c	$\nu_e$	standard parameters
tau3	all species	none
tau3c	all species	standard parameters
tau3ca	all species	convective braking
tau3ctp	all species	turbulent pressure
tau3ctpa	all species	turbulent pressure and convective braking
tau3nd	all species	neutrino advection

Table 5.1: List of model runs

convection and was intended as a control against which models with convection were to be compared. Model tau3c was a model with the standard parameters for convection described earlier. Model tau3ca contained an extra convective term in order to take into account, albeit in a crude fashion, for the mechanism of Burrows, Hayes, and Fryxell (1995) in which convection decreases the net infall velocity and therefore increases the “residence time” which material has to heat within the gain radius. Because non-electron neutrinos and convection were turned off before bounce, the characteristics of the infall phase in all of the models were identical. Bounce occurred 203 milliseconds after the start of the simulation, and the maximum central density was  $2.8 \times 10^{14}$  grams/cm<sup>3</sup>.

## 5.2 The non-convective models

Figures 5.1 to 5.14 present the behavior of model tau3. The behavior of the shock radius versus time is illustrated in figure 5.1. After bounce a shock wave is formed and moves outward. Over the course of the next 50 milliseconds, the shock moves from an initial radius of  $1 \times 10^6$  cm to a maximum radius of  $1 \times 10^7$

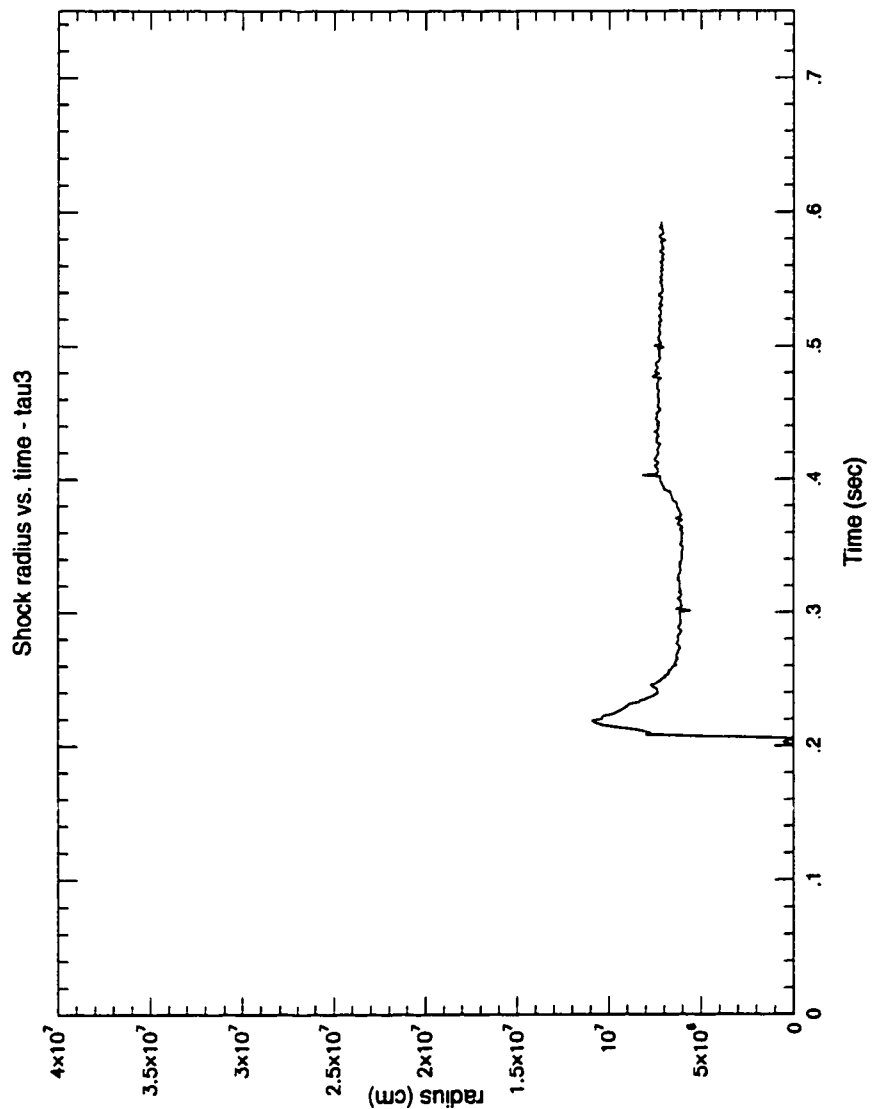


Figure 5.1: Shock radius versus time - Non-convective - All neutrino species

cm. The shock then retreats to a radius of a few times  $10^6$  cm. There the proto-neutron star continues to accrete material for the next several hundred milliseconds. There is no sign in the model of any explosion or indeed of any significant outward movement of the shock in radius space. This result is also expressed in the velocity evolution of the model (figure 5.26) which contains sharply negative velocities throughout the entire simulation.

Figures 5.3 through 5.6 illustrate the entropy evolution of the model, and figure 5.7 shows the evolution in  $Y_e$ . One characteristic of the post-shock entropy profile is that its profile in mass space appears very different than its profile in radius space. When plotted in mass space, there appears to be a very narrow spike of high entropy in the vicinity of the shock (figure 5.4). By contrast a plot versus either radius (figure 5.5) or log radius (figure 5.6) shows that the high entropy spike is actually a large volume behind the shock. This mass concentration is reflected in a plot of model density (figure 5.9) which illustrates that the density varies by seven orders of magnitude from on the order of  $10^7$  g/cm<sup>3</sup> in the immediate post shock area to the order of  $10^{14}$  g/cm<sup>3</sup> near the center of the shock. A plot of the radius versus mass profile (figure 5.8 also illustrates this mass concentration. From the profile, it can be seen how most of the mass of the proto-neutron star lies within  $10^6$  cm of the center even as the shock is an order of magnitude further out.

The entropy evolution can be divided into two phases. There is a “prompt shock phase” (figure 5.3) which lasts for 50 milliseconds after bounce during which the shock moves forward and then stalls. There is also a “stalling phase” (figure 5.4) which begins once the shock has reached quasi-equilibrium and extends, in the current calculation, several hundred of milliseconds until the end of the simulation.

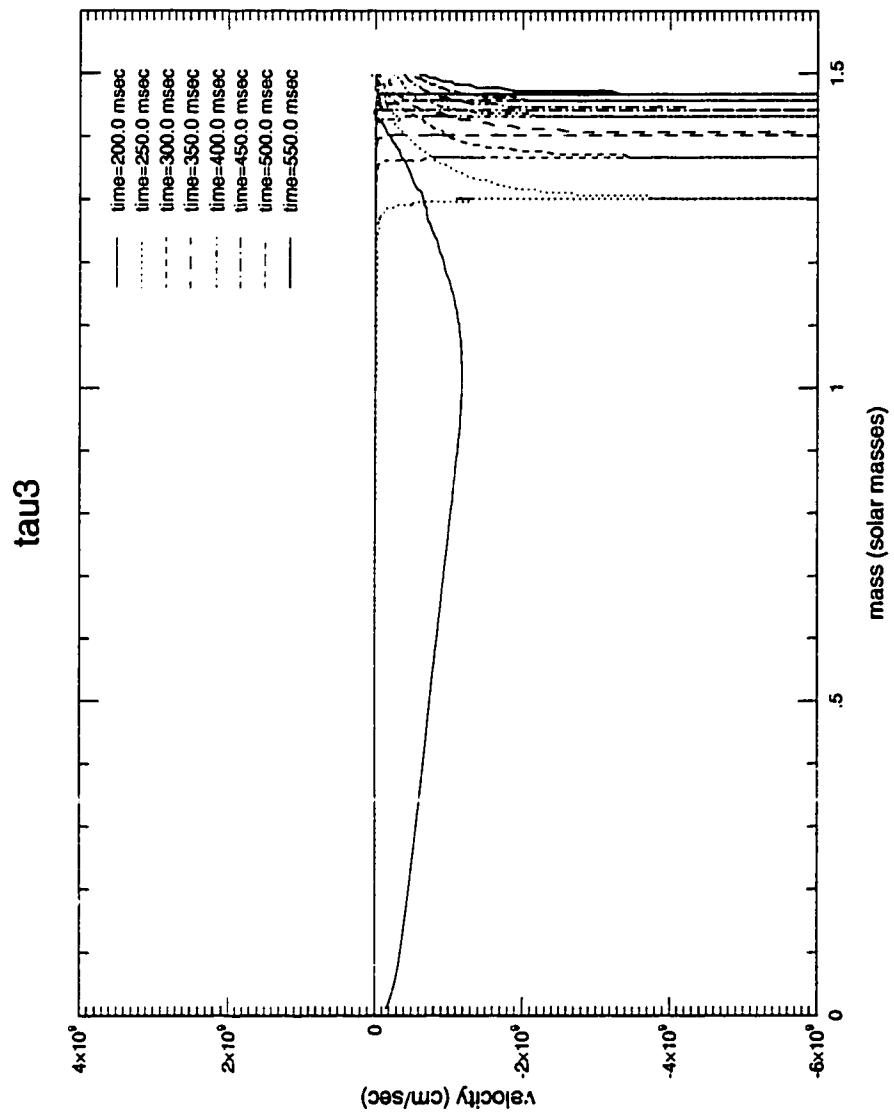


Figure 5.2: Velocity evolution - Non-convective - All neutrino species

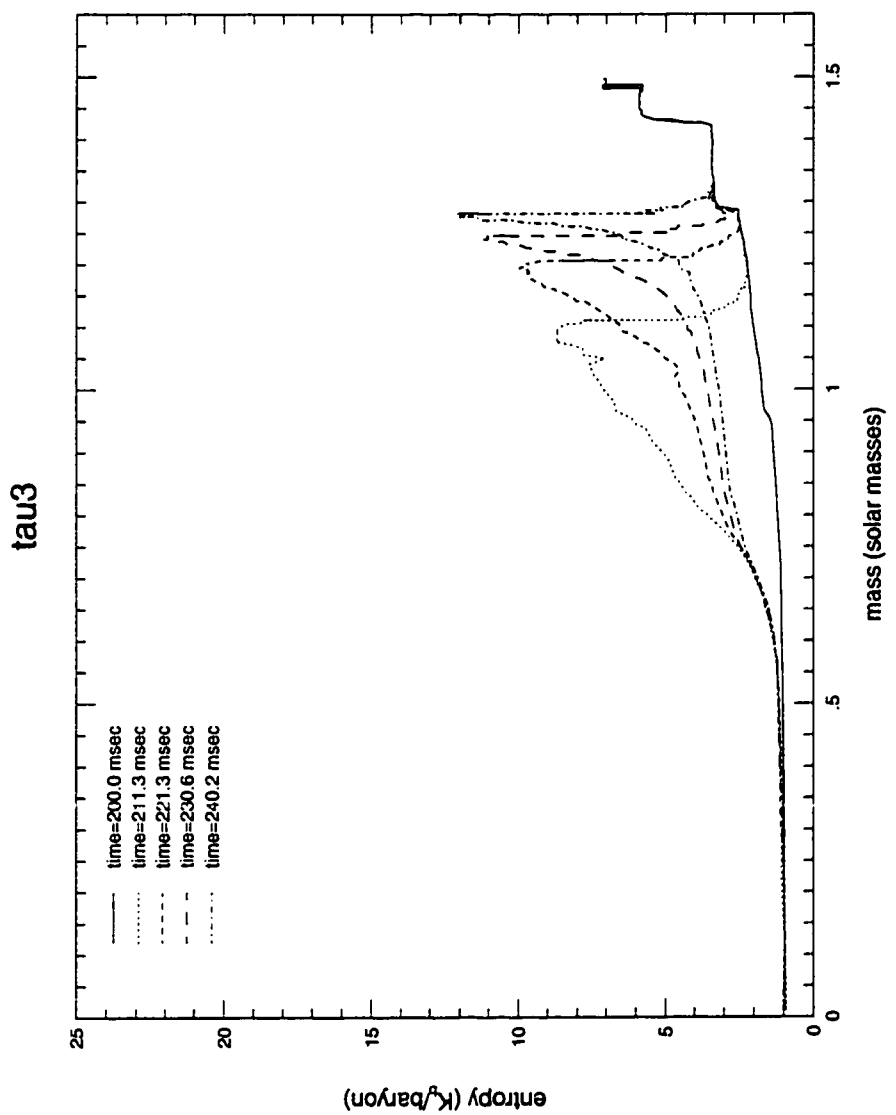


Figure 5.3: Early entropy evolution - Non-convective - All neutrino species

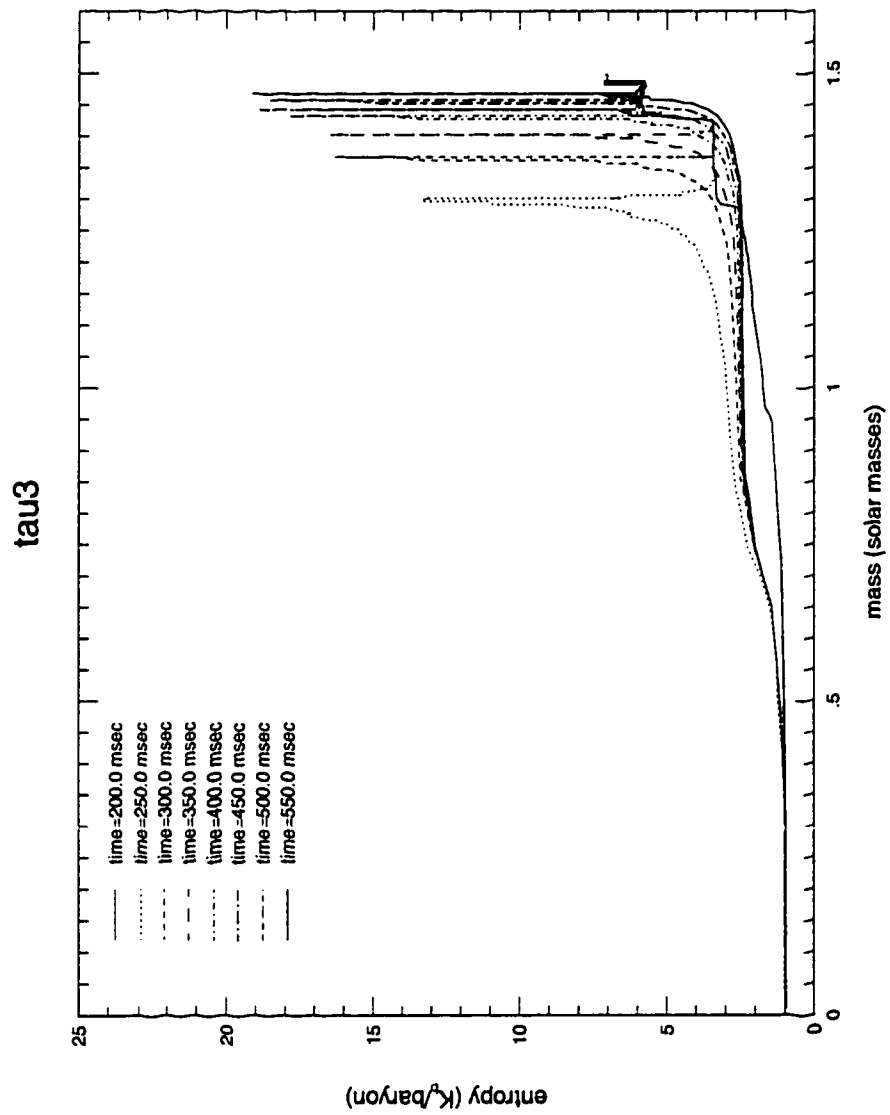


Figure 5.4: Entropy versus mass evolution - Non-convective - All neutrino species

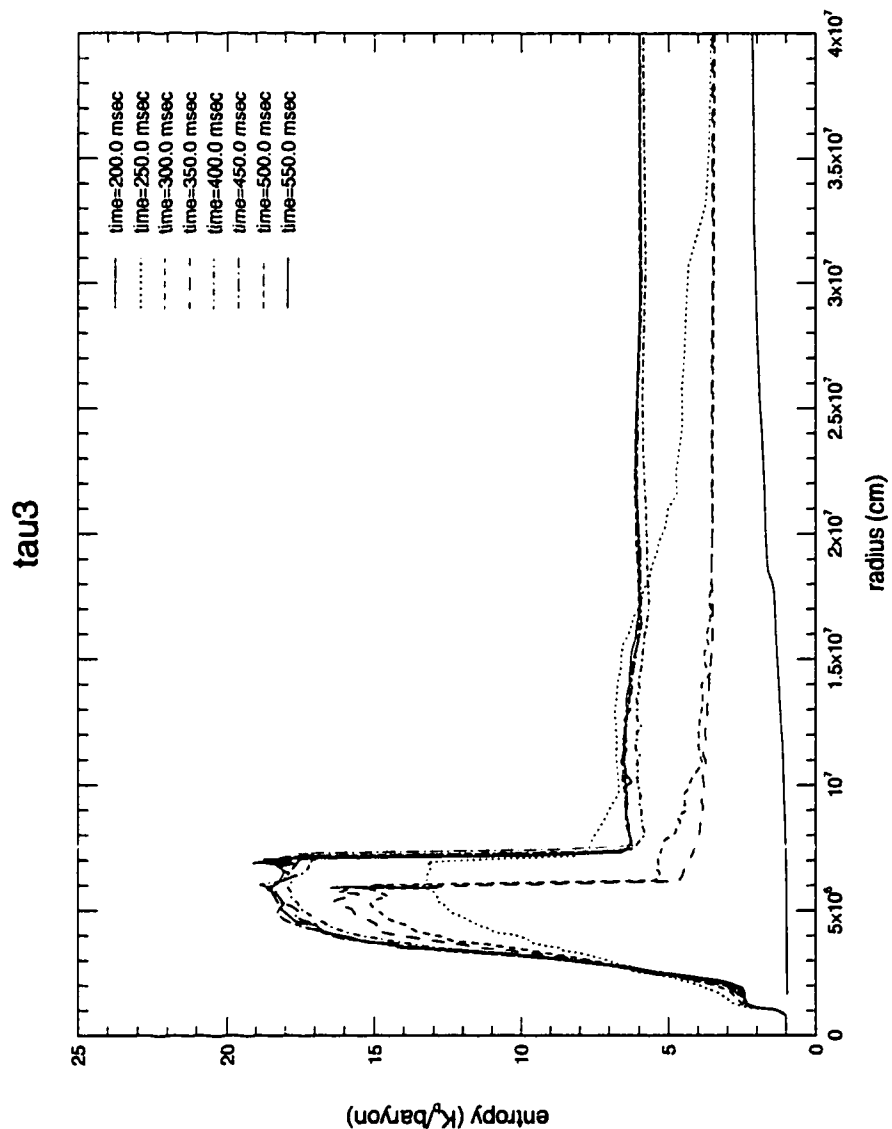


Figure 5.5: Entropy versus radius evolution - Non-convective - All neutrino species

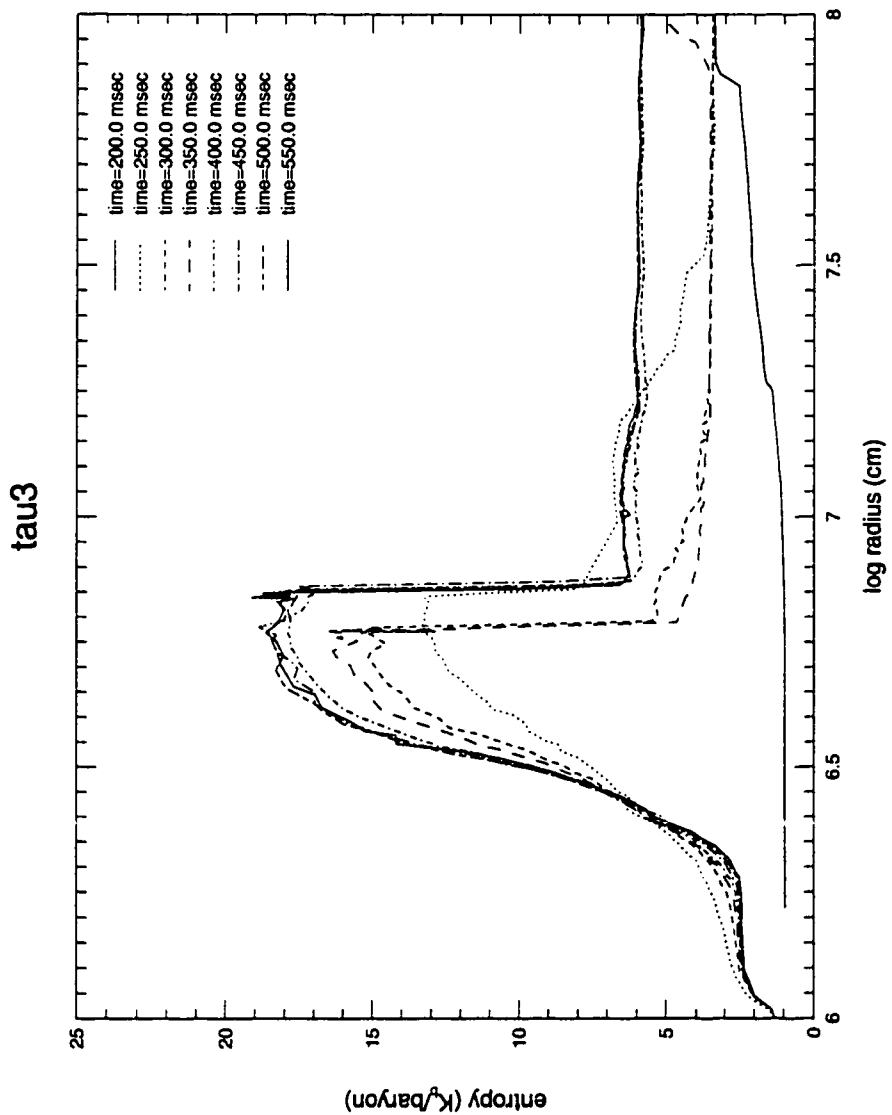


Figure 5.6: Entropy versus log radius evolution - Non-convective - All neutrino species

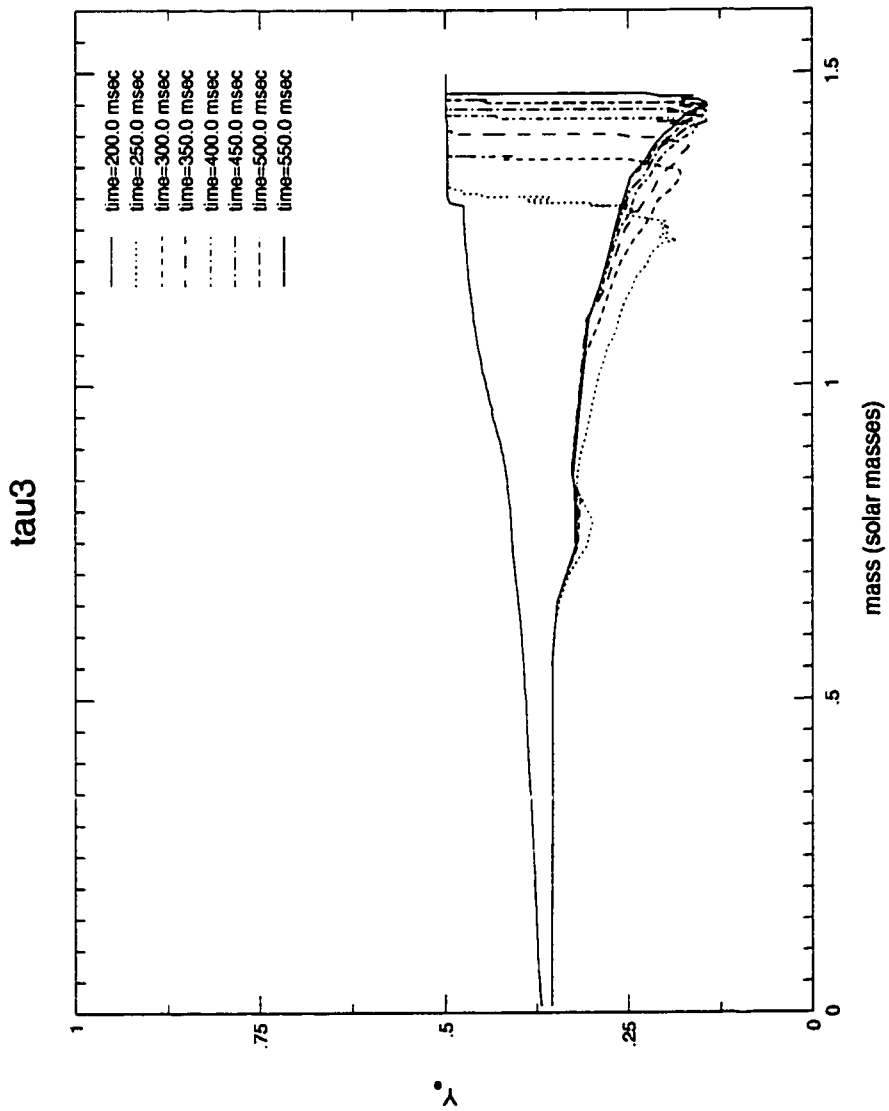


Figure 5.7:  $Y_e$  evolution - Non-convective - All neutrino species

During the prompt shock phase, there is considerable evolution of the entropy profile as the profile is flattened in the inner regions of the proto-neutron star and becomes sharply peaked near the shock. The behavior of the entropy profile in this model is broadly consistent with the models of Janka and Mueller (1996) and Burrows et al. (1995), in which the initial entropy peak disappears over a time scale of several milliseconds, and a second peak with a maximum entropy of 12 to 15 appears near the shock. The plots in radius space are similar to those of Mezzacappa et al. (1998).

The neutrino heating and cooling curves (figures 5.10 and 5.11) are also broadly consistent with those of Mezzacappa et al. (1998) with a loss region between the radii of  $3 \times 10^6 \text{ cm}$  and  $6 \times 10^6 \text{ cm}$  and a gain region extending from that radius to the shock. In the plots there is a positive spike at approximately  $2.5 \times 10^6 \text{ cm}$ . This spike is an artifact which exists at the inner boundary of the location at which  $\mu$  and  $\tau$  neutrinos are calculated and is not believed to affect the model calculation.

Although there is a neutrino heating region behind the shock, it is believed that the source of the post-shock entropy peak is not the thermodynamic transfer of energy, but rather a hydrodynamic effect. The neutrino energy losses cause cooling of the post-shock region which results in the contraction of the region. This compaction allows the shock infall velocity to increase thereby creating higher shock heating. It is shock heating rather than neutrino heating which produces the post shock entropy spike.

Another piece of evidence that the heating spike behind the shock is hydrodynamic and not radiative in nature comes from the temperature profile of the model. As the proto-neutron star evolves, a small but noticeable temperature inversion occurs at about  $2 \times 10^7 \text{ cm}$  (figure 5.12). This temperature

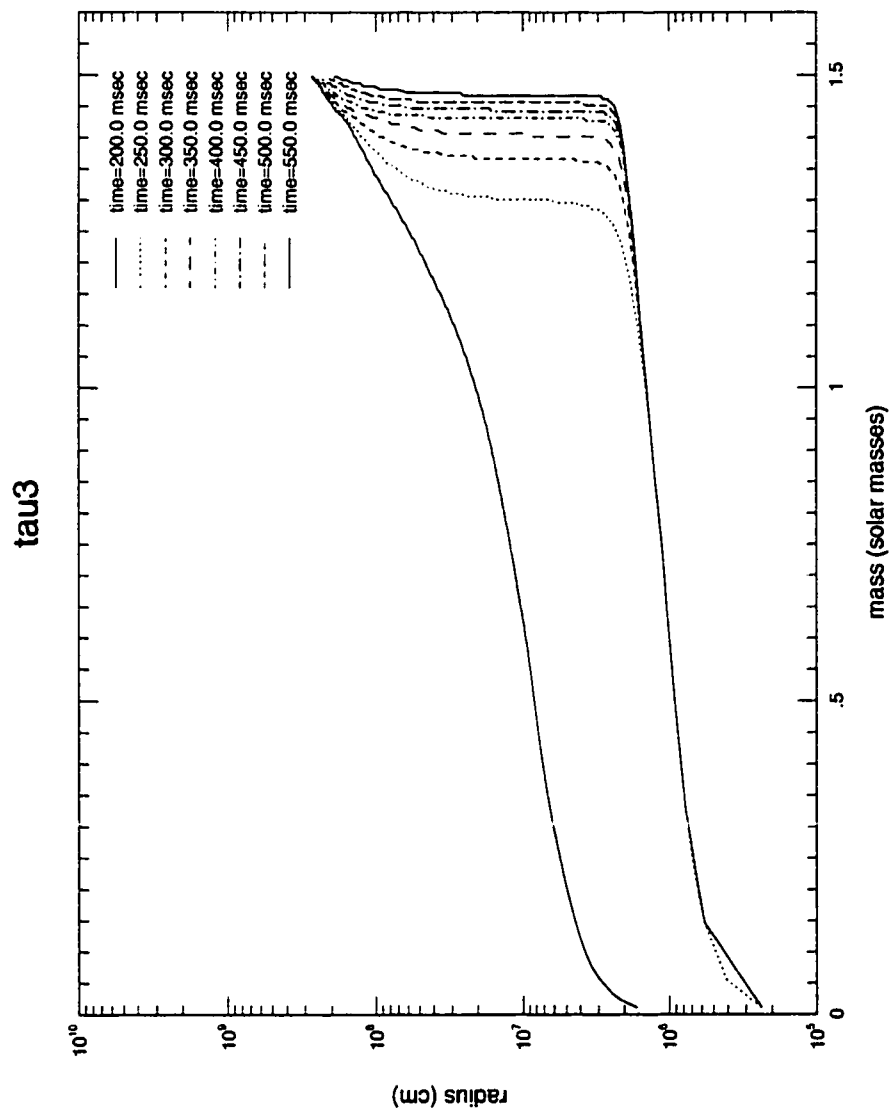


Figure 5.8: Radius versus mass evolution - Non-convective - All neutrino species

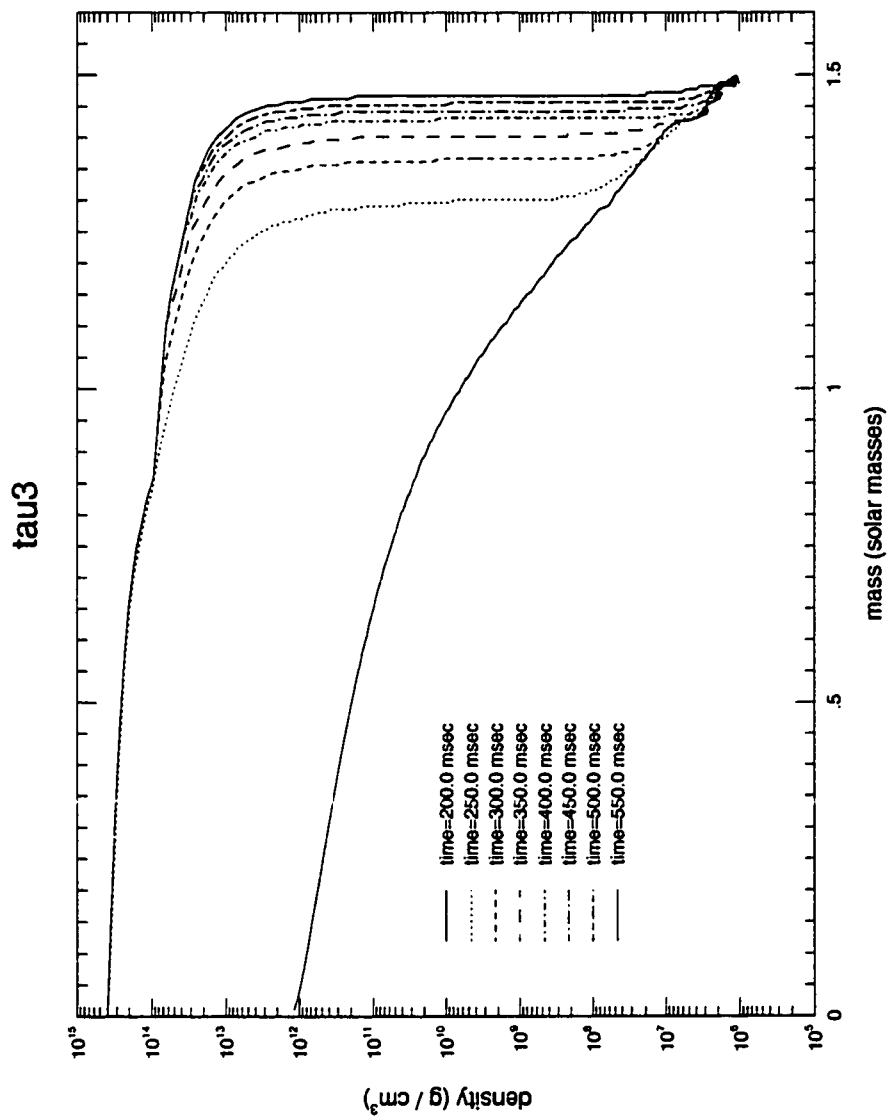


Figure 5.9: Density evolution - Non-convective - All neutrino species

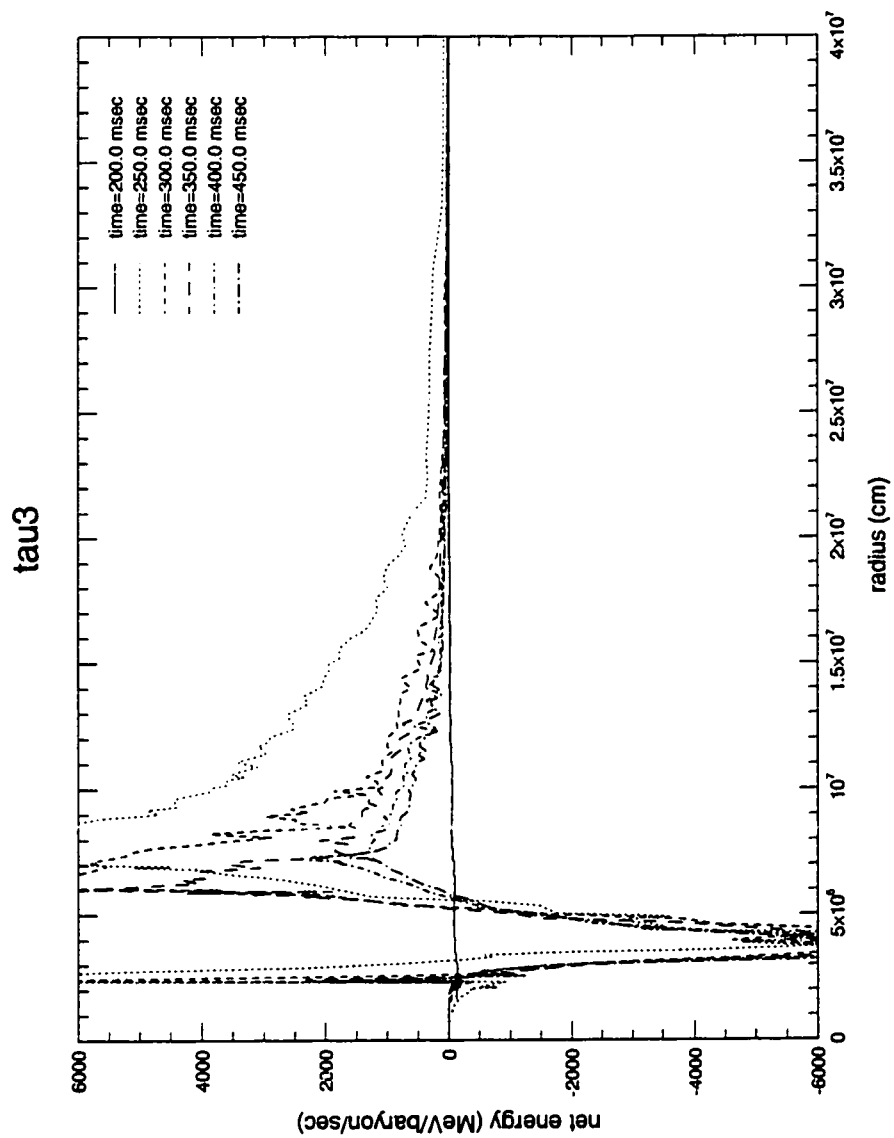


Figure 5.10: Neutrino heating/cooling - Non-convective - All neutrino species

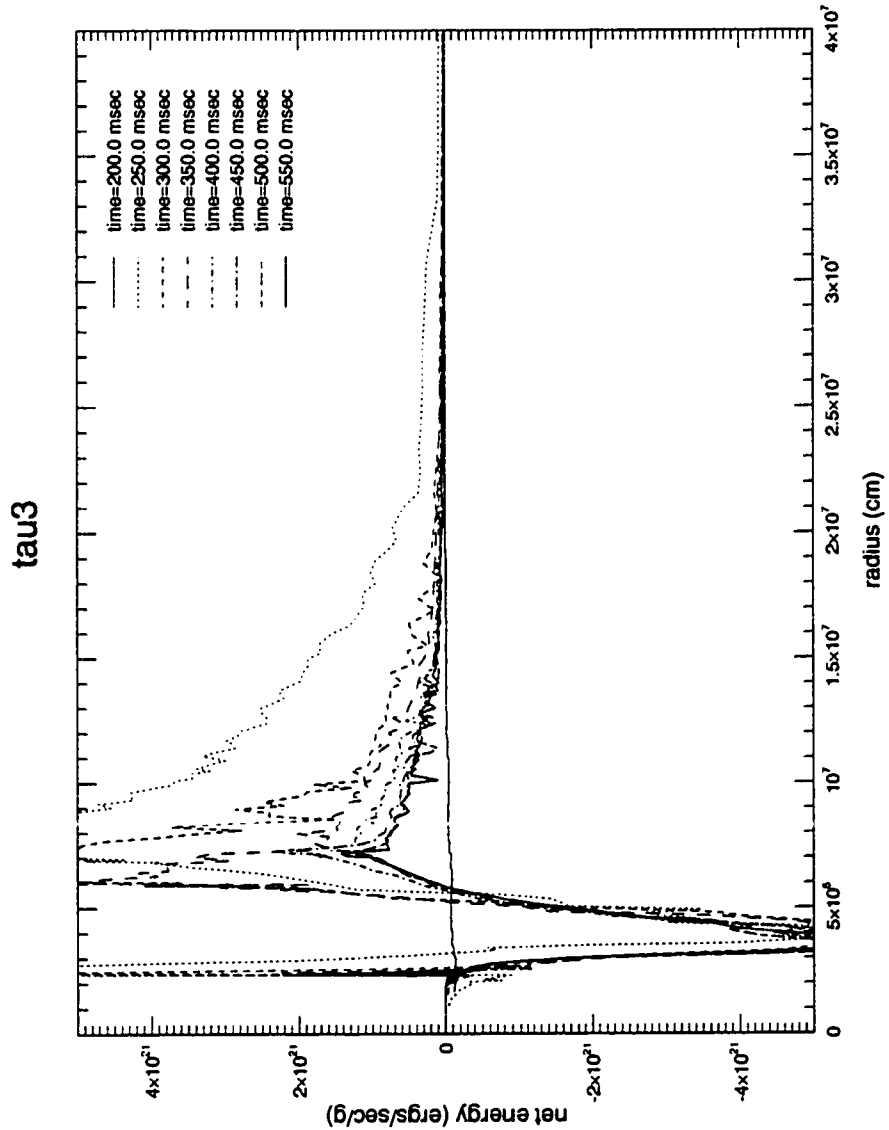


Figure 5.11: Neutrino heating/cooling - Non-convective - All neutrino species

inversion cannot be explained in terms of radiative transfer, which does not transfer energy from low temperatures to higher temperatures. Rather, it is believed that this temperature inversion is caused by shock heated material settling onto the inner core.

Because neutrino emission is a sensitive function of temperature, this temperature inversion has profound impact on the neutrino emission produced by model *tau3* (figures 5.13 to 5.14). Typically, one would expect  $\tau$  and  $\mu$  neutrinos to have the highest energies, anti-electron neutrinos to have lower energies, and electron neutrinos to have the lowest energies. (Janka 1993) This is due to differential scattering cross sections. Because  $\mu$  and  $\tau$  neutrinos are not affected by charged current reactions they therefore have the lowest cross section and decouple from matter at the deepest layers. Anti-electron neutrinos decouple from matter deeper than electron neutrinos because there are fewer protons than neutrons to undergo charge current scattering. The root mean square energy of the neutrino spectra is a monotonic function of the matter temperature at the region where the neutrinos decouple from the matter. Therefore, with a temperature gradient which is decreasing outward, one would expect  $\mu$  and  $\tau$  neutrinos to have the highest energies since they decouple from deeper and therefore hotter regions of the proto-neutron star.

However in the current models, the temperature inversion caused by shock heating reverses the sequence of energies. Because deeper layers in the neutrino decoupling region are cooler than outer layers, neutrino species which decouple from matter further in the proto-neutron star, have lower root mean square energy than the species which decouple in regions that are further out and therefore warmer. Hence, at late times, electron neutrinos have the highest energies, anti-electron neutrinos have intermediate energies, and  $\tau$  neutrinos

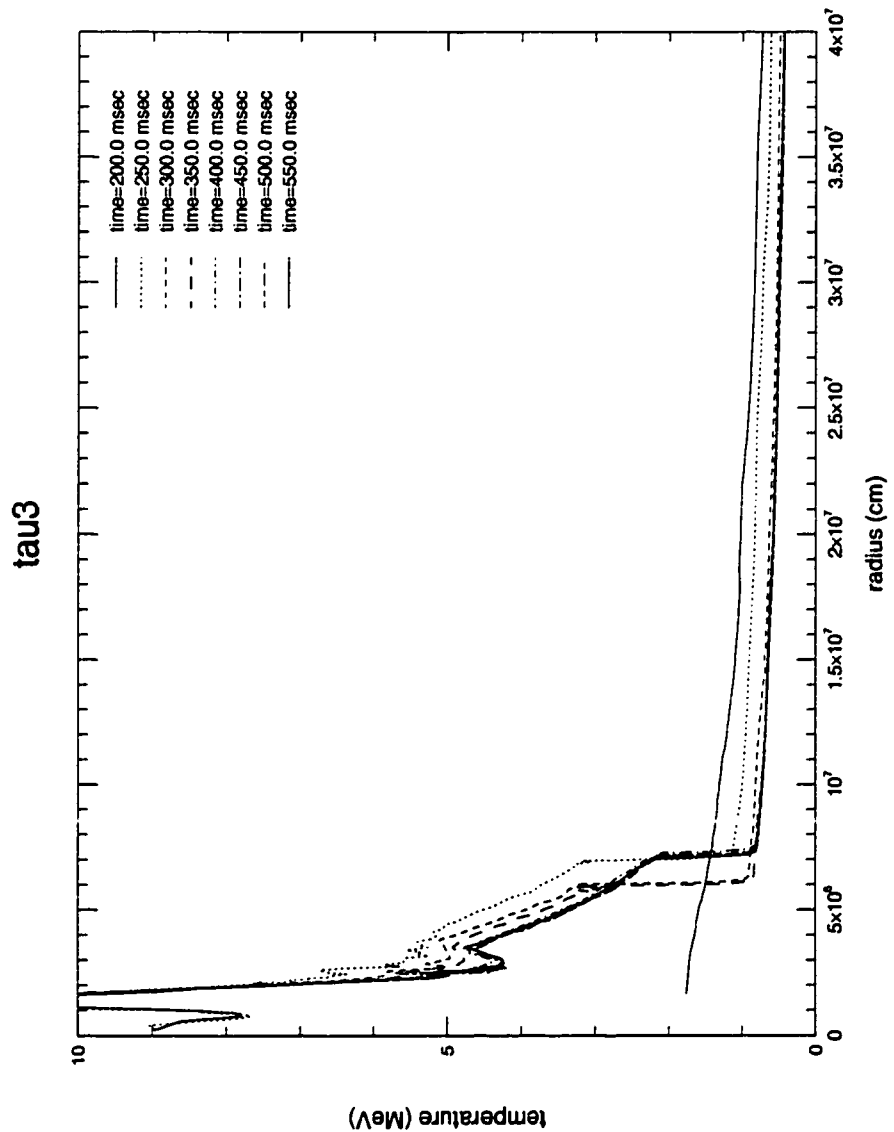


Figure 5.12: Temperature - Non-convective - All neutrino species

have the lowest energies. This interpretation is supported by the observation that the order of energies reverse shortly after bounce, as the temperature inversion forms (figure 5.13).

### 5.3 Comparison with electron neutrino only models

Insight into the dynamics of the explosion can be gained by comparing the models with all species of neutrinos with model *test3* which contains electron neutrinos only. Although this case is physically unrealistic, examining the behavior of this model helps in understanding the dynamics of the supernova problem.

One commonality between the models with all neutrino species and the models in which some of the species are suppressed is the division between a prompt shock phase lasting a few milliseconds and a late heating phase which may last for hundreds of milliseconds. As with the models with all species, most of the evolution in entropy profile occurs in the prompt shock phase, and there is little change in the entropy profiles in the late heating phase. Another similarity is the lack of anything that may be a sign of a delayed explosion.

A plot of the shock radius (figure 5.16) shows the shock stalling at  $3 \times 10^7$  cm in model *test3* which is considerably higher than the stall radius in model *tau3*. At about 600 milliseconds into the simulation, there is a sudden movement outward of the shock. This is caused by the edge of the iron core falling through the shock, and the accretion of low density silicon material. That this does not produce an explosion can be seen in a velocity plot (figure

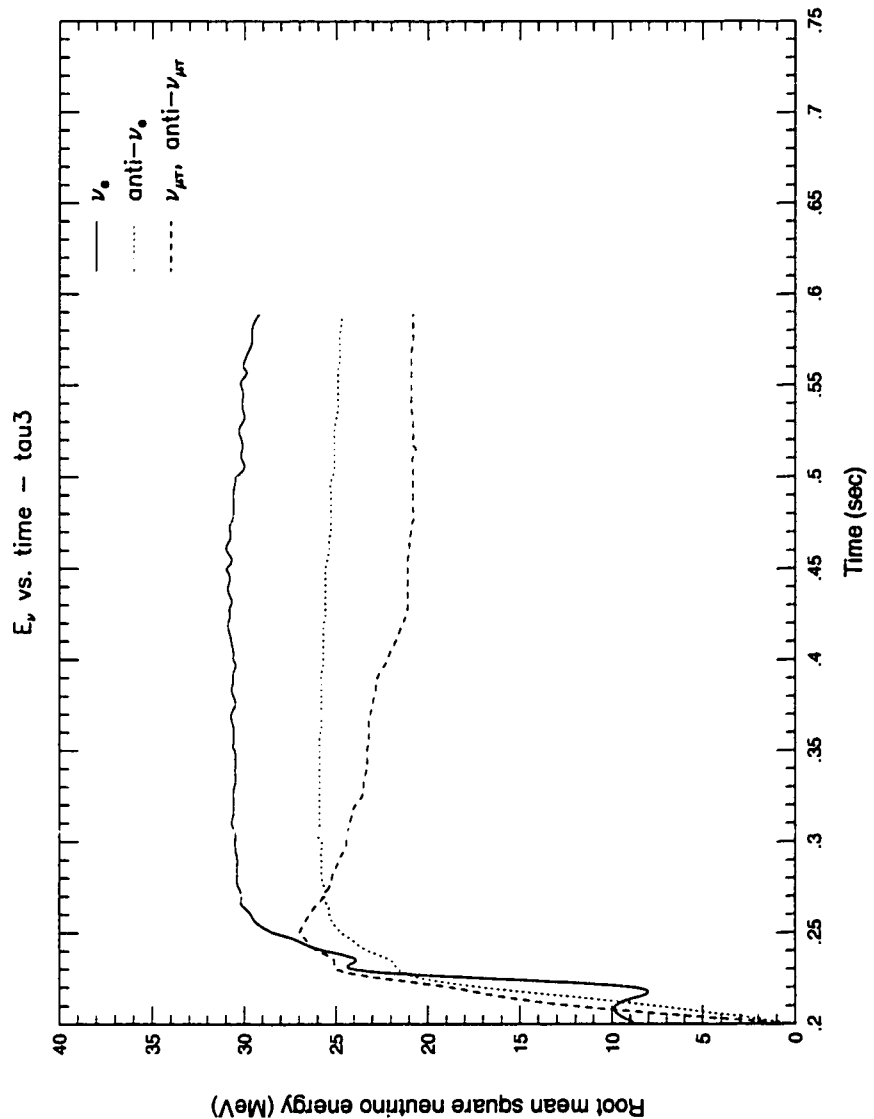


Figure 5.13: Neutrino energy versus time - Non-convective - All neutrino species

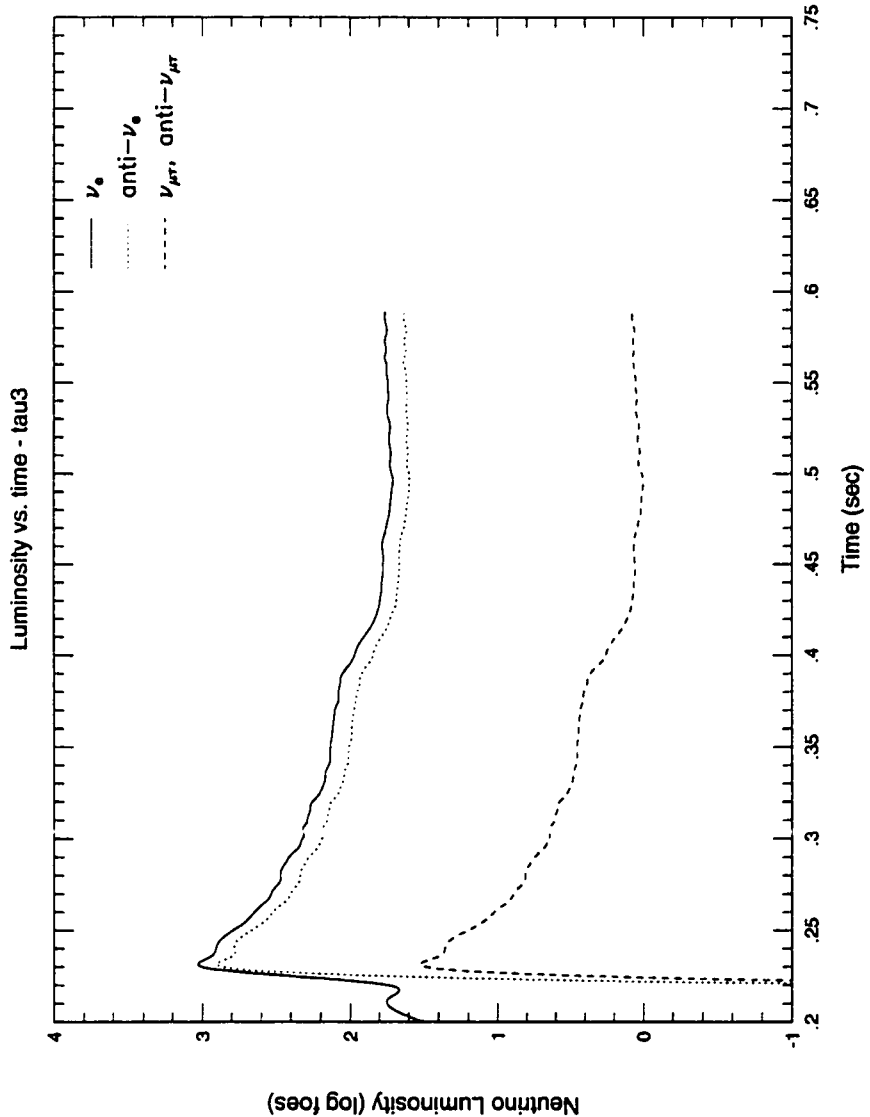


Figure 5.14: Neutrino luminosity versus time - Non-convective - All neutrino species

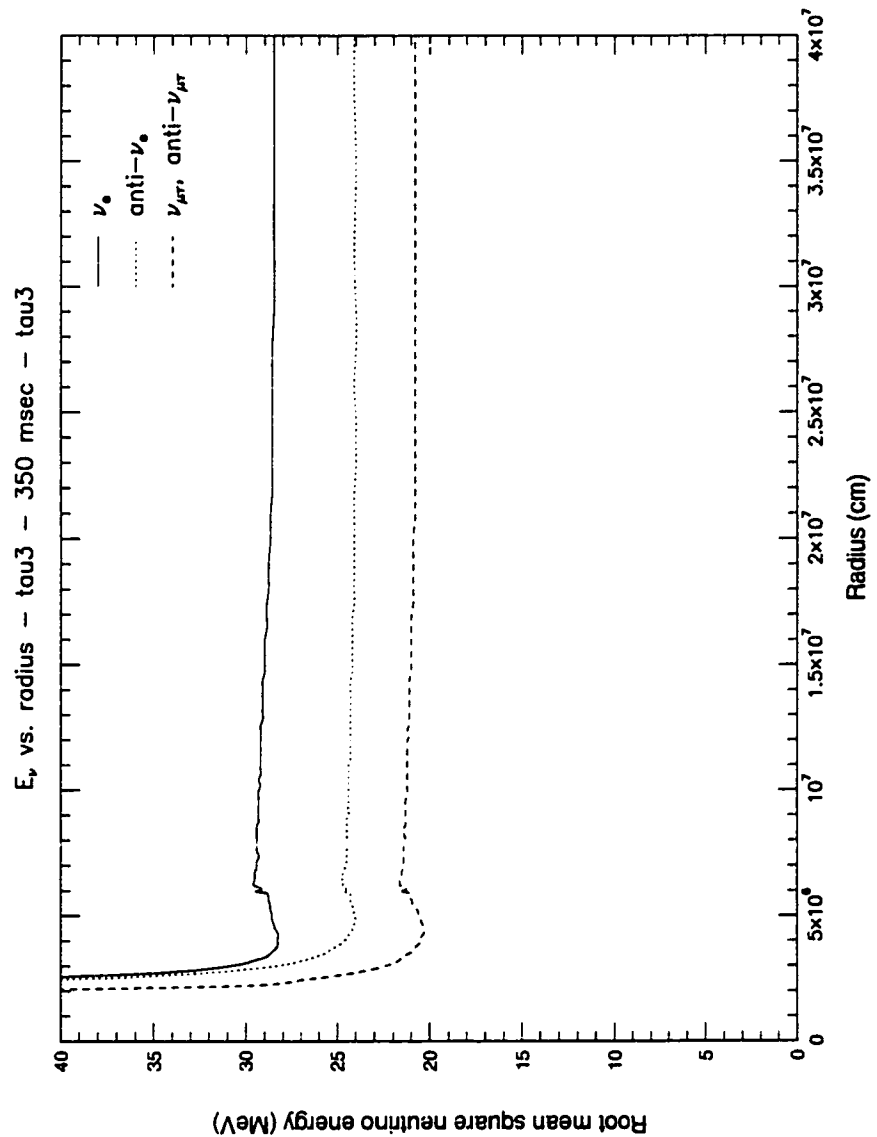


Figure 5.15: Neutrino energy versus radius - Non-convective - All neutrino species

5.17) which shows that the post shock velocities remain zero.

Another difference is that in the electron neutrino only case there is no flattening of the original entropy peak and that a spike does not form in the immediate post shock region (figure 5.18; compare to 5.4). Plotting the entropy in radius space and velocity curves reveals further differences. The post-shock region for the electron neutrino only case is considerably less compact than for the case where all of the neutrino species are included. The differences between models *test3* and *tau3* more clearly presented in (figure 5.22) which compares the models in terms of mass space and (figure 5.23) which compares the models in radius space. These figures represent conditions 50 milliseconds after bounce. At this time, the prompt shock phase evolution is complete, and the shock is entering the stalling phase. In the plot with respect to mass space (figure 5.22 ) one can see that the entropy peak which lies between 0.8 and 1.2 solar masses in *test3* has disappeared in the corresponding region of model *tau3*. Furthermore, model *tau3* has developed an sharp entropy spike of a height of about 15 which lies within 0.1 solar masses of the shock.

In comparing entropy profiles with respect to radial space (figure 5.23) one sees large differences in the structure of model *tau3*. The first difference is that the volume behind the shock is considerably smaller for model *tau3*. Although the post-shock region contains roughly the same amount of mass in both models, the radius of the shock in model *tau3* is one-third the radius for model *test3*. This difference in compactness also extends to features within the proto-neutron star. In model *test3* the entropy peak lies between  $3 \times 10^6 \text{ cm}$  and  $1 \times 10^7 \text{ cm}$ . The corresponding region in model *tau3* lies within  $2 \times 10^6 \text{ cm}$ .

The source of these differences can be seen to arise from differences in neutrino heating and cooling (figures 5.24 and 5.25). In contrast to model

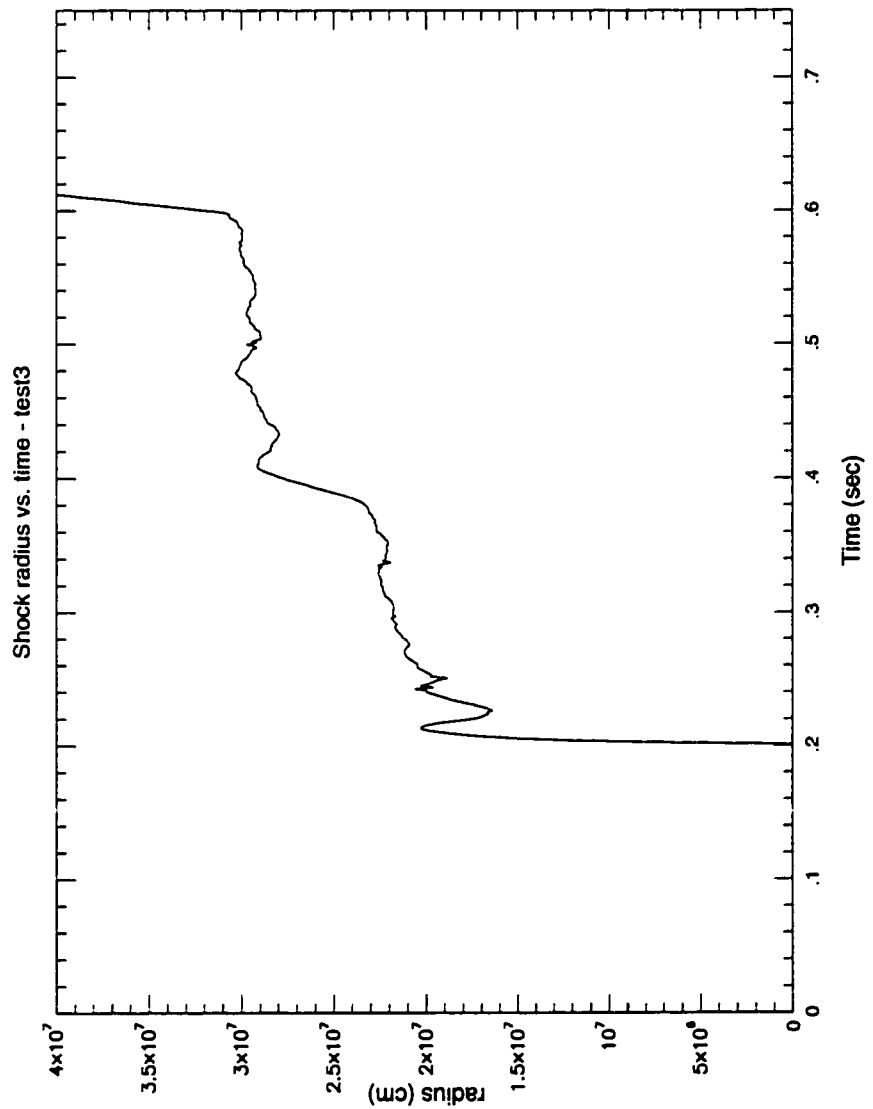


Figure 5.16: Shock versus time - Non-convective - Electron neutrino only

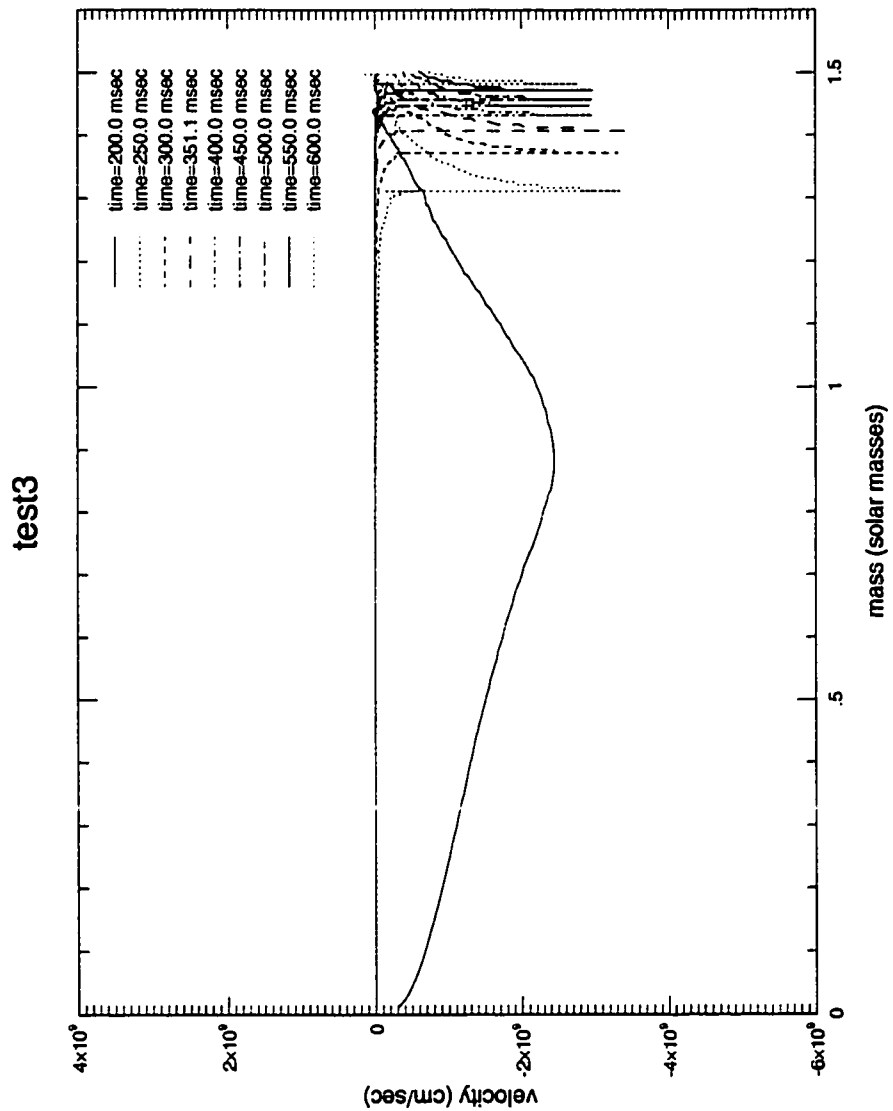


Figure 5.17: Velocity evolution - Non-convective - Electron neutrino only

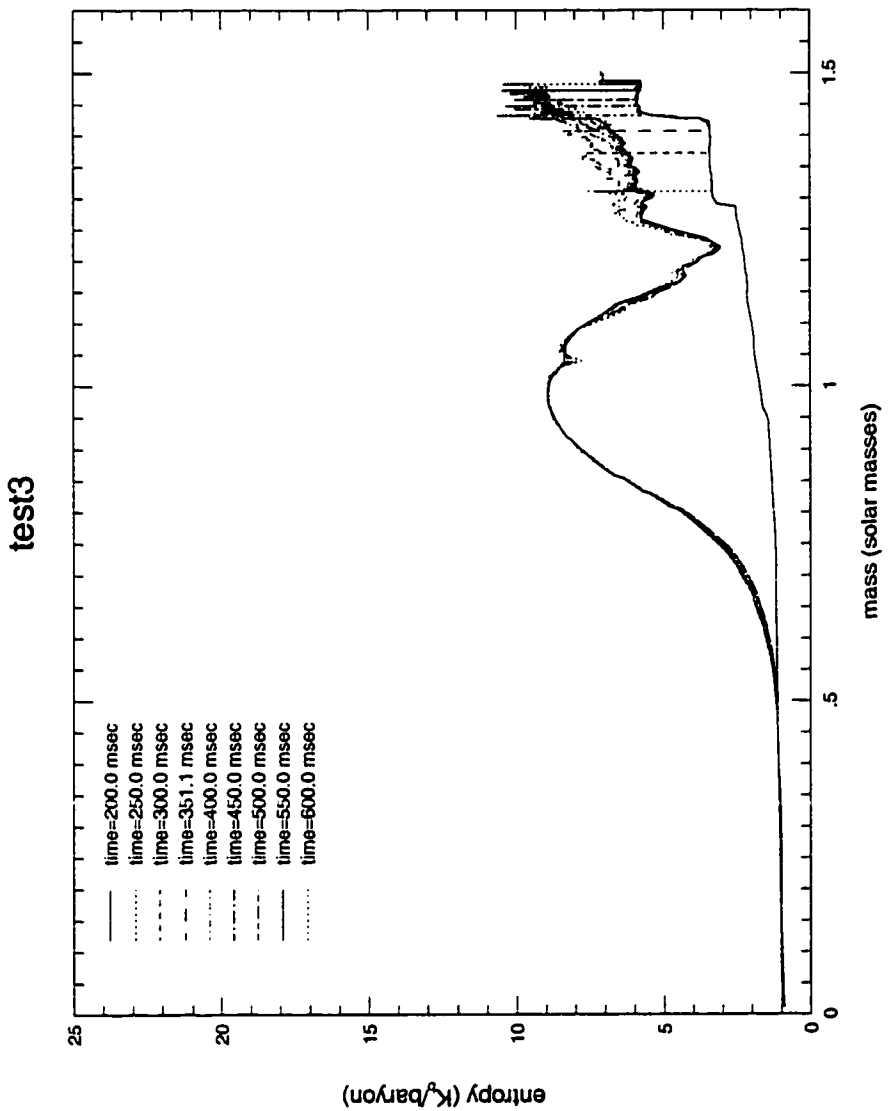


Figure 5.18: Entropy evolution - Non-convective - Electron neutrino only

test3

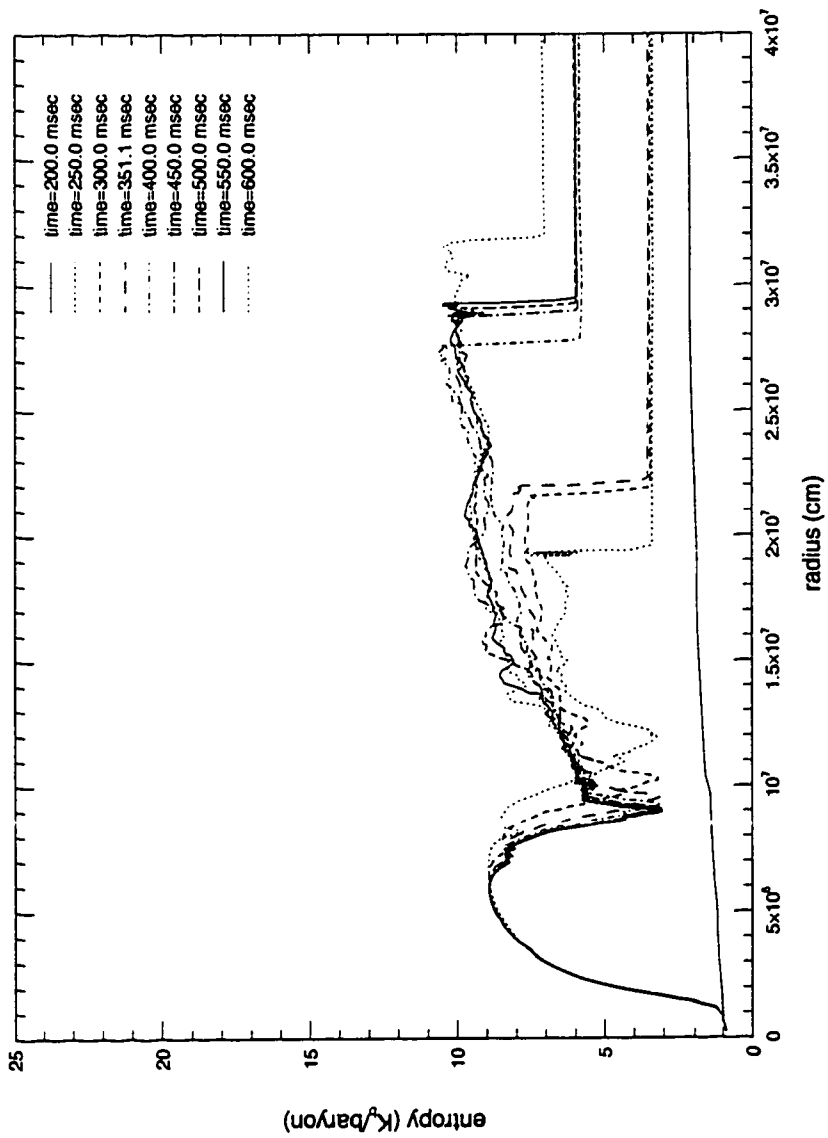


Figure 5.19: Entropy evolution - Non-convective - Electron neutrino only

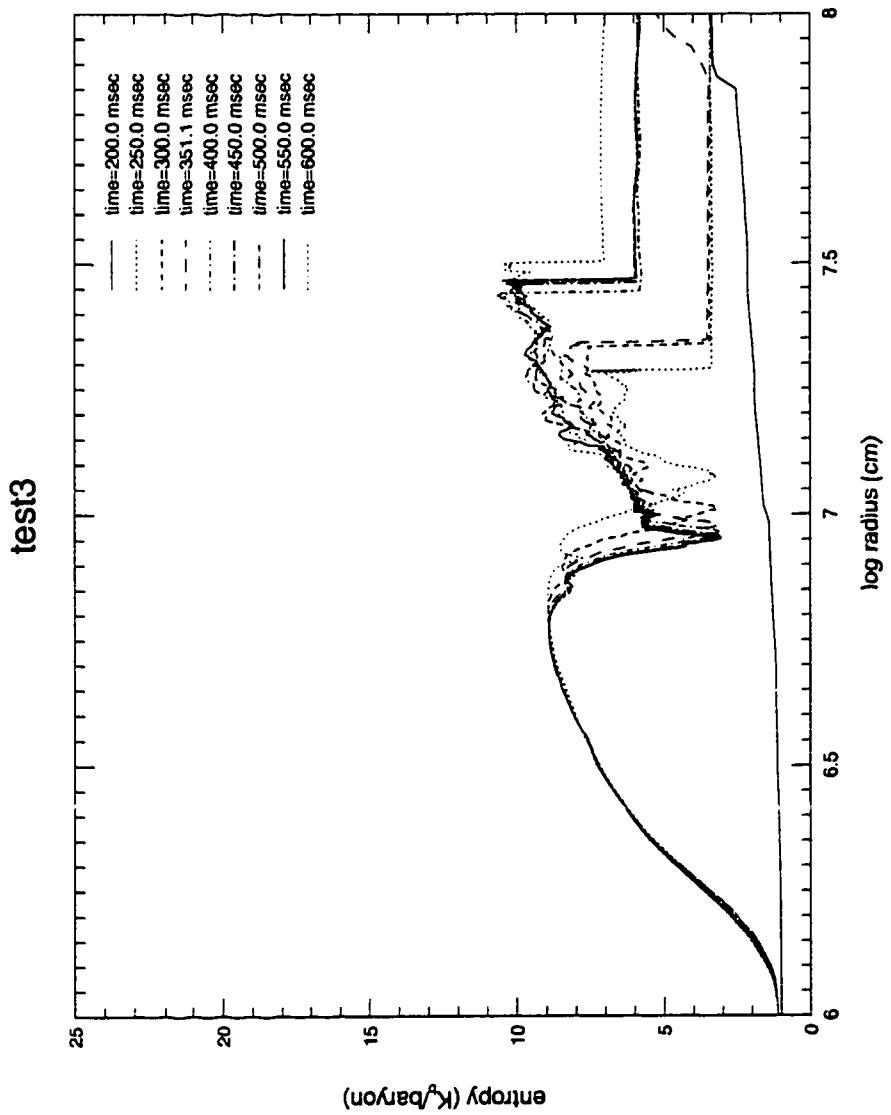


Figure 5.20: Entropy evolution - Non-convective - Electron neutrino only

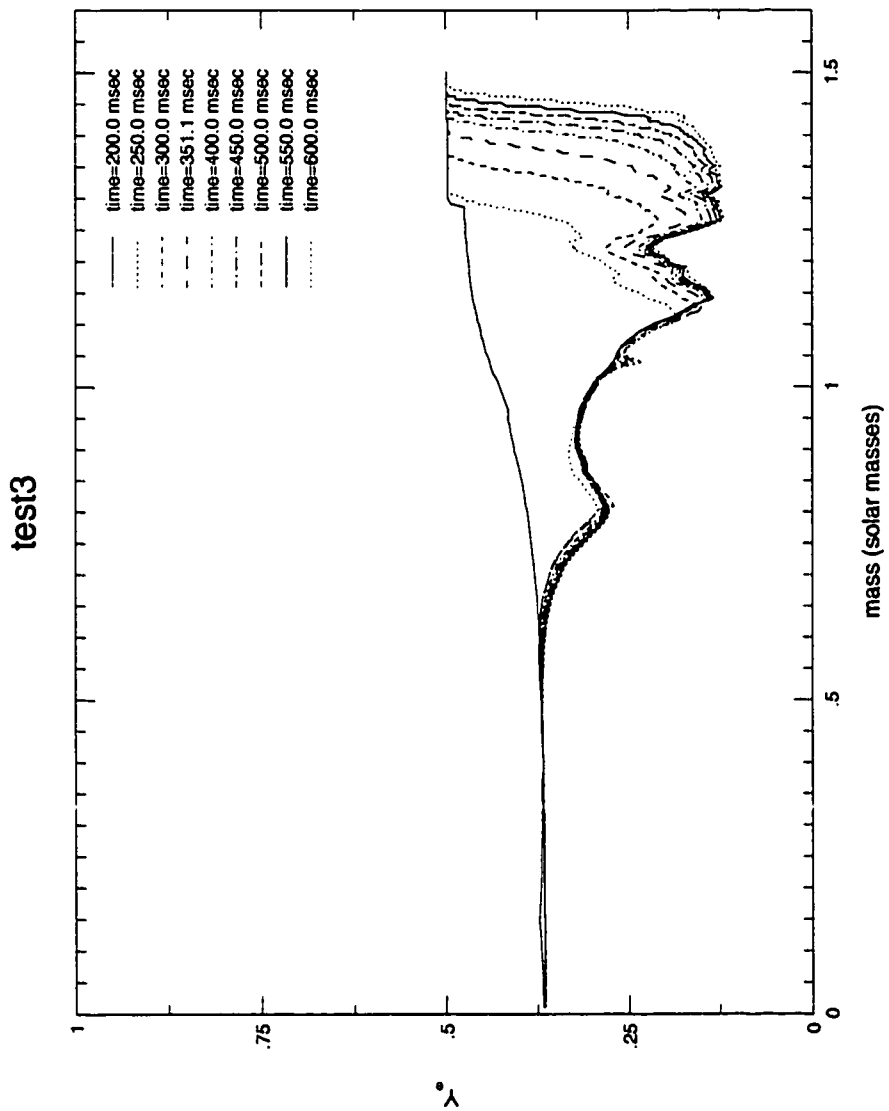


Figure 5.21:  $Y_e$  evolution - Non-convective - Electron neutrino only

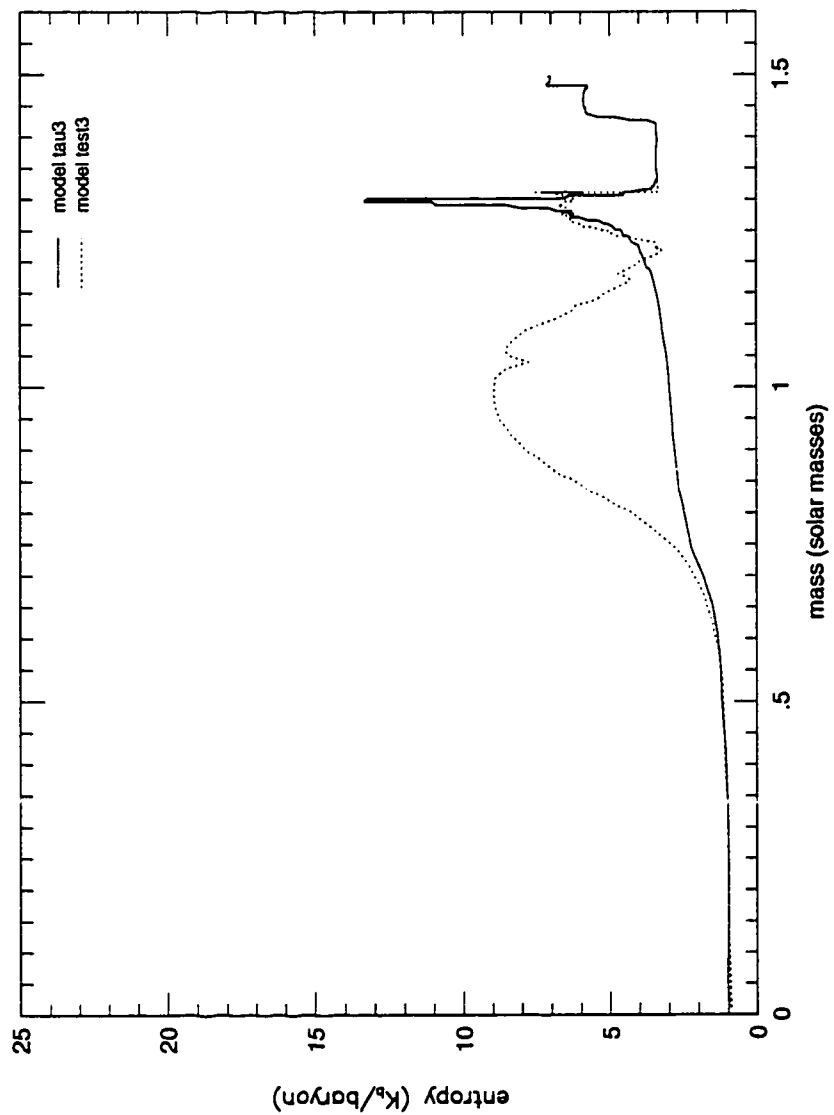


Figure 5.22: Comparison of entropy versus mass profiles

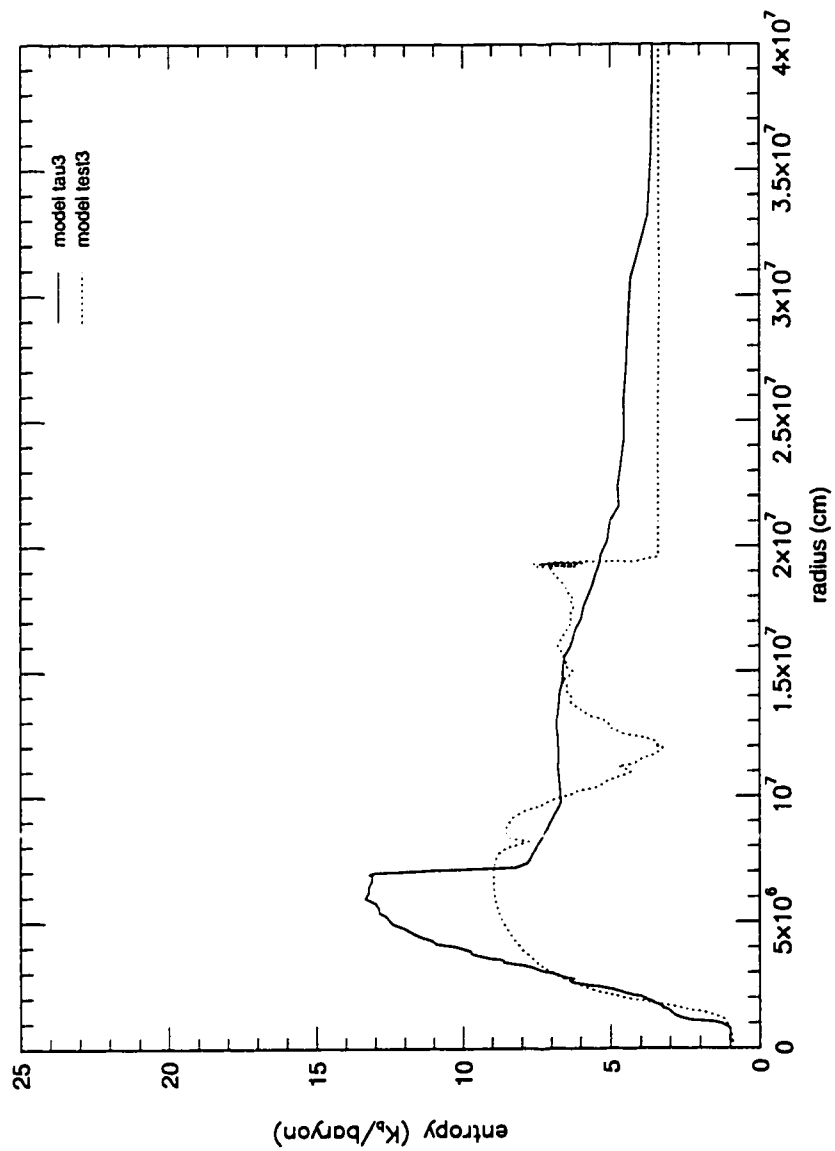


Figure 5.23: Comparison of entropy versus radius profiles

*tau3* which has sharp gain and loss regions (figures 5.10 and 5.11), *test3* has relatively small amounts of heating and cooling.

The high entropy spike within 0.1 solar masses of the shock in model *tau3* is a significant difference between the models *tau3* and *test3*. Although the spike occupies only a small amount of mass, it occupies a large volume. The presence of the spike has traditionally been taken as a sign of neutrino heating and of the transfer of energy from the interior of the proto-neutron star to the shock. However, in examining the velocity profiles of model *tau3* and *test3* (figures 5.2 and 5.26, it becomes apparent that an alternate explanation for the post-shock entropy spike is possible. Because the shock in model *tau3* stalls at a smaller radius than model *test3*, the pre-shock infall velocity in model *tau3* is higher by a factor of three. This velocity difference leads to increased shock heating and a higher entropy behind the shock.

The implication of this interpretation is that the post-shock entropy spike is an indication of shock failure rather than of shock success. Although there is neutrino heating in the entropy spike region, the spike arises as a consequence of the contraction of the proto-neutron star post-shock region in response to the loss of pressure support associated with neutrino losses. Even if there were no gain region, the high entropy spike would exist as a consequence of post-shock region contraction. That high entropy near the shock is associated with failing shocks rather than successful ones can be illustrated via a simple argument.

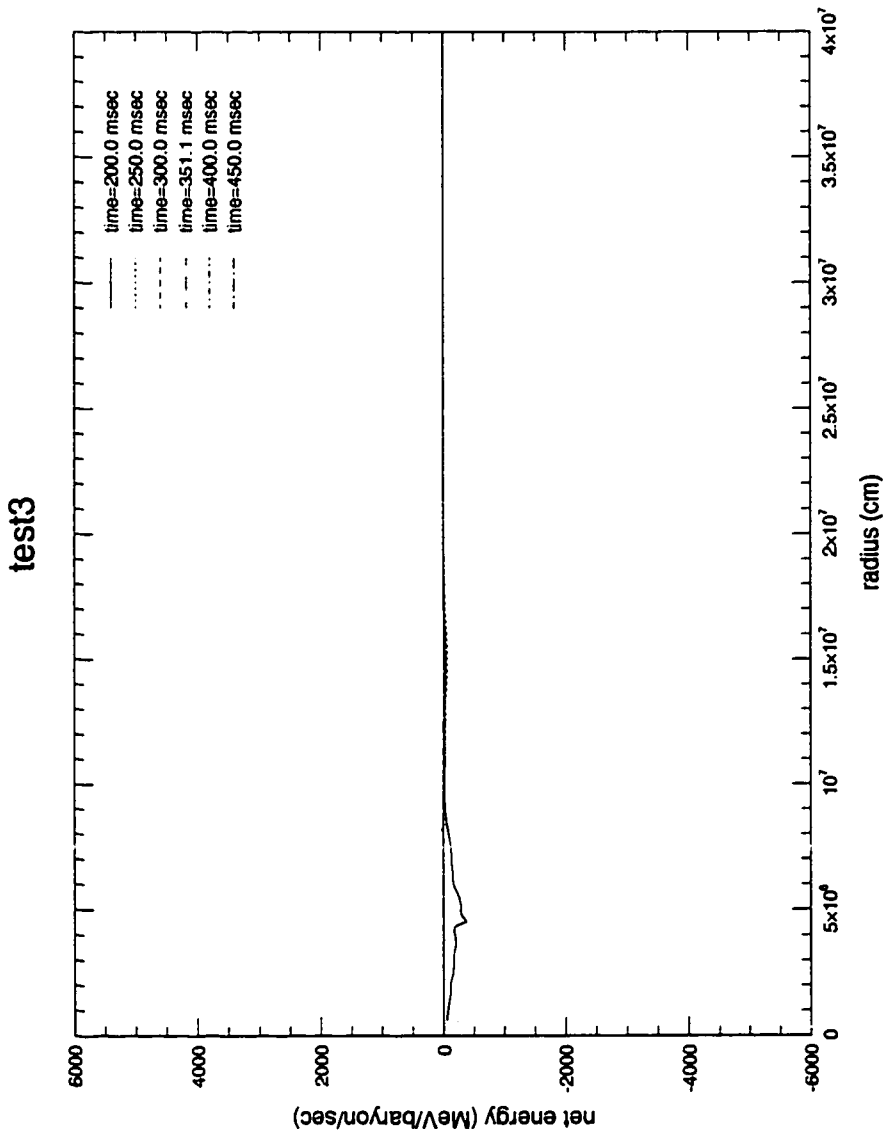


Figure 5.24: Neutrino heating/cooling - Non-convective - Electron neutrino only

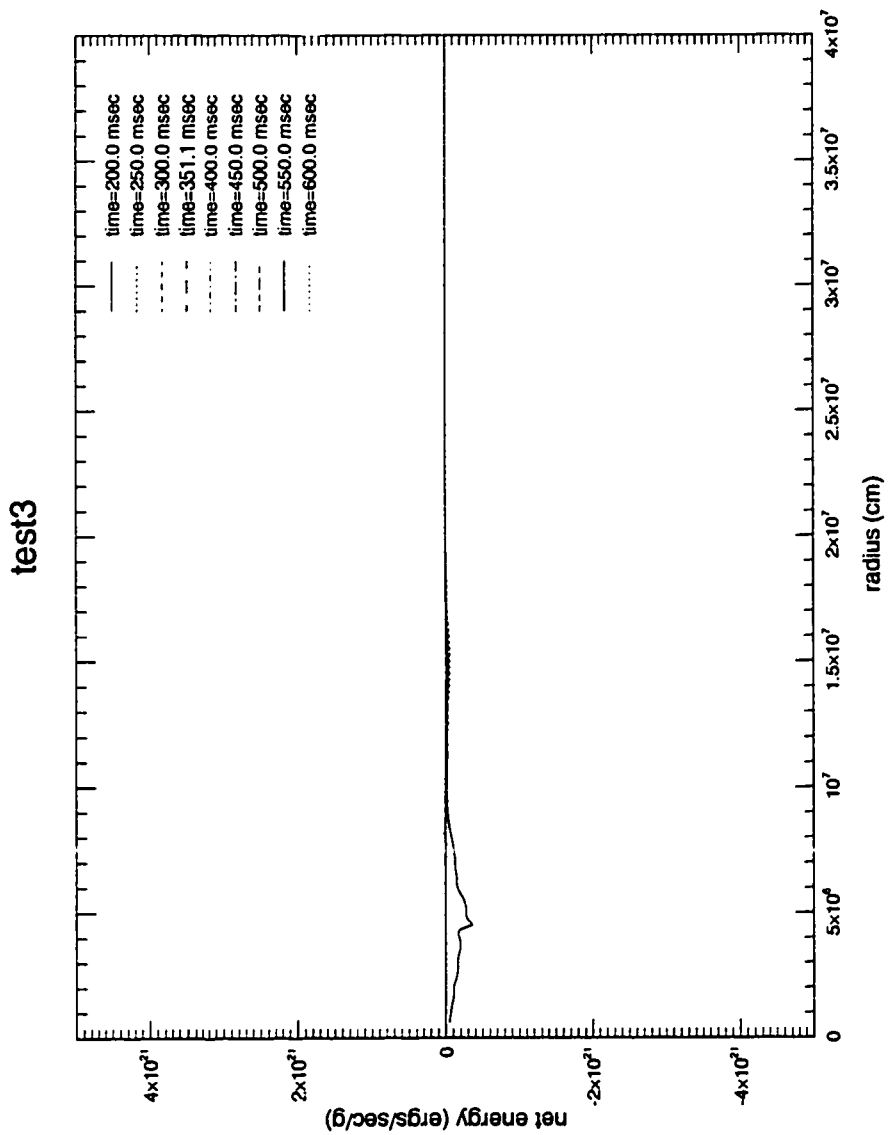


Figure 5.25: Neutrino heating/cooling - Non-convective - Electron neutrino only

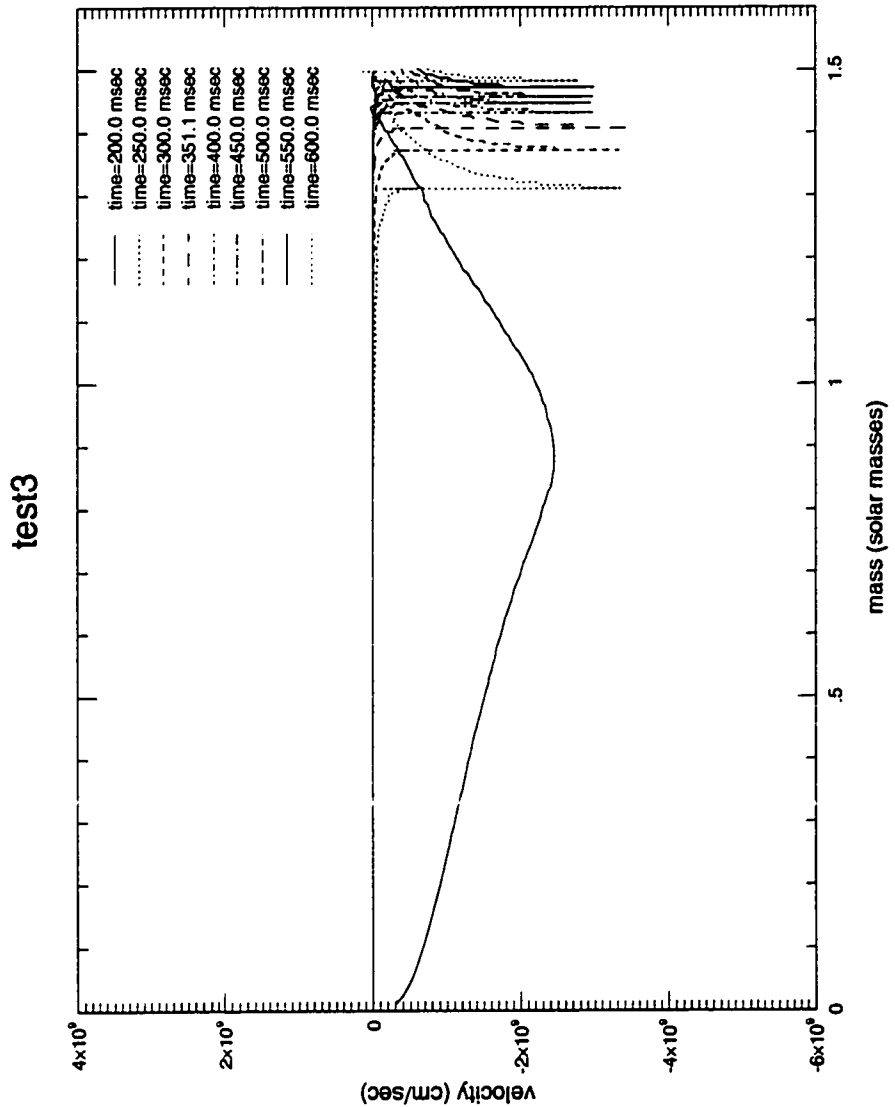


Figure 5.26: Velocity evolution - Non-convective - Electron neutrino only

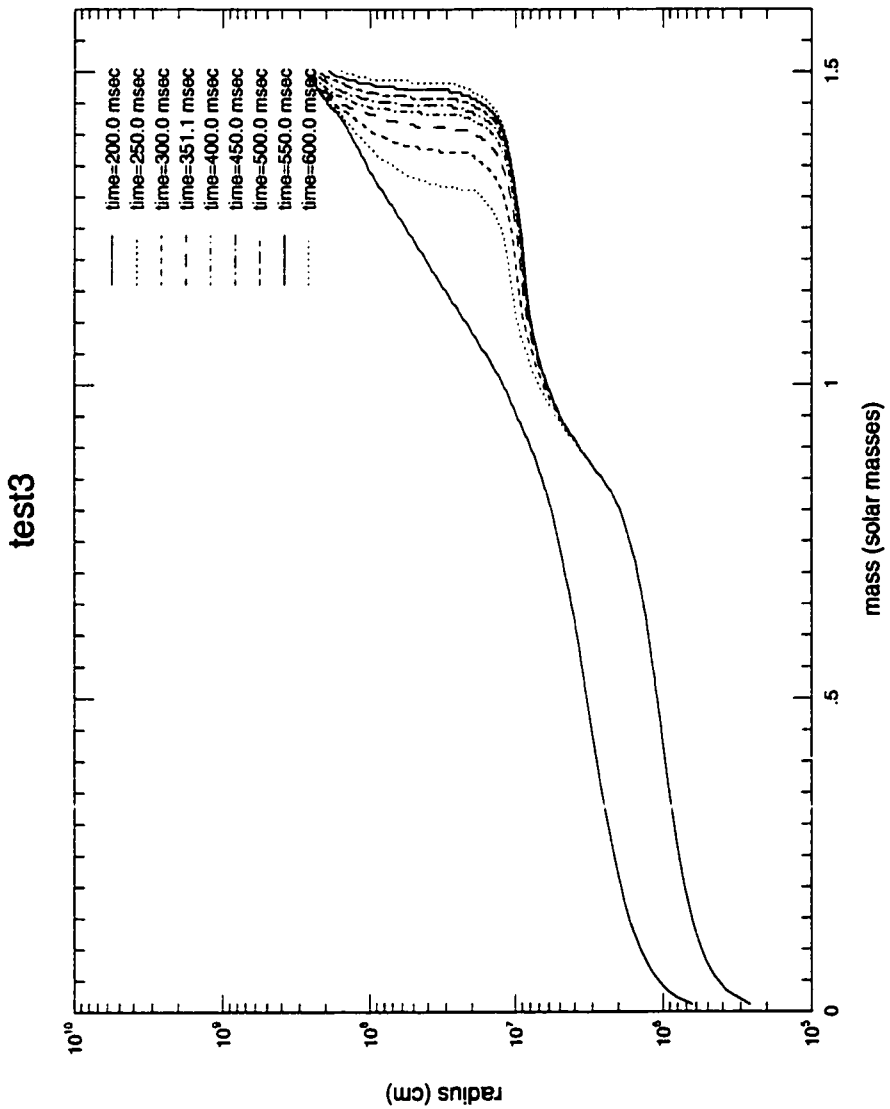


Figure 5.27: Radii evolution - Non-convective - Electron neutrino only

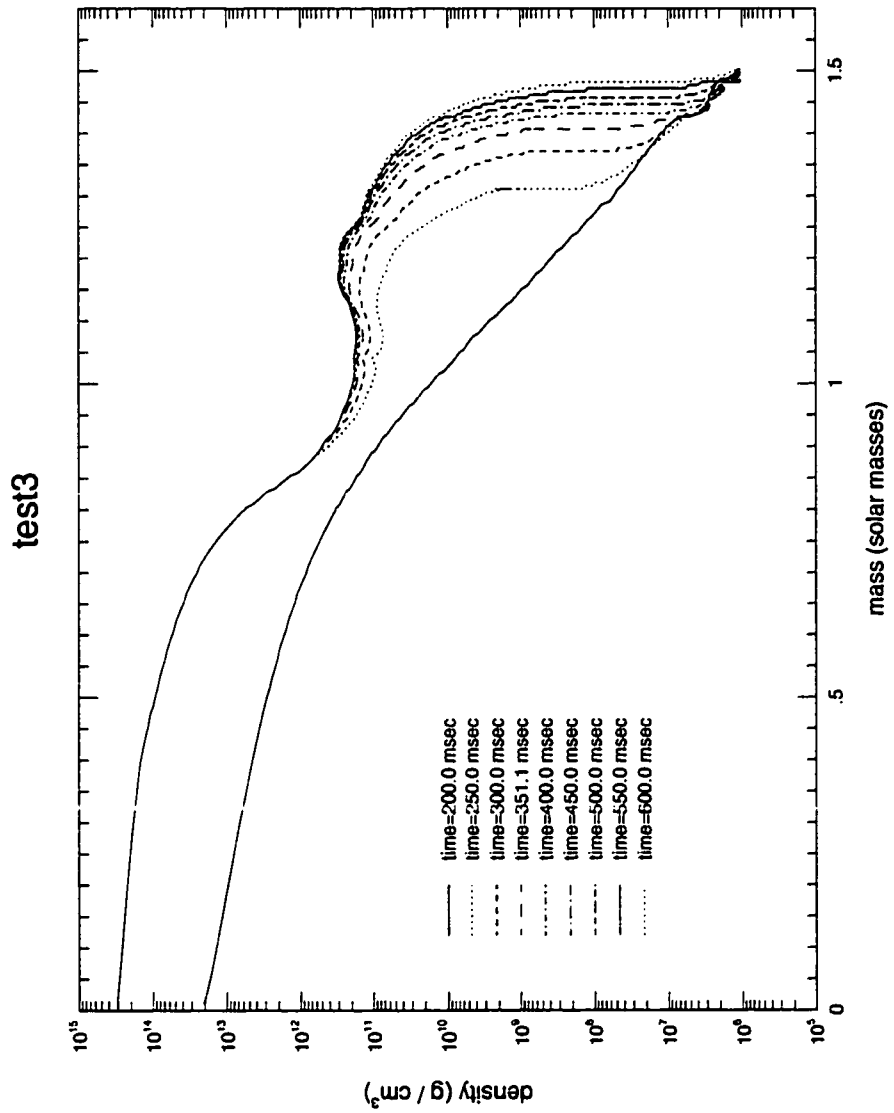


Figure 5.28: Density evolution - Non-convective - Electron neutrino only

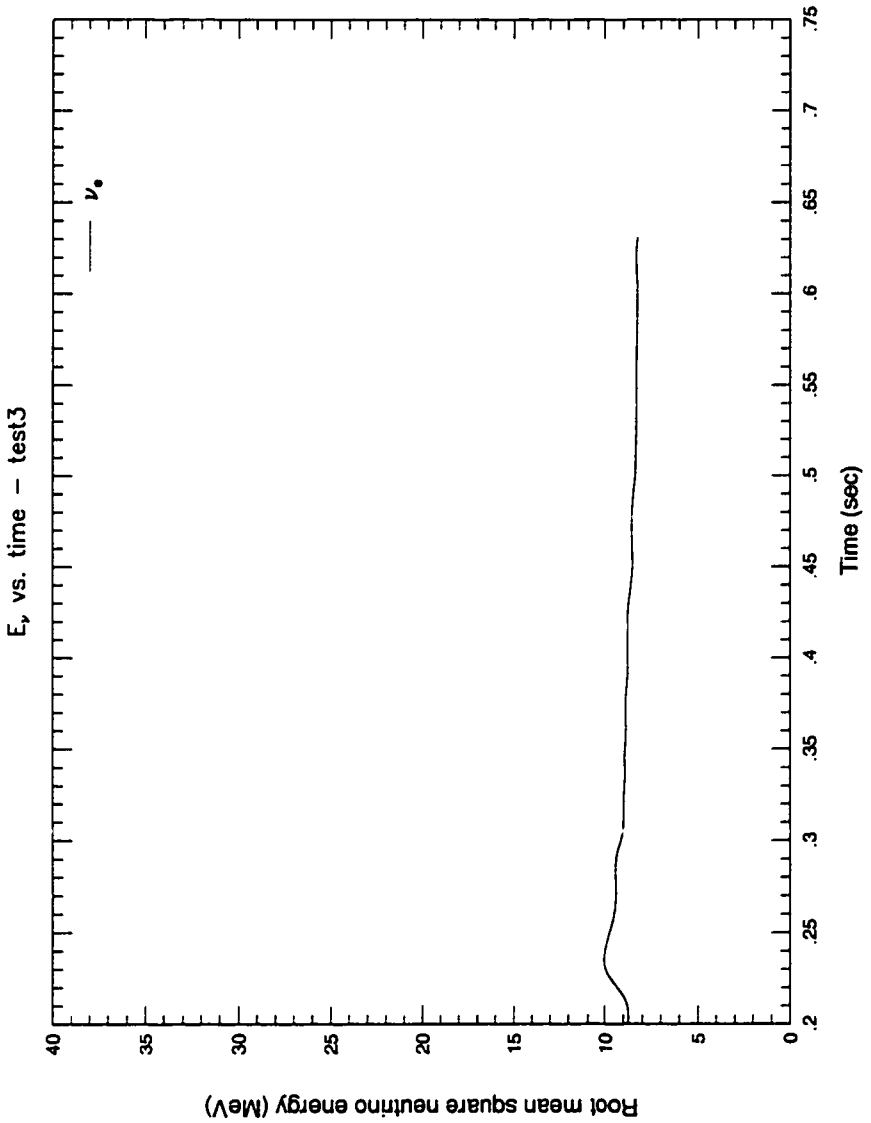


Figure 5.29: Neutrino energy versus time - Non-convective - Electron neutrino only

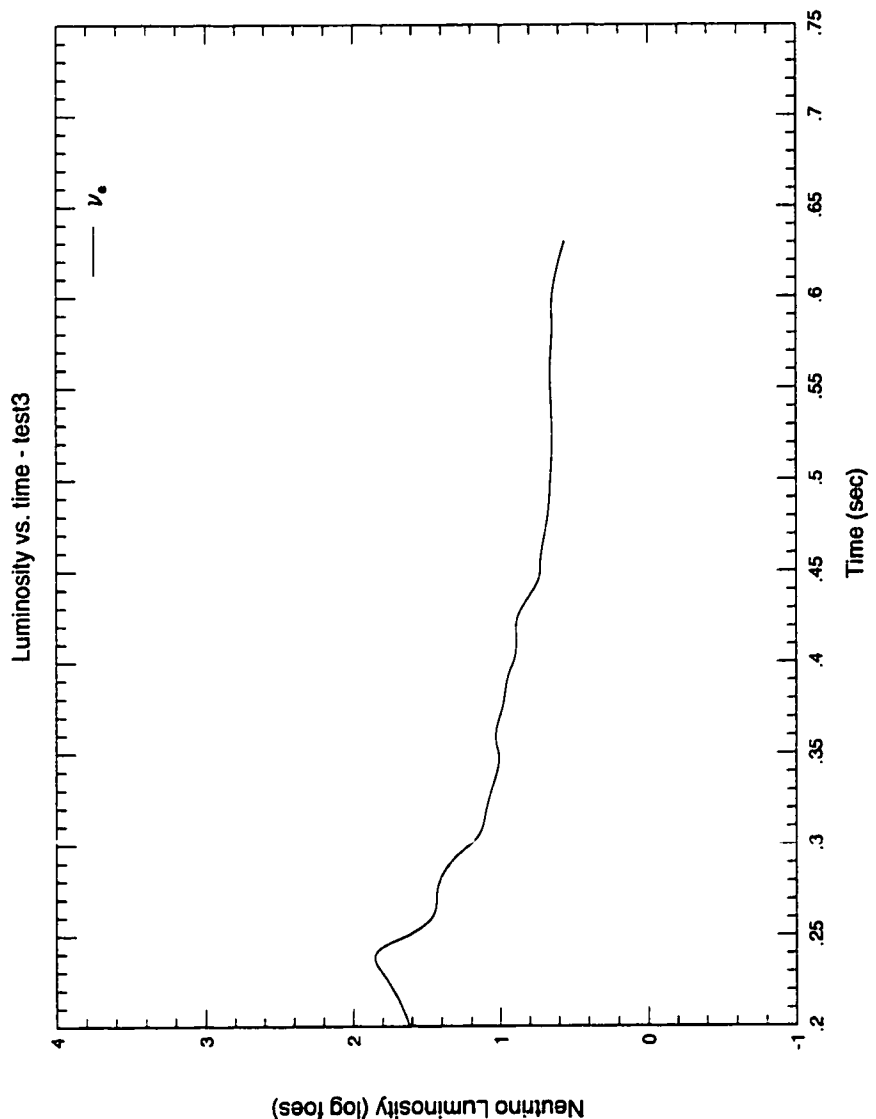


Figure 5.30: Neutrino luminosity versus time - Non-convective - Electron neutrino only

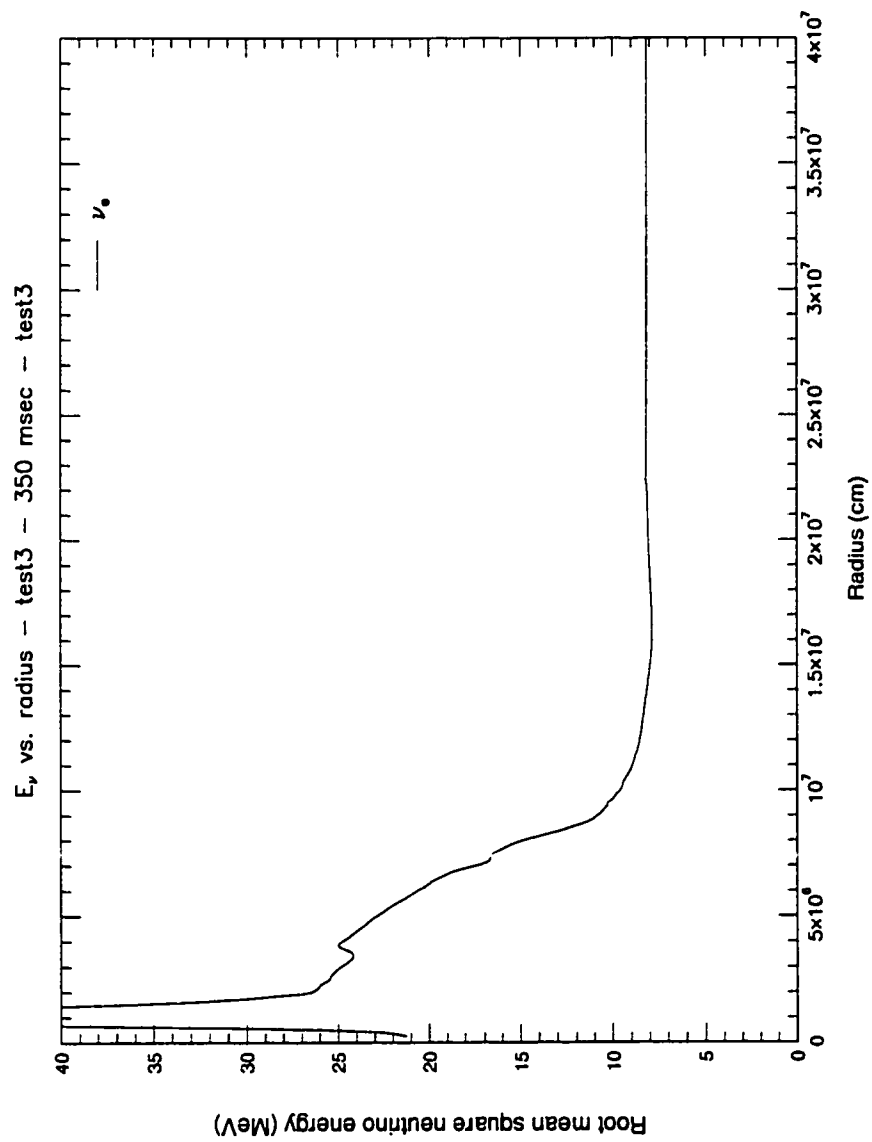


Figure 5.31: Neutrino energy versus radius - Non-convective - Electron neutrino only

## 5.4 The heating dilemma

One begins with the following assumptions about the behavior of the shock region

- that the post shock material is in hydrostatic equilibrium
- that the shock obeys the condition that higher post-shock entropies result a greater velocity difference across the shock
- that the material in the vicinity of the shock evolves quasi-statically

The second condition can be written as

$$\frac{\partial \Delta v}{\partial s_{post}} > 0. \quad (5.1)$$

Since the material behind the shock is assumed to be in hydrostatic equilibrium, the infall velocity must be identical to the shock velocity  $v_{infall}$  hence

$$\frac{\partial v_{infall}}{\partial s_{post}} > 0. \quad (5.2)$$

In the proto-neutron star the infall material is moving inward at supersonic speed relative to the shock. As a result, information about events behind the shock cannot acoustically propagate to affect material in front of the shock. Therefore, the post-shock entropy is uncorrelated with the pre-shock velocities. The shock therefore must, if the evolution is quasi-static, rather be located where the velocity of the infall matches the velocity difference across the shock. Using the assumption of quasi-static evolution, we ignore the time variation of the infalling velocity field and look only at the spatial variation. Because the free fall velocity increases as one moves deeper in the proto-neutron star,

that is

$$\frac{\partial v_{\text{infall}}}{\partial r} < 0, \quad (5.3)$$

increased post-shock entropy must correspond to a deeper shock.

Although this may at first appear counter-intuitive, a simple thought experiment may shed light on the dynamics of the heating dilemma. Suppose one has a standing shock whose post-shock region is in hydrostatic equilibrium. If one were to simply add entropy to the region immediately behind the shock, the shock would begin to propagate outward, but would not be in hydrostatic equilibrium. For hydrostatic equilibrium to be maintained, there must be a loss of pressure support in some other area of the post shock region. The heating dilemma asserts that an increase in the entropy behind the shock corresponds to a small shock stall radius. This argument is similar to an argument by Bethe, Brown and Cooperstein (1987) that in flattening the entropy profile, convection has a detrimental effect on the prospects for an explosion. Their argument can be generalized to an transfer of heat from the core of the proto-neutron star to the shock which occurs quasi-statically.

In short, the heating dilemma is that so long as there exist the three conditions of hydrostatic equilibrium behind the shock, satisfaction of the shock jump conditions, and quasi-static evolution, an increase in post-shock entropy corresponds to a shock that is deeper in the gravity well and therefore one in which an explosion is even more unlikely. It explains why in the current models, the more compact post-shock region corresponds to the model with the stronger shock.

Although the heating dilemma appears to exist in the current models, which do not explode, it is unlikely to exist in real supernovae, which do

explode. Therefore, it is necessary to discuss the assumptions behind the dilemma in detail to find ways in which the conditions that give rise to this behavior are not satisfied in actual supernova.

### 5.4.1 Resolving the heating dilemma

In order to resolve the heating dilemma, it is necessary to find conditions that break the three assumptions which give rise to the dilemma. In breaking the condition of hydrostatic equilibrium, one can assume either that the material behind the shock never settles into hydrostatic equilibrium or that material has attained hydrostatic equilibrium and that heating, such as that from neutrinos or convection heats the post-shock region in a manner that causes it to evolve dynamically. The former is a “prompt shock” model and is subject to the weaknesses discussed earlier.

The second possibility is related to the “critical luminosity” concept developed by Burrows and Goshy (1993). Using a semi-analytic model, they have demonstrated that once neutrino luminosity increases beyond a critical value, the material behind the shock cannot maintain hydrostatic equilibrium. Attempting to resolve the heating dilemma by breaking the assumption of hydrostatic equilibrium raises the question of under what circumstances will the post-shock material be unable to achieve hydrostatic equilibrium? Although Burrows and Goshy have answered this question for one specific set of assumptions, it should be possible to develop criteria for more general cases.

Another possibility for resolving the heating dilemma is by breaking the assumption that conditions across the shock jump are not described by a

relationship in which

$$\frac{\partial \Delta v}{\partial s_{post}} > 0. \quad (5.4)$$

One mechanism by which this may be accomplished is by assuming that multi-dimensional effects affect the shock. Multi-dimensional effects may allow for the shock to move non-perpendicularly to infall thereby removing the equality between infall velocity and shock velocity difference. Furthermore, in a multi-dimensional shock, there may be variations in conditions in the neighborhood of the shock which cause the global evolution of the shock to be different from normal shock jump conditions, which describe the local evolution of the shock. Whether these effects allow for the shock to avoid the heating dilemma remains a topic for future research. Furthermore, an investigation should be made into whether the reaction of the shock in response to the heating dilemma could create shock instabilities or promote asymmetries in the shock.

The final assumption that may be broken is the assumption of quasi-static evolution. One mechanism by which this may be done, is by strong heating which breaks hydrostatic equilibrium as described earlier. Another possibility is a “gentle push” mechanism. At a fixed radius, there is a gradual increase in infall velocity as time passes. Hence there may be trajectories which move out in radius space even as the infall pre-shock infall velocities.

## 5.5 Neutrino energy

The other major difference in the models with and without anti-electron neutrinos and the  $\tau$  and  $\mu$  neutrinos is the large difference in root mean square neutrino energies in the electron neutrino only case (figure 5.29) and the case

with all species (figure 5.13). The correlation appears to be that as the shock stall radius decreases, the root mean square energy of the neutrinos increases. The cause of this difference can be illustrated in plots of the radial dependence of root mean square neutrino energy in figures 5.31 and 5.15. When the shock stalls at a lower radius, the neutrinosphere is deeper and so the neutrinos decouple from the matter at a lower depth. Second and more importantly, a lower shock stall radius corresponds to a stronger shock and higher temperatures. This produces higher energy neutrinos.

## 5.6 Convective models

The model *tau3c* was a convective model using the standard parameters. The development of convection is illustrated in figure 5.32 which presents the convective velocities within the current model. Figure 5.35 and in 5.38 show the behavior of the “standard model” including convection (model *tau3c*). When the convection algorithm is included with standard parameters, convection develops between 1.0 and 1.5 solar masses, and grows to a maximum velocity of approximately  $2 \times 10^8$  cm/sec with a time scale of several tens of milliseconds. These convective velocities are somewhat smaller than the velocities of other groups, which typically find velocities on the order of a few times  $10^9$  cm/sec. (Burrows, Hayes & Fryxell 1995; Mezzacappa et al. 1998; Janka & Mueller 1995). In comparing the radial locations of the convection, it is found that the main differences in convective velocity are near the shock.

Examining the profile of the convective luminosity (figure 5.37) reveals that convection in the all neutrino species case transports only a very small amount of energy. These small differences do not cause any qualitative change

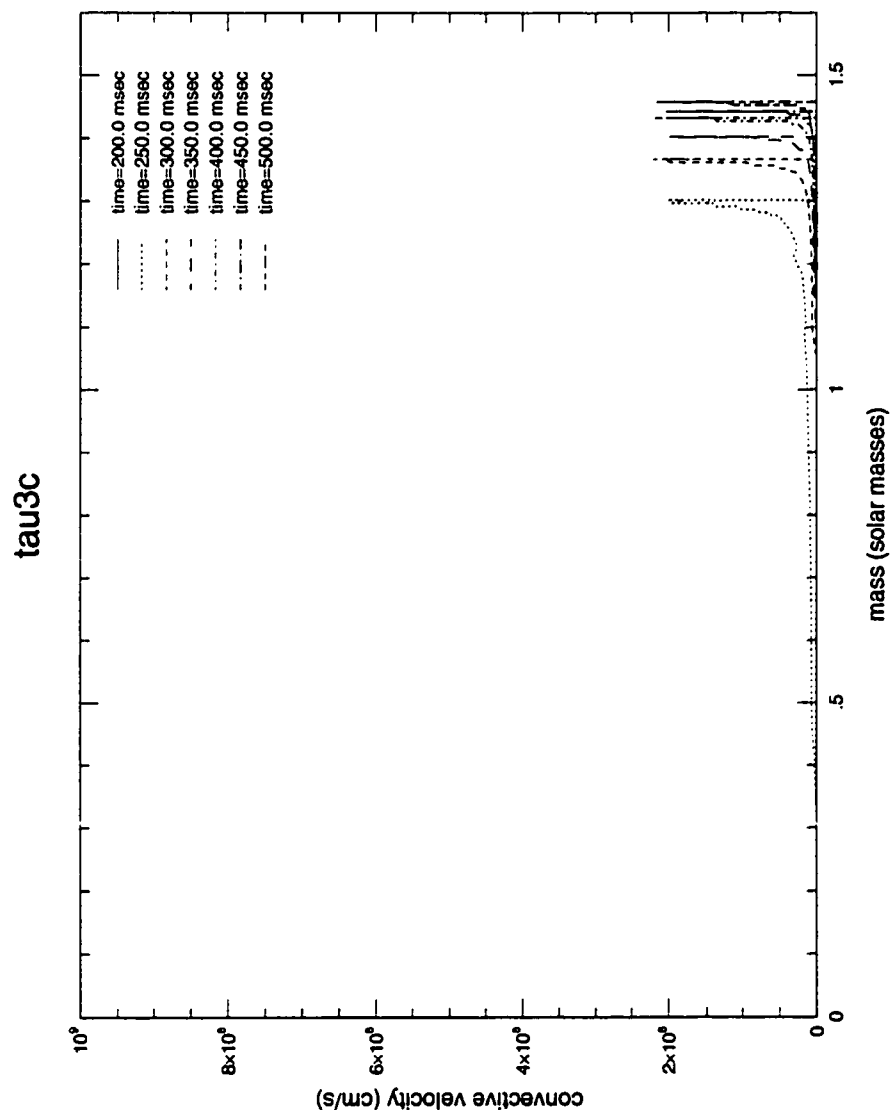


Figure 5.32: Convective velocity versus mass evolution - Convective - All neutrino species

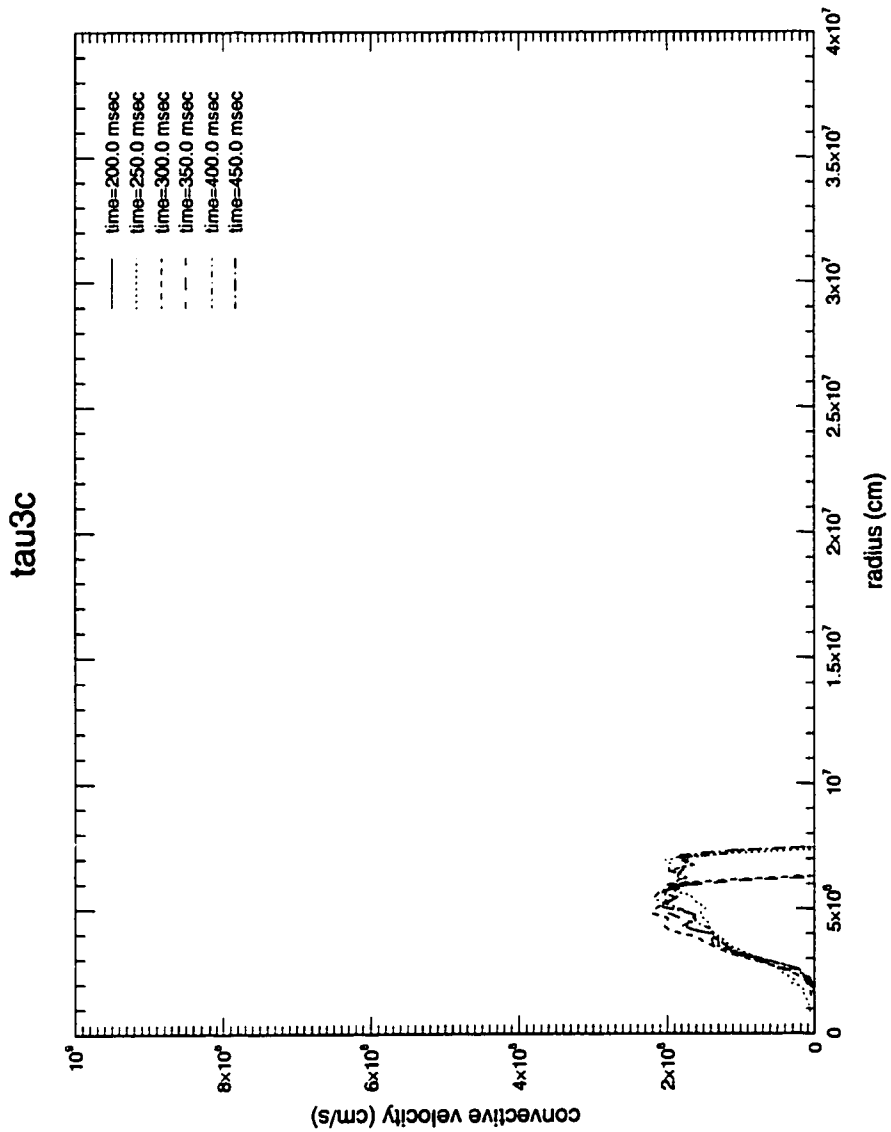


Figure 5.33: Convective velocity evolution versus radius - Convective - All neutrino species

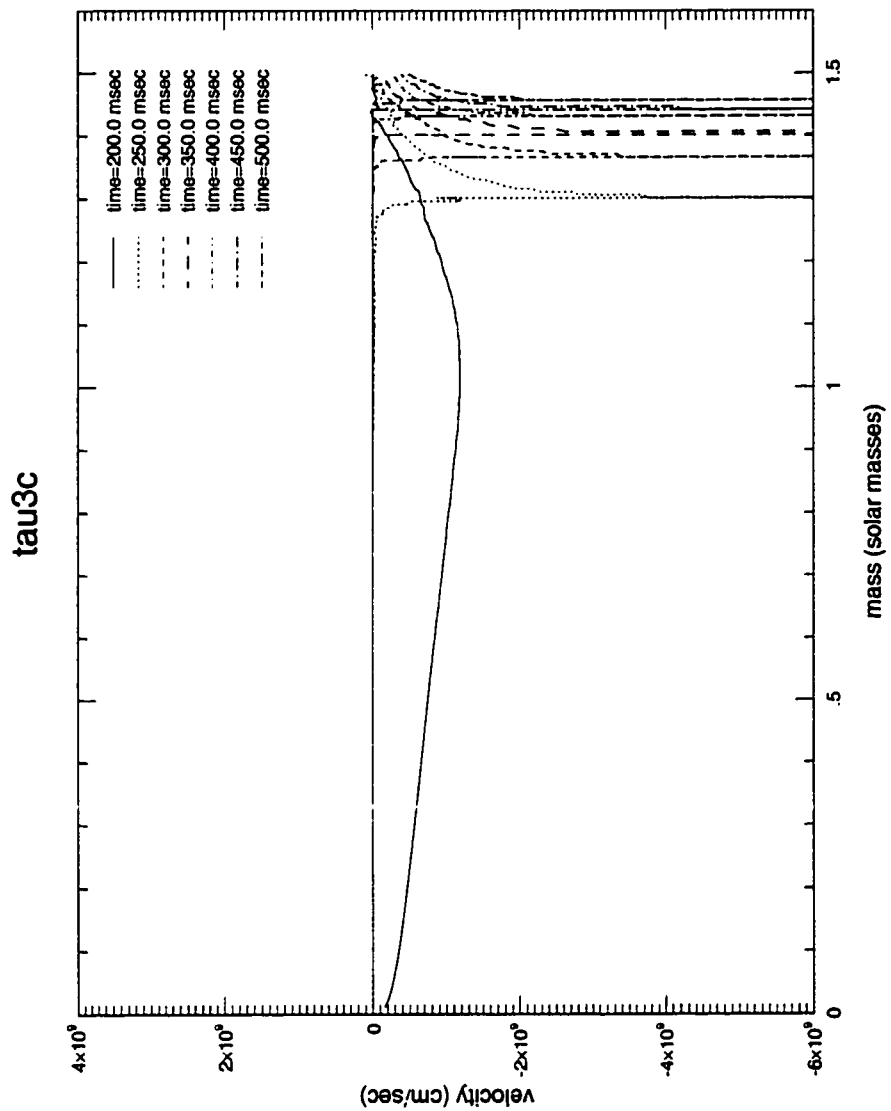


Figure 5.34: Velocity evolution - Convective - All neutrino species

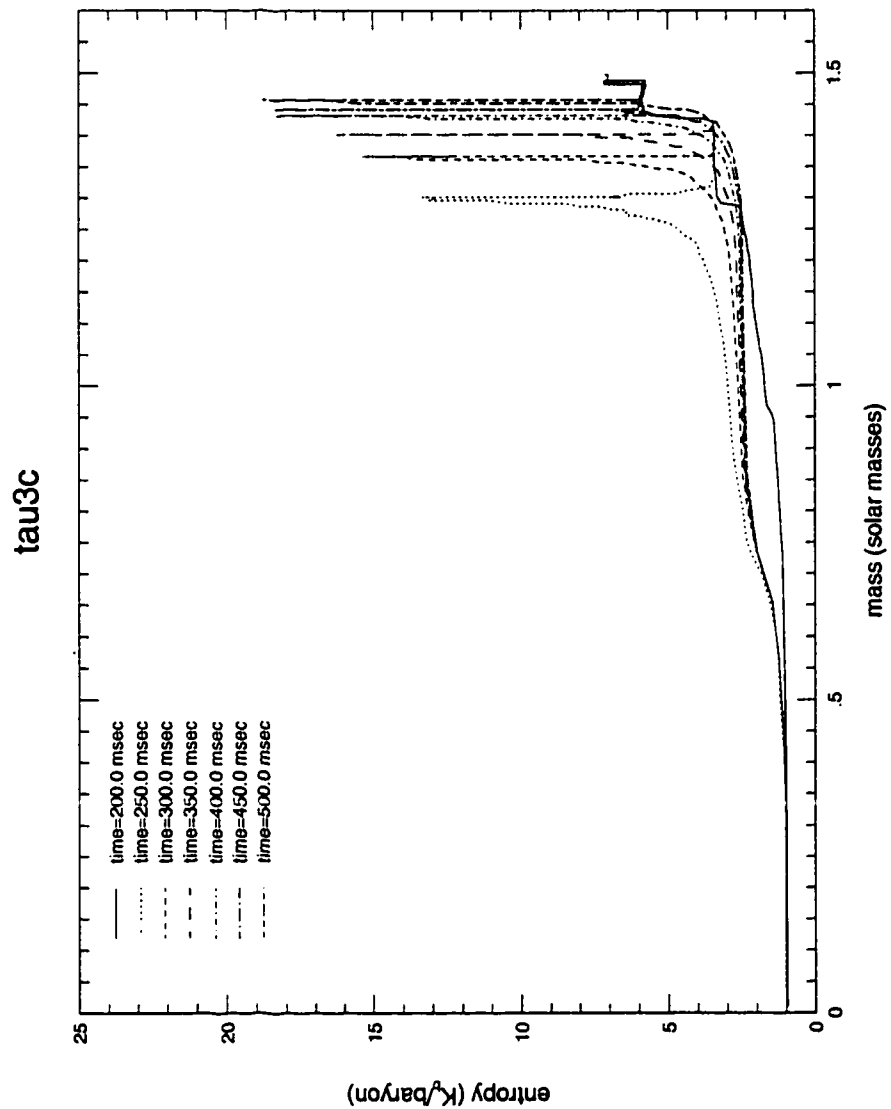


Figure 5.35: Entropy evolution - Convective - All neutrino species

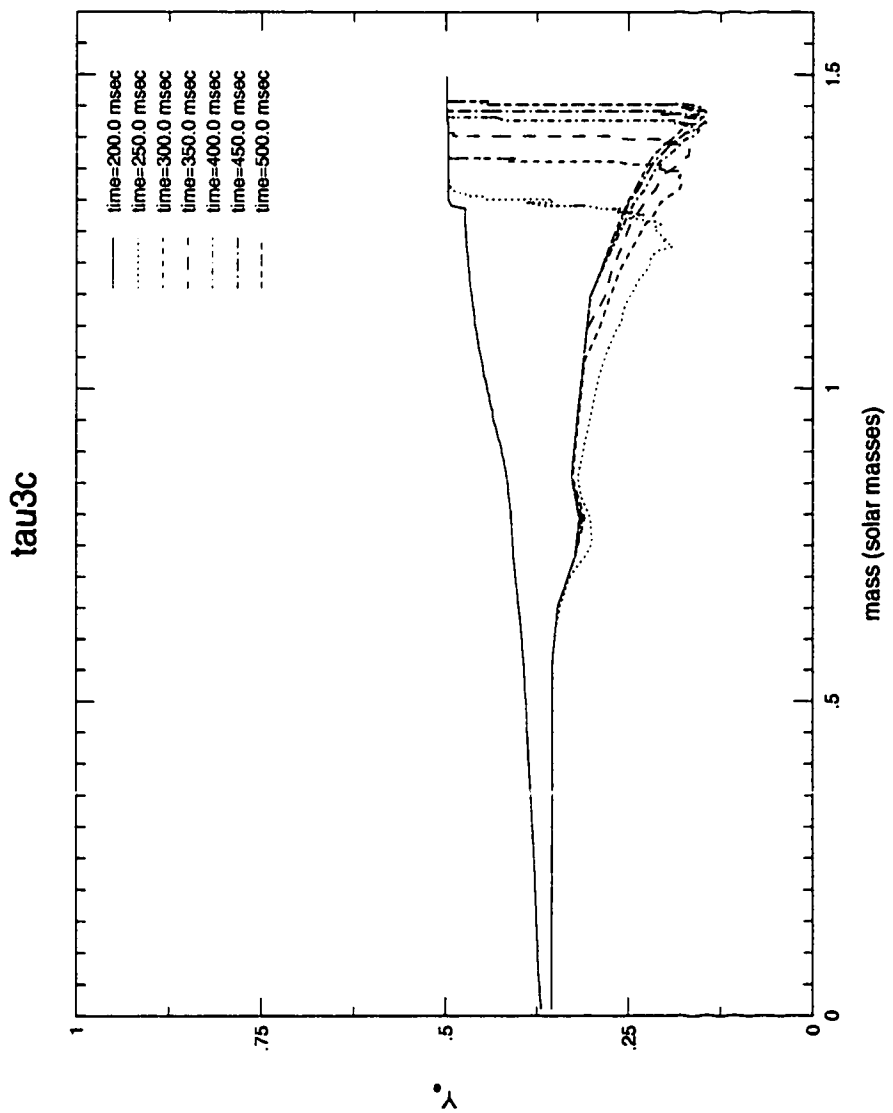


Figure 5.36:  $Y_e$  evolution - Convective - All neutrino species

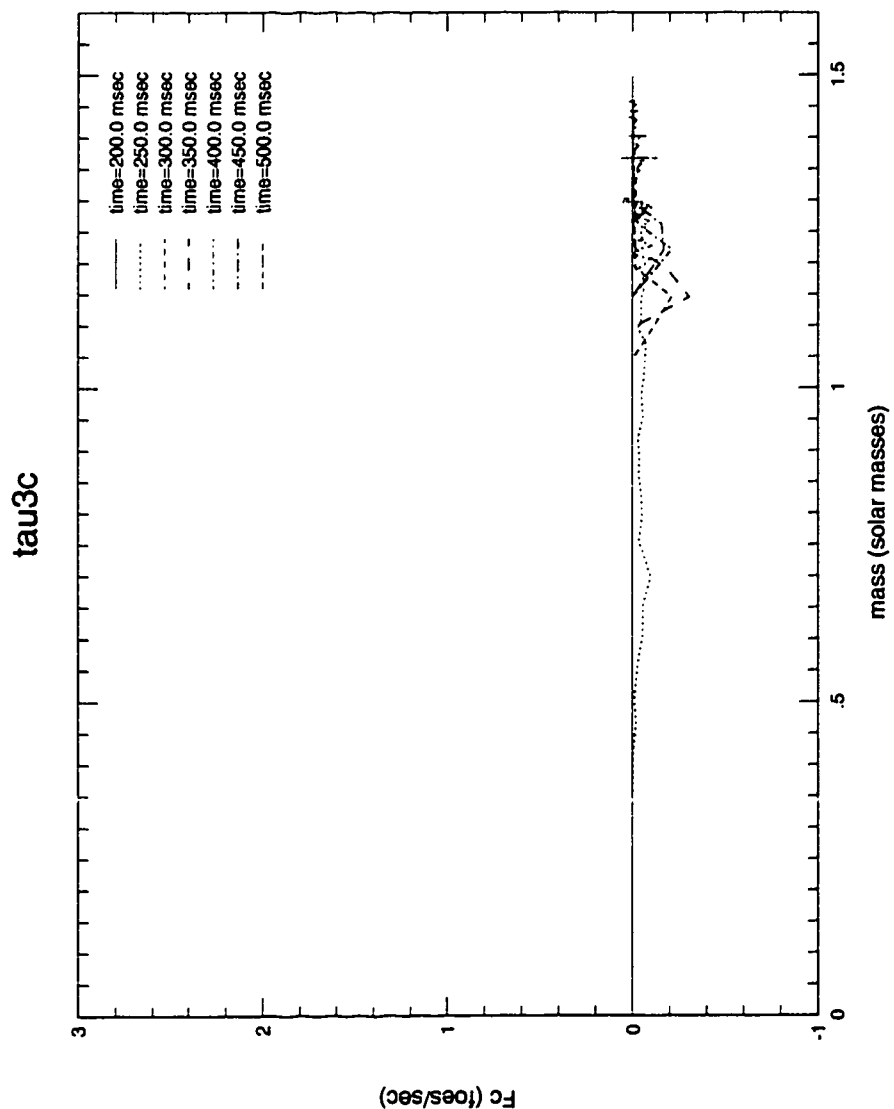


Figure 5.37: Convective luminosity - Convective - All neutrino species

in a plot of the shock position (figure 5.38) or in any of the neutrino emission parameters (figures 5.39 to 5.42).

In general, there appears to no qualitative differences between the current convective and non-convective models. The plots of neutrino heating and cooling appear identical between the convective case (figure 5.39) and the non-convective case (figure 5.10). Furthermore, a plot of the convective luminosity (figure 5.37) indicates that the luminosity provided by convection is much smaller than those provided by neutrino heating.

Further insight into the effects of convection can be gained by studying the effects of convection on the electron neutrino only case. Figure 5.43 illustrates the convective velocities in the electron neutrino only case. As can be seen, the distribution of convective velocities are considerably different than the all neutrino species case. These differences are unsurprising considering the differences in entropy distribution between models *tau3* and *test3*. In the case of the electron neutrino only case, there is a large entropy peak onto which convection can act. The effects of this convection is illustrated in figures 5.44 and 5.45.

However, as in the case of the all neutrino species case, convection does not appear to have any qualitative impact on the outcome of the models. We also do not observe evidence of other convective mechanisms which have been invoked in the literature. This is due to differences in neutrino heating and cooling distributions which prevent the operation of these mechanisms. Burrows et al. (1995) suggest that convection can improve prospects for an explosion by decelerating material behind the shock and increasing the time that material spends in the gain region. This effect is not seen in the current models since the immediate post shock region has relatively small convective

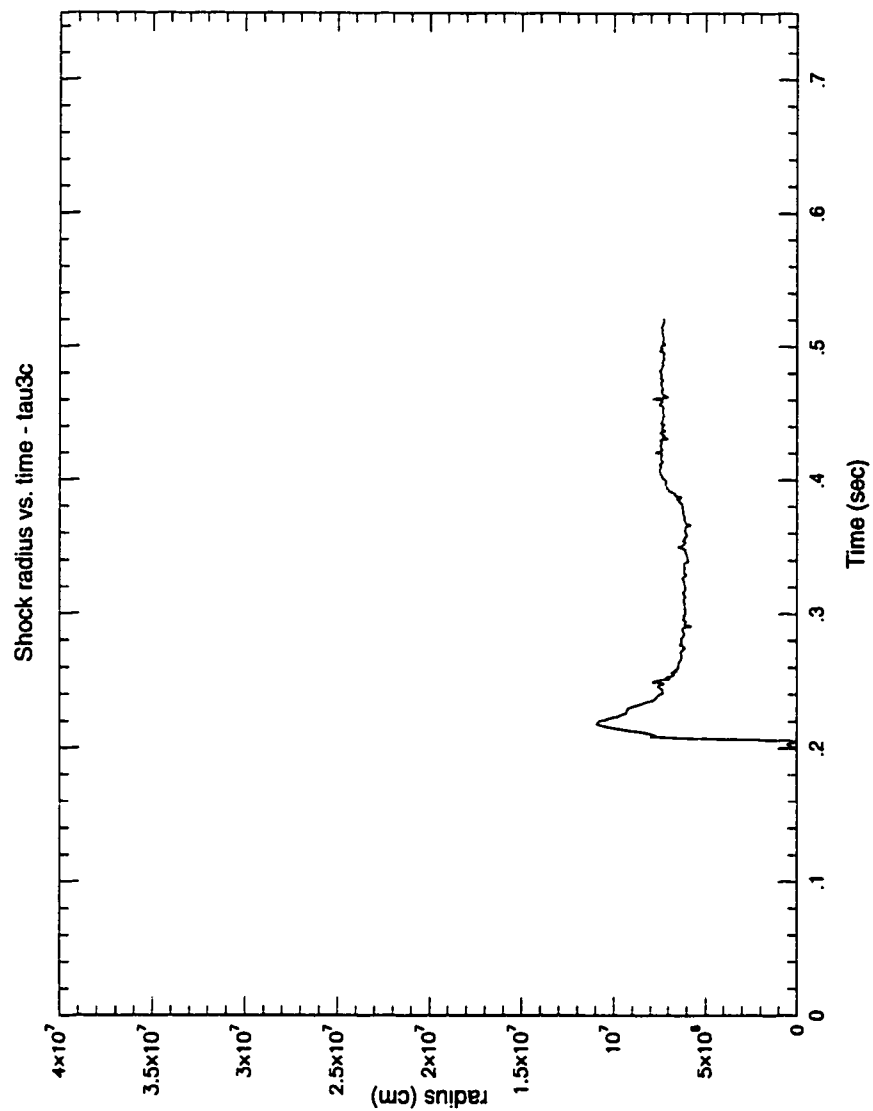


Figure 5.38: Shock versus time - Convective - All neutrino species

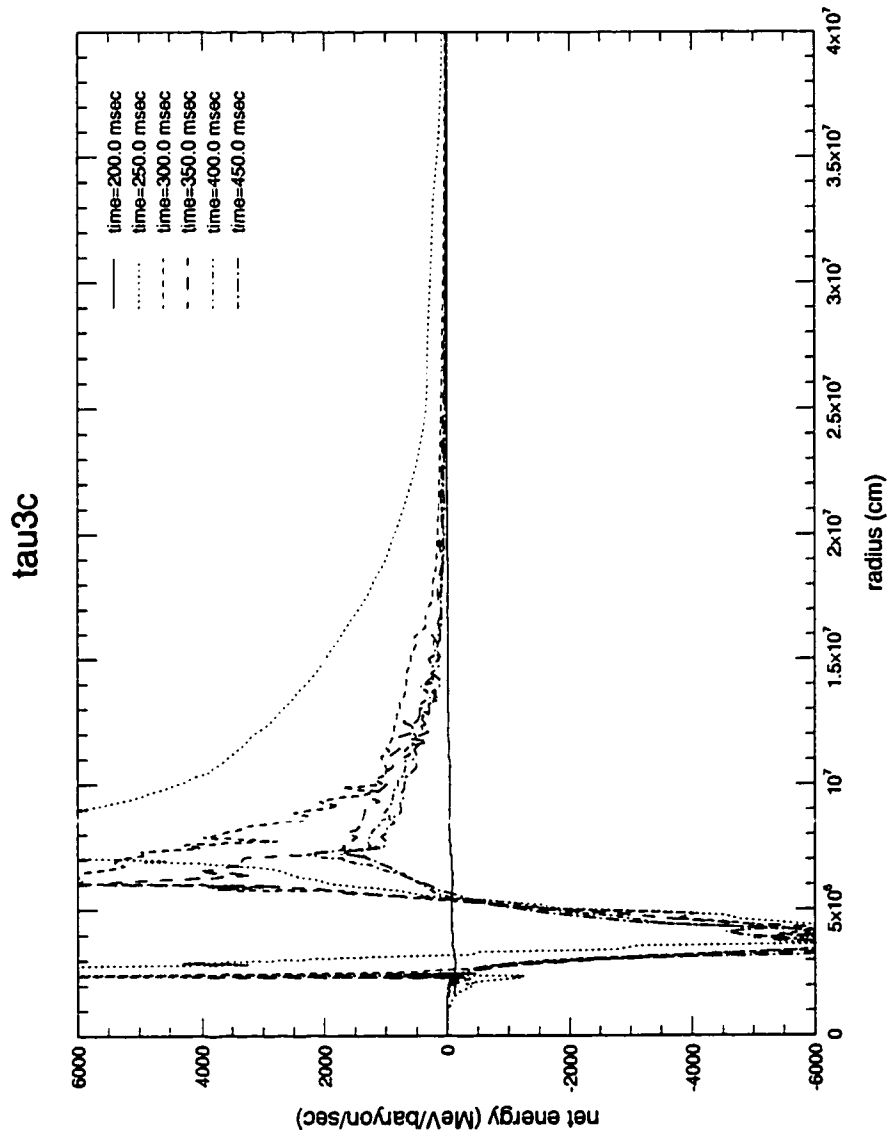


Figure 5.39: Neutrino heating/cooling - Convective - All neutrino species

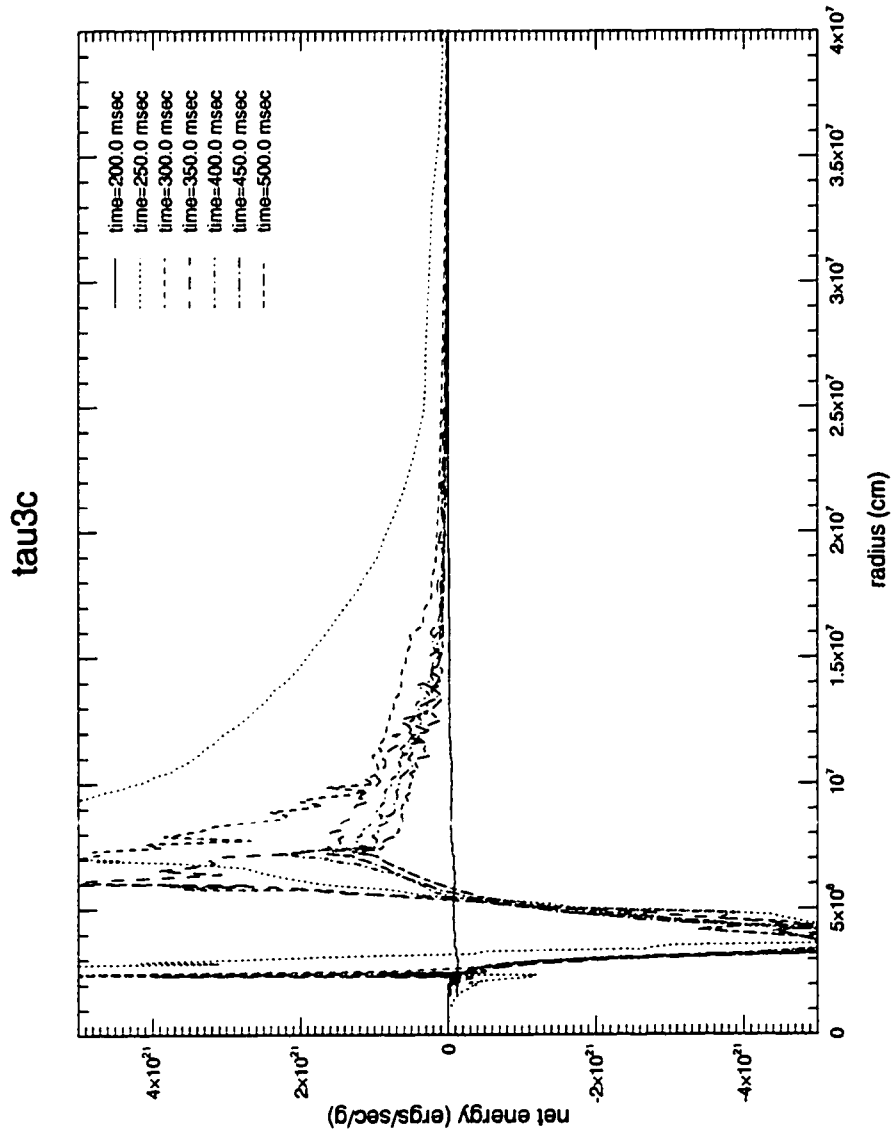


Figure 5.40: Neutrino heating/cooling - Convective - All neutrino species

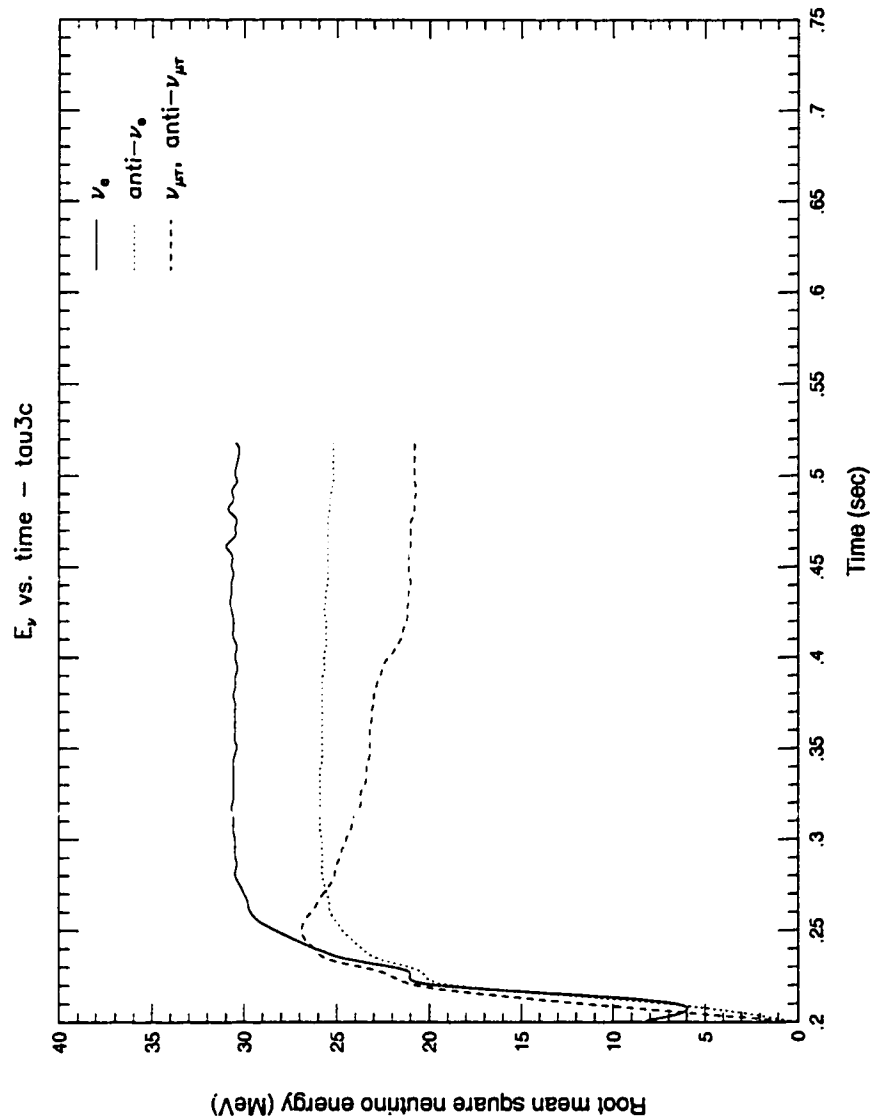


Figure 5.41: Neutrino energy versus time - Convective - All neutrino species

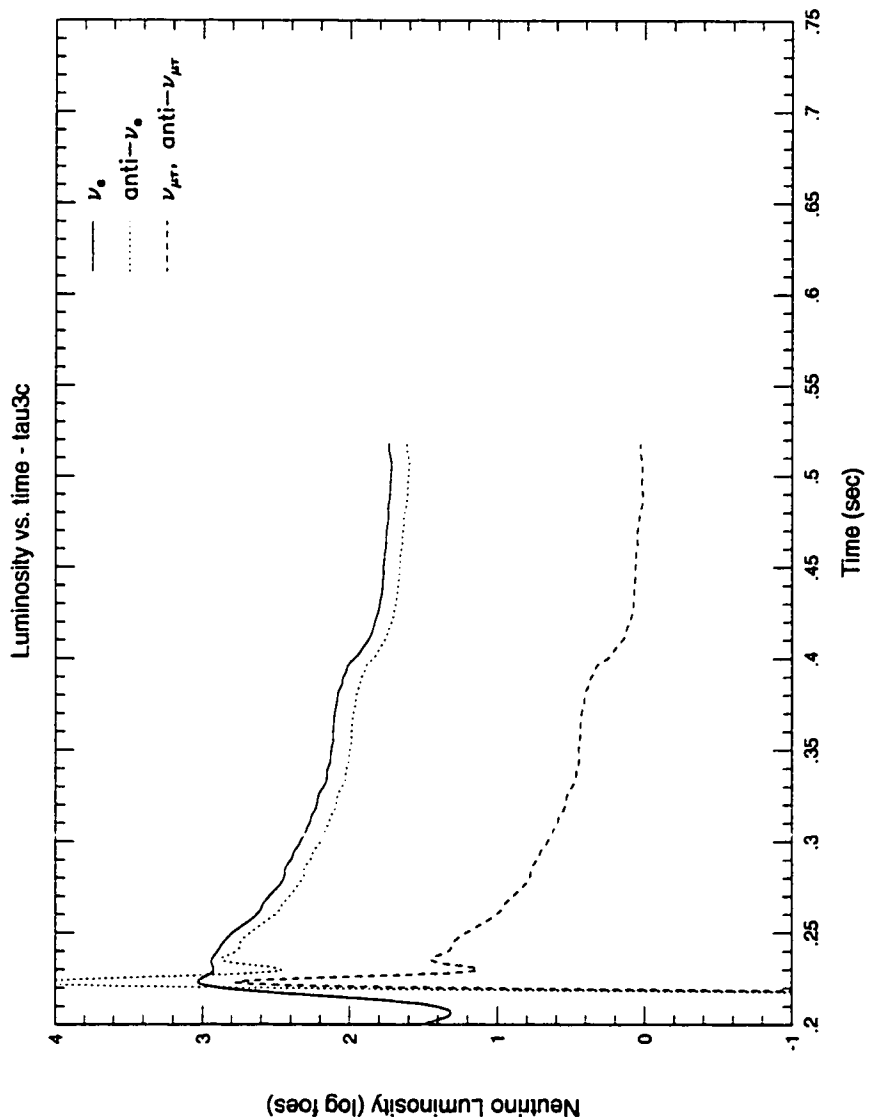


Figure 5.42: Neutrino Luminosity versus time - Convective - All neutrino species

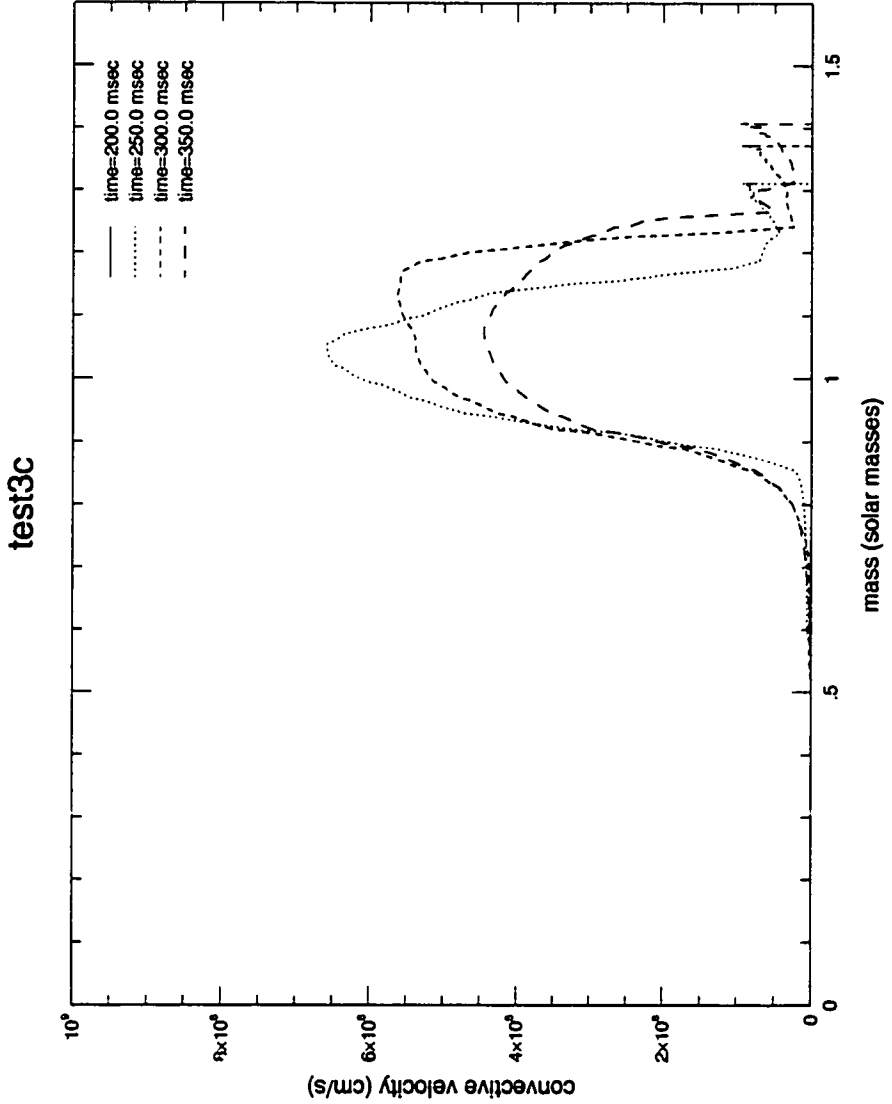


Figure 5.43: Convective velocity evolution - Convective - Electron neutrinos only

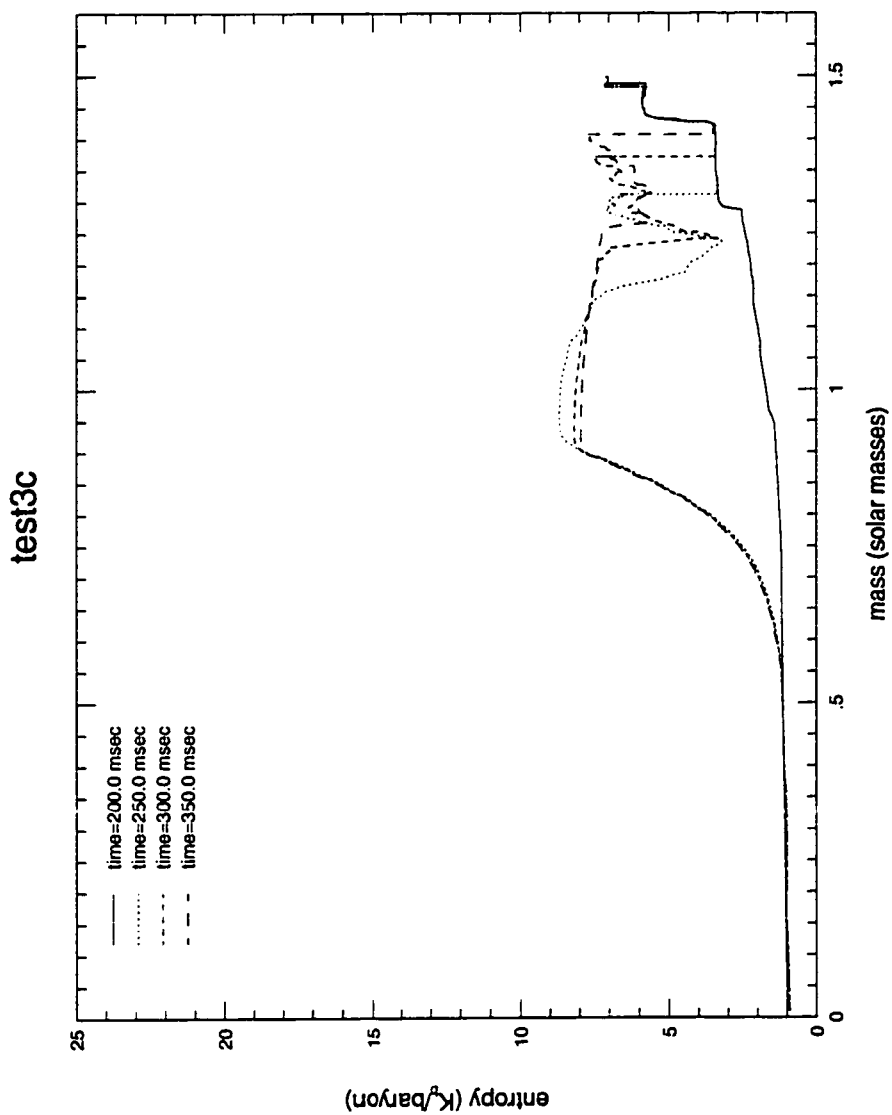


Figure 5.44: Entropy evolution - Convective - Electron neutrino only

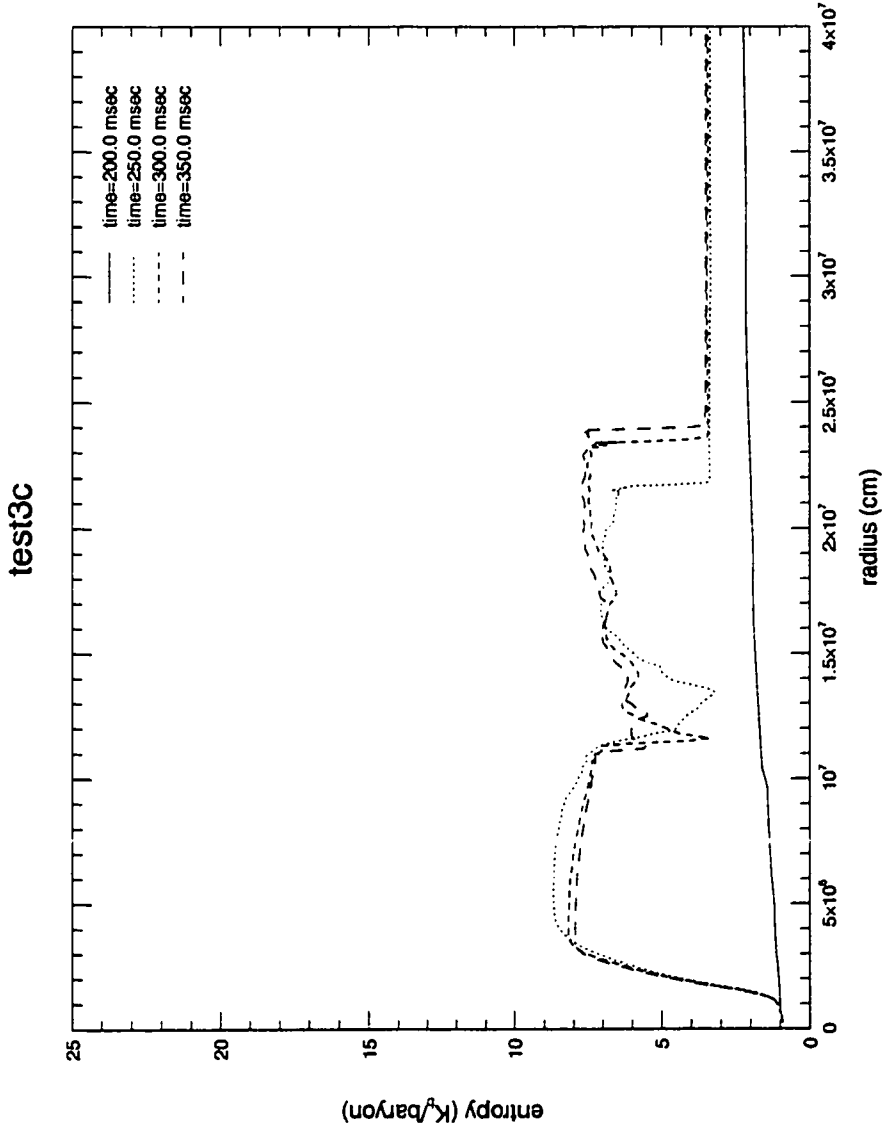


Figure 5.45: Entropy versus radius evolution - Convective - Electron neutrinos only

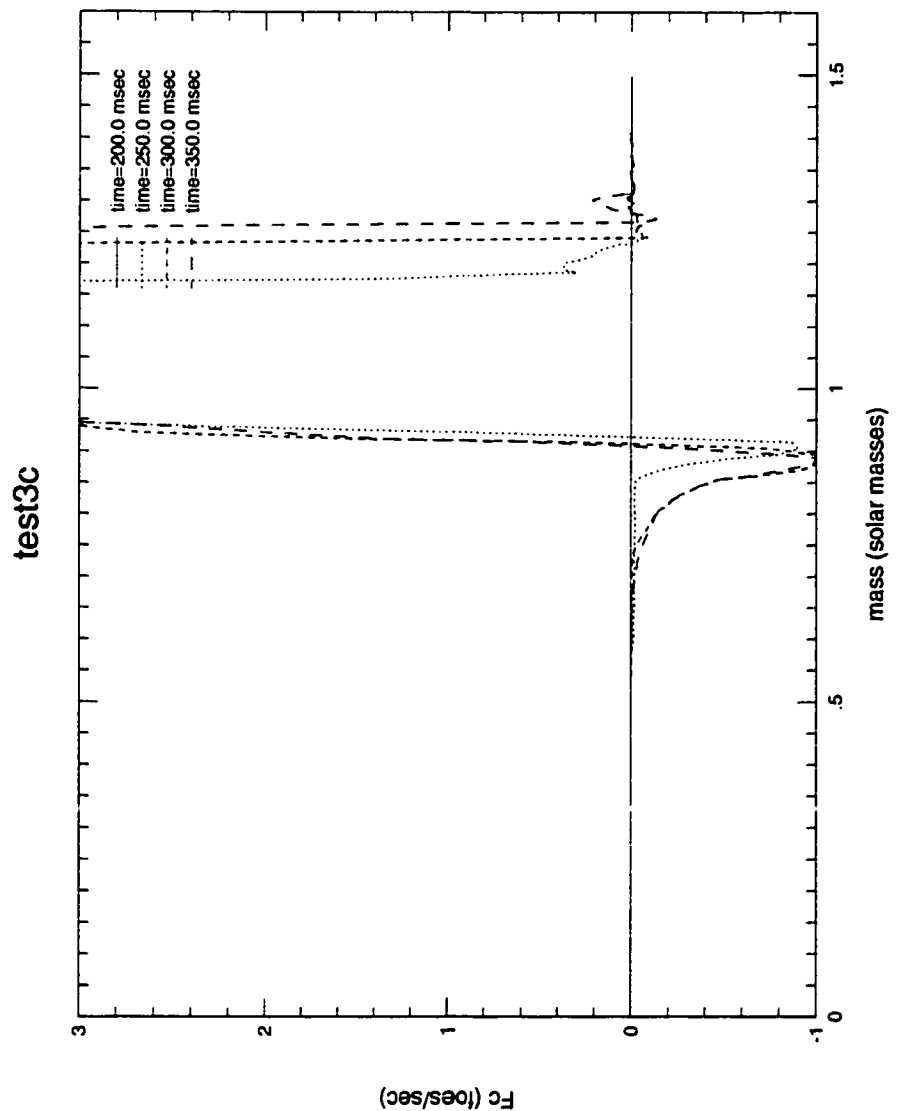


Figure 5.46: Convective luminosity - Convective - Electron neutrinos only

velocities.

The results of these models are also inconsistent with models which rely on a “heat engine” to transfer energy from the interior of the star to the shock (Herant, Benz, & Colgate 1994). In the current models, convection does not appear to deliver significantly more heat to the shock than neutrinos and does not appear to make any qualitative change in the evolution of the shock. It has also been suggested that convection may affect the explosions by altering the temperature profiles in such a way as to increase neutrino luminosities (Wilson & Mayle 1993). There is also no evidence that convection affects the neutrino luminosity in the current models.

Finally, there is no sign in the current convective models of the inner core Ledoux convection observed in the two dimensional models of Janka and Muller (1995) and the one dimensional models of Burrows (1987). In the current models, the large positive entropy gradient at the base of the entropy spike has the effect of suppressing Ledoux convection. This positive entropy gradient is in turn caused by the rapid neutrino cooling of material having passed through the shock. In order to create the conditions necessary for inner core Ledoux convection, it is necessary to reduce neutrino energy loss while maintaining a negative  $Y_e$  gradient. This may be accomplished by decreasing neutrino production by pair-production. At the same time, it is unclear how changing the neutrino opacity or electron capture rates will affect inner core Ledoux convection. While increasing opacity or decreasing electron capture will decrease the positive entropy gradient, it will also soften the  $Y_e$  gradient making unclear how this will affect inner core Ledoux convection.

It should be clear from the forgoing discussion that the existence of inner core Ledoux convection is sensitive to the input neutrino physics, and

that further study is needed to define the conditions under which it will appear.

## 5.7 Convective models with nonstandard parameters

Further insight into the role of convection in supernova explosions can be gained by examining some models with convective extensions. Several models containing all neutrino species were run with combinations of convective braking and turbulent pressure. In no case did the addition of these elements into the convective model result in any qualitative change in the behavior of the models. Figure 5.47 is a typical example of the evolution of this group of models and contains both turbulent pressure and convective braking.

To test for the interaction between neutrinos and convection, a model *tau3nd* was run assuming that the convection would fully convect neutrinos. As illustrated in figures 5.48 and figures 5.49 results of this model were similar to the non-advection model *tau3c*.

There were differences in the neutrino emission immediately following bounce. In particular the neutrino-advection model did not show the peak and dip in neutrino emissions that were present in the models with standard convective parameters (see figures 5.50 and 5.51). The dip in the standard convective models exists because the contracting post-shock region advects neutrinos inward. When the neutrinos are advected, this inward advection is canceled by the advection that results from convection. However, besides this initial difference, there were no qualitative difference in the neutrino luminosity and energies, and because the difference after bounce do not appear to persist

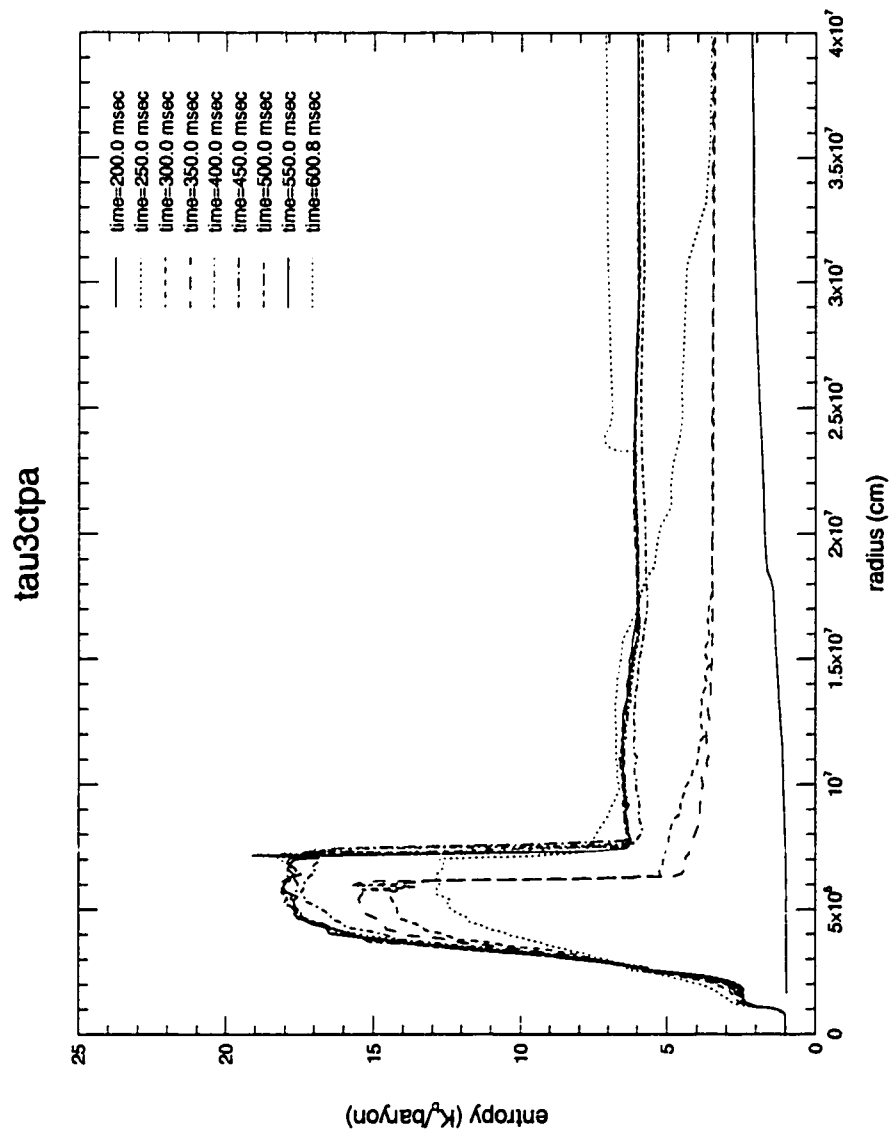


Figure 5.47: Entropy versus radius evolution - Convective with braking and turbulent pressure - All neutrino species

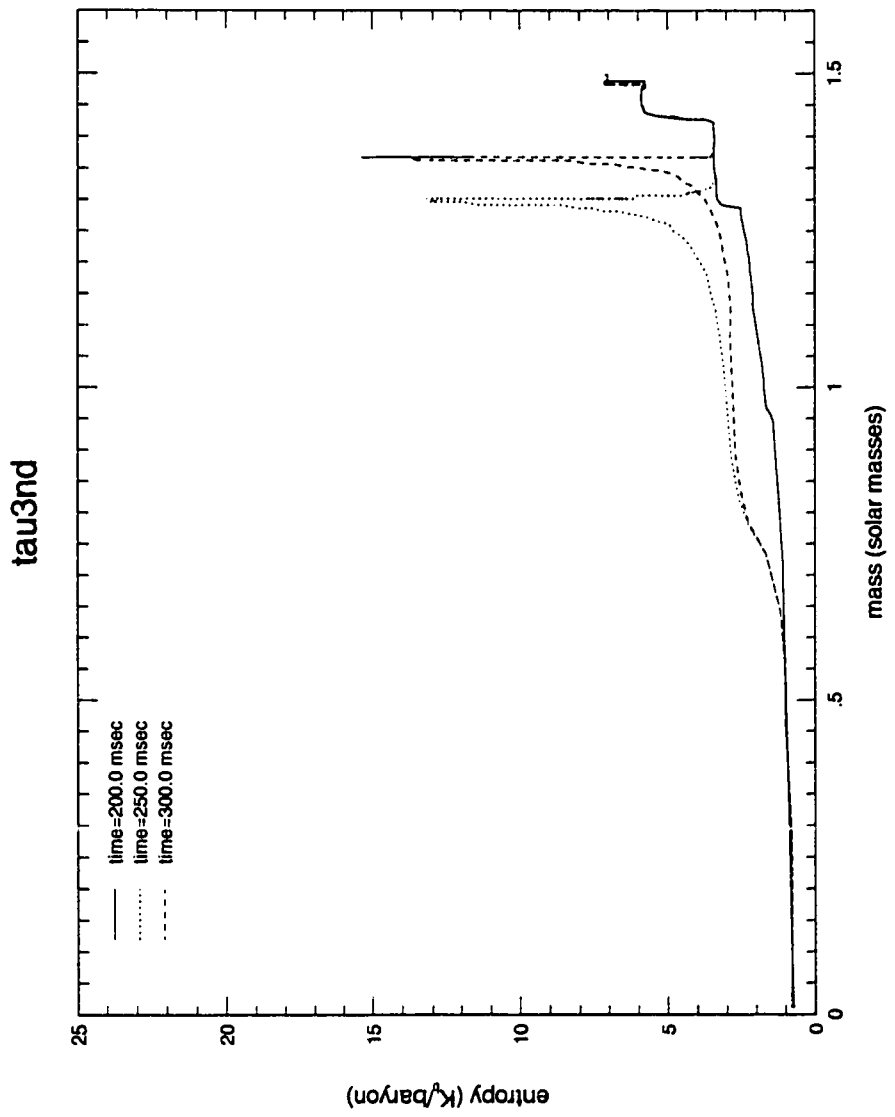


Figure 5.48: Entropy evolution - Convective with neutrino advection - All neutrino species

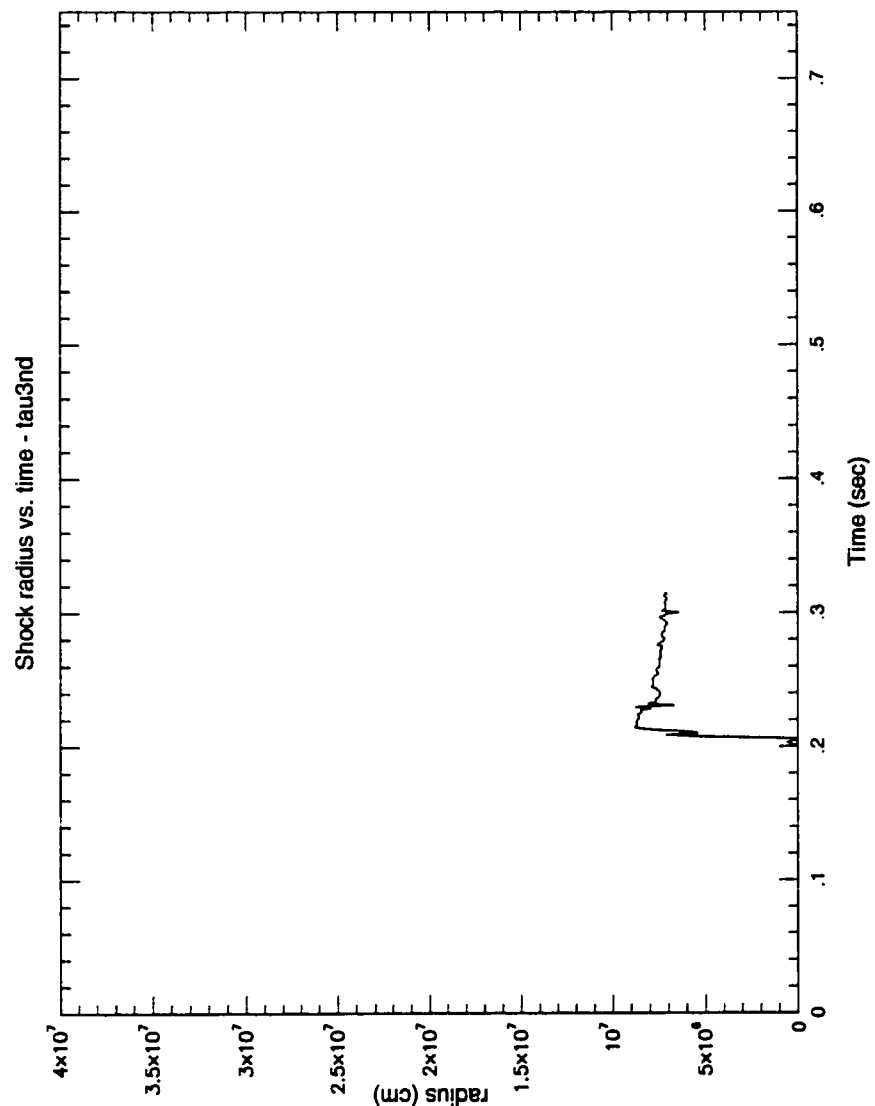


Figure 5.49: Shock radius versus time - Convective with neutrino advection - All neutrino species

into later times, there were no differences in the subsequent heating and cooling rates and no differences in shock evolution.

## 5.8 Analysis of the convective models

It appears that across a wide set of model assumptions, convection does not qualitatively affect the evolution of the proto-neutron star. This results is unsurprising given the discussion of the non-convective models. Convective instabilities take several times of milliseconds to develop, and therefore makes little impact on the entropy profile that exists once the proto-neutron star has left the early phase of shock development.

Once the proto-neutron star stalls and the post shock material is in hydrostatic equilibrium, it encounters the heating dilemma, and as long as the shock evolves quasi-statically convective heating will cause the shock to retreat and for an explosion to be more unlikely.

Convective heating is also unlikely to provide enough heating to break hydrostatic equilibrium as the follow argument indicates. To break hydrostatic equilibrium, the energy transfer rate must satisfy

$$F > \Delta E \frac{\Delta r}{\tau_{dyn}} \quad (5.5)$$

where  $F$  is the energy transfer rate,  $\Delta r$  is the length scale across which energy is to be transferred, and  $\Delta E$  is the energy difference across the length scale. If the energy is transferred only by convection, one can write

$$\Delta E v_{conv} > \Delta E \frac{\Delta r}{\tau_{dyn}}. \quad (5.6)$$

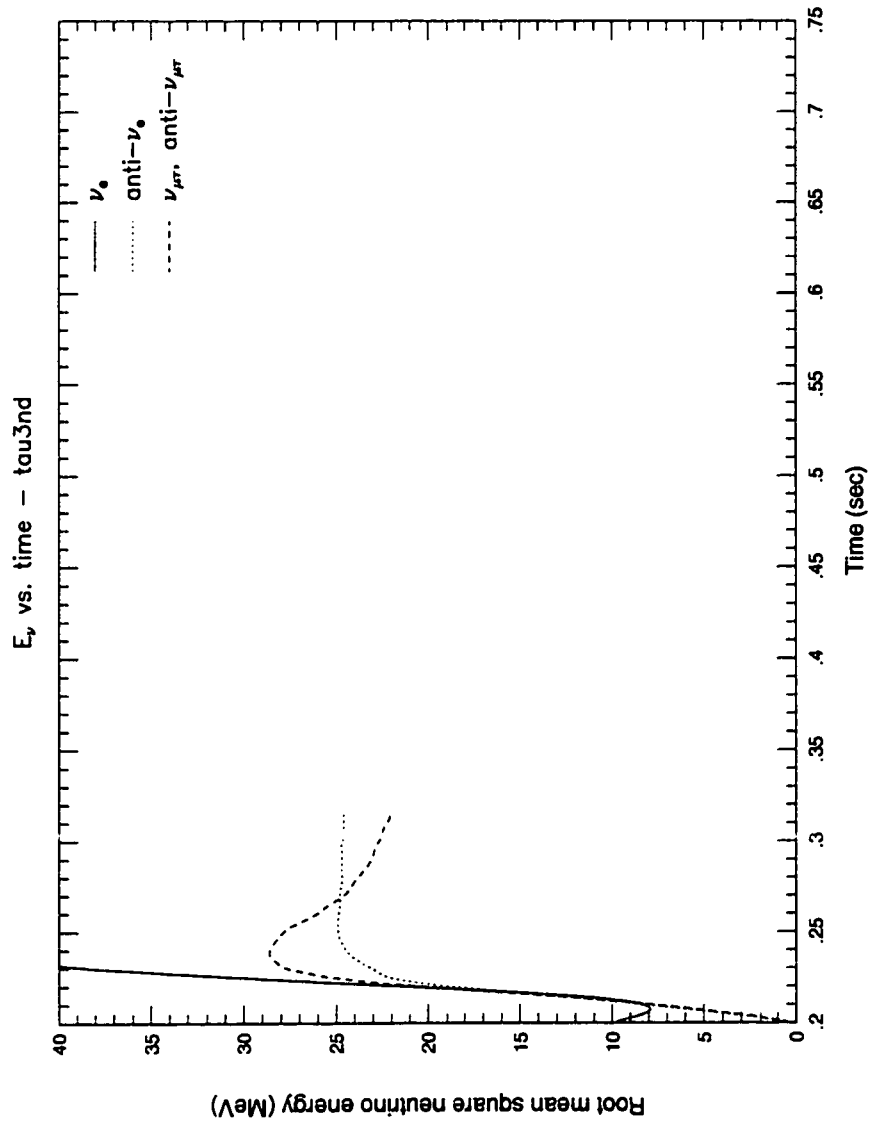


Figure 5.50: Neutrino energy versus time - Convective with neutrino advection  
- All neutrino species

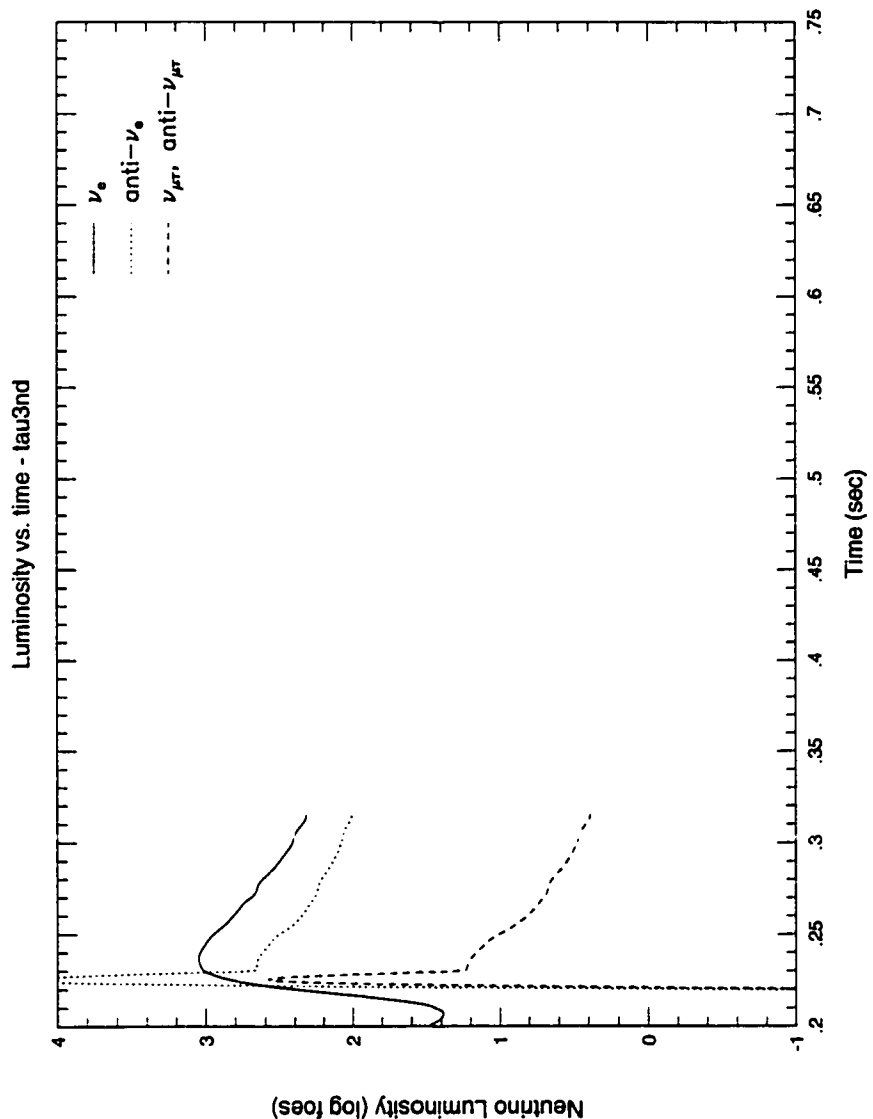


Figure 5.51: Neutrino luminosity versus time - Convective with neutrino advection - All neutrino species

The dynamical time scale can be estimated from the Mach number  $M$  as

$$\tau_{dyn} = M \Delta r. \quad (5.7)$$

Substituting and canceling terms, we obtain

$$v_{conv} > M. \quad (5.8)$$

Therefore to revive a shock via convective heating alone requires that the convective velocities exceed the Mach number. This is physically unrealistic.

The forgoing discussion suggests ways in which convection can affect the explosion. First, if there is a threshold beyond which hydrostatic equilibrium cannot be maintained, convection may, in combination with neutrino heating, push shock heating over this threshold. Second, convection may serve to distort the shape of the shock, causing the global behavior of the shock to differ from the behavior expected from the local shock jump conditions. Nevertheless, it appears that convection plays, at best a marginal role. While it may convert a near-fizzle to an explosion, the role of convection is secondary to neutrino heating.

# Chapter 6

## Conclusion

In recent years, it has become increasingly clear that core collapse supernova are fundamentally multi-dimensional phenomenon. In the words of Burrows (1996), “Supernova do not explode as spheres, but aspherically in plumes, resembling cauliflower and broccoli more than oranges.” This multi-dimensionality of core collapse supernovae poses a dilemma for numerical studies in that it forces numerical theorists to choose between one-dimensional codes which leave out important aspects of the core collapse, and multi dimensional codes whose computational demands make them impractical for use in parameter searches. Moreover, the results of multi-dimensional calculations threaten to render obsolete the one dimensional codes which have been developed to calculate neutrino interactions more accurately (Mezzacappa & Bruenn 1993a, 1993b, 1993c; Eastman & Pinto 1993) or to study supernova nucleosynthesis (Woosley & Weaver 1995 ; Hasimoto, Nomoto & Shigeyama 1995).

The main purpose of this dissertation is to resolve this dilemma by demonstrating that some of the multi-dimensional convective aspects of the core collapse can be simulated in a one dimensional code. Moreover, such a

code is essential for parameter studies of core collapse supernova. Because the behavior of supernova models appears to change in complex qualitative ways in response to details of neutrino and convective modeling, and because some of the parameters that appear to affect supernova models are not well constrained physically, such parameter studies are essential for determining how the input physics of a supernova model affects the supernova outcome. Moreover, the complex behavior of the models presented here suggest that there is much left to be understood about the mechanisms of supernovae.

The models in this dissertation suggest that, under the given assumptions, convection can be unimportant in the outcome of the development of a supernova models. In these models, there were few differences in the evolution of models by the addition of convection. Furthermore, the failure of convection to radically change the dynamics of the explosion appears to be a robust result extending across the various parameter assumptions in this investigation.

At the same time, this investigation may make clearer the fundamental difficulties in producing explosions via the delayed shock model. In comparing models with different species of neutrinos there appears to be a “heating dilemma” in which increasing heating behind the shock causes the shock to move inward rather than outward. This finding suggests that one fruitful avenue of research is to develop analytic and semi-analytic models to establish the conditions under which the heating dilemma no longer applies. This line of inquiry would seek to provide answers to questions such as: under what conditions is hydrostatic equilibrium behind the shock? are there positive feedback mechanisms which would allow for a large increase in neutrino emissions? and do asymmetric shocks allow a means of bypassing the heating dilemma.

## **6.1 Future Application of the Convective Algorithm**

The one dimensional convection algorithm described in this dissertation can be easily added to existing one dimensional codes. One area of further research would be to incorporate this convective algorithm in codes with different neutrino algorithms such as a full Boltzmann calculation (Mezzacappa & Bruenn 1993a, 1993b, 1993c) or a lambda-relaxation model (Eastman & Pinto 1993) to explore the effects of different neutrino algorithms.

Another use of this convective model is to investigate how changes in the neutrino cross sections affect the dynamics of the explosion. Recent papers have suggested large uncertainties in the absorption and emission cross sections of neutrinos at high densities due to large scale nuclear correlation effects (Burrows & Sawyer 1998) or ion screening (Bruenn & Mezzacappa 1997). Furthermore, there are neutrino processes which have not been included in this investigation such as Bremsstrahlung (Burrows 1997) which may have important effects on the outcome of the explosion. As has been noted in this paper, neutrino heating and cooling may interact in a complex way with convection, and a parameter study is needed to investigate how these neutrino elements affect the supernova process.

## **6.2 Applicability of this model to other astrophysical convection problems**

The convective model developed in this dissertation was designed specifically to deal with the problem of core collapse supernovae and contains assumptions and approximations which may limit its usefulness. Nevertheless, it is useful to think about the relationship between this model and convective models in other astrophysical contexts.

There are a number of distinguishing features of convection in the context of a supernova. First of all, unlike convection in most other astrophysical situations, the convection in a core collapse supernova occurs on the same time scale as the dynamical phenomena of interest. Second, the convection occurs within a large entropy gradient that has been imposed from the outside. Finally, the physical process of interest lies in the development of convection rather than in the steady state nature of convection. These conditions are radically different from convection in main sequence stars. In that case convection is essentially steady state.

The cases in which the convective model presented may be useful include Cepheid variables and the later stages of the evolution of high mass stars. Unlike standard stellar convection, in which the star is in dynamic equilibrium, stars at these stages of evolution are changing on dynamic time scales.

## **6.3 Further research**

The results of these investigations have implications for future research of iron core collapse. One strategy for theoretical numerical work is to use increasingly

sophisticated and complex models in the hopes that one will converge toward the actual phenomenon being studied. As consensus is reached on the basic questions and issues, the research community focuses on extending the basic models to generate more details predictions and to extend the basic models to explore new phenomenon. An example of an astrophysical field in which this strategy has been used successfully is the evolution of solar mass main sequence stars. In this field, there is consensus on the basic mechanism and physics needed to model the stars, and progress in this field is largely a story generating increasingly sophisticated models which model a larger variety of phenomenon.

Unfortunately, this strategy does not seem to be successful in increasing our understanding of convection in core collapse supernova. The problem with this strategy is that the basic mechanisms which govern core collapse supernova are poorly understood. Because the explosion mechanism may vary qualitatively as the input physical assumptions are changed and because the physics is not sufficiently known to constrain the models to one mechanism, there is no reason for models for different groups to converge as physics is added.

Instead of relying only on developing more numerically complex and intensive models, it is also necessary to develop codes which can map out how the mechanisms change as the physical assumptions change. In addition to developing codes which are numerically intensive, there is a need of codes and analytic models which are less numerically intensive and which can therefore explore the parameters which affect core collapse. In performing this investigation, one important point is that the input models need not be physically realistic in order to provide insight in the behavior of the proto-neutron star.

Stated another way, examining how a supernova model behaves when given physically unrealistic input assumptions may illustrate some of the underlying dynamics of the model.

The present investigation reveals some of the benefits of this approach. Using the current model, we can demonstrate that within the realm of the assumptions used in the current investigation, that the behavior of the model is relatively insensitive to the details of the convective algorithm. By contrast, the models underwent qualitatively different behaviors when the types of neutrino species were varied. This suggests that one line of further results is to vary the details of the neutrino emission and absorption rates to see how they vary the outcomes of the models.

In addition, this investigation has pointed out a number of interpretational issues which need to be addressed in supernova models. The existence of a heating dilemma in which increased heating leads a retreat of the shock suggests that attention should be focused in developing mechanism to break the assumptions that give rise to the dilemma. Finally, the apparent inverse relationship between emitted root mean square neutrino energy and shock depth, which be further examined to see if it may provide an observational diagnostic of conditions within the proto-neutron star. Clearly, this investigation has provided the beginning steps for what may prove to be a long but interesting road.

# Bibliography

- [1] J. D. Anand, A. Goyal, V. K. Gupta, and S. Singh. Burning of two-flavor quark matter into strange matter in neutron stars and in supernova cores. *Astrophysical Journal*, 481:954+, May 1997.
- [2] D. Arnett, Bahcall J.N., Kirshner R. P., and S. E. Woosley. Supernova 1987A. *Annual Reviews of Astronomy and Astrophysics*, 27:629–700, 1989.
- [3] M. B. Aufderheide, E. Baron, and F. K. Thielemann. Shock waves and nucleosynthesis in Type II supernova. *Astrophysical Journal*, 370:630–642, 1991.
- [4] R. Barbieri and R. N. Mohapatra. Limit on the magnetic moment of the neutrino from supernova 1987A observations. *Physical Review Letters*, 61:27–30, July 1988.
- [5] E. Baron and J. Cooperstein. The effect of iron core structure on supernovae. *Astrophysical Journal*, 353:597–611, April 1990.
- [6] O. G. Benvenuto and J. E. Horvath. Evidence for strange matter in supernovae ? *Physical Review Letters*, 63:716–719, August 1989.

- [7] H. A. Bethe, G. E. Brown, and J. Cooperstein. Convection in supernova theory. *Astrophysical Journal*, 322:201–205, November 1987.
- [8] H. A. Bethe and J. R. Wilson. Revival of a stalled supernova shock by neutrino heating. *Astrophysical Journal*, 295:14–23, August 1985.
- [9] S. I. Blinnikov and L. B. Okun. Supernova models and the neutrino magnetic moment. *Soviet Astronomy Letters*, 14:368+, September 1988.
- [10] I. A. Bonnell and J. E. Pringle. Gravitational radiation from supernovae. *Monthly Notices of the Royal Astronomical Society*, 273:L12–L14, March 1995.
- [11] R. Bowers and J. R. Wilson. Collapse of iron stellar cores. *Astrophysical Journal*, 263:366–376, December 1982.
- [12] N. Brandt and P. Podsiadlowski. The effects of high-velocity supernova kicks on the orbital properties and sky distributions of neutron-star binaries. *Monthly Notices of the Royal Astronomical Society*, 274:461–484, May 1995.
- [13] G. E. Brown and H. A. Bethe. A scenario for a large number of low-mass black holes in the galaxy. *Astrophysical Journal*, 423:659+, March 1994.
- [14] S. W. Bruenn. Stellar core collapse - numerical model and infall epoch. *Astrophysical Journal Supplement*, 58:771–841, August 1985.
- [15] S. W. Bruenn, J. R. Buchler, and M. Livio. Rayleigh-Taylor convective overturn in stellar collapse. *Astrophysical Journal Letters*, 234:L183–L186, December 1979.

- [16] S. W. Bruenn and T. Dineva. The role of doubly diffusive instabilities in the core-collapse supernova mechanism. *Astrophysical Journal Letters*, 458:L71–+, February 1996.
- [17] S. W. Bruenn and A. Mezzacappa. Prompt convection in core collapse supernovae. *Astrophysical Journal Letters*, 433:L45–L48, September 1994.
- [18] S.W. Bruenn and A. Mezzacappa. Ion screening effects and stellar collapse. *Physics Review D*, 56:7529–47, December 1997.
- [19] A. Burrows. Convection and the mechanism of Type II supernovae. *Astrophysical Journal Letters*, 318:L57–L61, July 1987.
- [20] A. Burrows. A statistical derivation of an upper limit to the electron neutrino mass from the SN 1987A neutrino data. *Astrophysical Journal Letters*, 328:L51–L54, May 1988.
- [21] A. Burrows. Towards a synthesis of core-collapse supernova theory. Los Alamos Physics Preprint Archive <http://xxx.lanl.gov> – preprint astro-ph/960635, 1996.
- [22] A. Burrows. New insights into core-collapse supernova theory. Los Alamos Physics Preprint Archive <http://xxx.lanl.gov> – preprint astro-ph/9706137, 1997.
- [23] A. Burrows and J. Goshy. A theory of supernova explosions. *Astrophysical Journal Letters*, 416:L76, 1993.
- [24] A. Burrows, J. Hayes, and B. A. Fryxell. On the nature of core-collapse supernova explosions. *Astrophysical Journal*, 450:830+, September 1995.

- [25] A. Burrows and J. M. Lattimer. The effect of trapped lepton number and entropy on the outcome of stellar collapse. *Astrophysical Journal*, 270:735–739, July 1983.
- [26] A. Burrows and J. M. Lattimer. The prompt mechanism of Type II supernovae. *Astrophysical Journal Letters*, 299:L19–L22, December 1985.
- [27] A. Burrows and R. F. Sawyer. The effects of correlations on neutrino opacities in nuclear matter. Los Alamos Physics Preprint Archive <http://xxx.lanl.gov> – preprint astro-ph/9801082, 1998.
- [28] V. M. Canuto. Turbulent convection with overshooting - reynolds stress approach. *Astrophysical Journal*, 392:218–232, June 1992.
- [29] V. M. Canuto. Turbulent convection with overshooting: Reynolds stress approach. II. *Astrophysical Journal*, 416:331+, October 1993.
- [30] V. M. Canuto, I. Goldman, and I. Mazzitelli. Stellar turbulent convection: A self-consistent model. *Astrophysical Journal*, 473:550+, December 1996.
- [31] J. I. Castor. Radiative transfer in spherically symmetric flows. *Astrophysical Journal*, 178:779–792, December 1972.
- [32] F. Cattaneo, N. H. Brummell, J. Tcomre, A. Malagoli, and N. E. Hurlburt. Turbulent compressible convection. *Astrophysical Journal*, 370:282–294, March 1991.
- [33] H. Y. Chiu, K. L. Chan, and Y. Kondo. Correlation mass method for analysis of neutrinos from supernova 1987A. *Astrophysical Journal*, 329:326–334, June 1988.

- [34] K. Choi, K. Kang, and J. E. Kim. Invisible-axion emissions from SN 1987A. *Physical Review Letters*, 62:849–851, February 1989.
- [35] K. Choi and A. Santamaria. Majorons and supernova cooling. *Physics Review D*, 42:293+, 1990.
- [36] S. A. Colgate. Mass ejection from supernova. *Astrophysical Journal*, 153:335, 1968.
- [37] S. A. Colgate and R. H. White. The hydrodynamic behavior of supernovae explosions. *Astrophysical Journal*, 143:626, 1964.
- [38] K. R. De Nisco, S. W. Bruenn, and A. Mezzacappa. The effects of general relativity on core collapse supernovae. Los Alamos Physics Preprint Archive <http://xxx.lanl.gov> – preprint astro-ph/9808048, 1998.
- [39] R. G. Eastman and P. A. Pinto. Spectrum formation in supernovae - numerical techniques. *Astrophysical Journal*, 412:731–751, August 1993.
- [40] R. I. Epstein. Lepton-driven convection in supernovae. *Monthly Notices of the Royal Astronomical Society*, 188:305–325, August 1979.
- [41] B. Freytag, H. G. Ludwig, and M. Steffen. Hydrodynamical models of stellar convection. the role of overshoot in da white dwarfs, a-type stars, and the sun. *Astronomy and Astrophysics*, 313:497–516, September 1996.
- [42] C. L. Fryer, A. Burrows, and W. Benz. Pulsar velocity distributions from natal kicks. *Bulletin of the American Astronomical Society*, 188:7310+, May 1996.

- [43] G. M. Fuller, R. Mayle, B. S. Meyer, and J. R. Wilson. Can a closure mass neutrino help solve the supernova shock reheating problem? *Astrophysical Journal*, 389:517–526, April 1992.
- [44] D. O. Gough. The anelastic approximation for thermal convection. *Journal of the Atmospheric Sciences*, 26:448–456, May 1969.
- [45] S. A. Grossman. A theory of non-local mixing-length convection - III. comparing theory and numerical experiment. *Monthly Notices of the Royal Astronomical Society*, 279:305–336, March 1996.
- [46] S. A. Grossman and R. Narayan. A theory of nonlocal mixing-length convection. II – generalized smoothed particle hydrodynamics simulations. *Astrophysical Journal Supplement*, 89:361–394, December 1993.
- [47] S. A. Grossman, R. Narayan, and D. Arnett. A theory of nonlocal mixing-length convection. I – the moment formalism. *Astrophysical Journal*, 407:284–315, April 1993.
- [48] I. Hachisu, T. Matsuda, K. Nomoto, and T. Shigeyama. Nonlinear growth of Rayleigh-Taylor instabilities and mixing in SN 1987A. *Astrophysical Journal Letters*, 358:L57–L61, August 1990.
- [49] D. Hartmann, S. E. Woosley, and M. F. El Eid. Nucleosynthesis in neutron-rich supernova ejecta. *Astrophysical Journal*, 297:837–845, October 1985.
- [50] M. Hasimoto, K. Nomoto, and T. Shigeyama. Explosive nucleosynthesis in supernova 1987A. *Astronomy and Astrophysics*, 210:L5–L8, 1989.

- [51] M. Herant and W. Benz. Postexplosion hydrodynamics of SN 1987A. *Astrophysical Journal*, 387:294–308, March 1992.
- [52] M. Herant, W. Benz, W. R. Hix, C. L. Fryer, and S. A. Colgate. Inside the supernova: A powerful convective engine. *Astrophysical Journal*, 435:339–361, November 1994.
- [53] M. E. Herant, W. Benz, and S. A. Colgate. Postcollapse hydrodynamics of SN 1987A - two-dimensional simulations of the early evolution. *Astrophysical Journal*, 395:642–653, August 1992.
- [54] R. D. Hoffman, Y. Z. Qian, and S. E. Woosley. Model independent r-process nucleosynthesis - constraints on the key parameters. *Bull. American Astron. Soc.*, 187, #97.05, 187:9705+, December 1995.
- [55] J. C. Houck and R. A. Chevalier. Steady spherical hypercritical accretion onto neutron stars. *Astrophysical Journal*, 376:234–244, July 1991.
- [56] H. T. Janka and E. Mueller. Neutron star recoils from anisotropic supernovae. *Astronomy and Astrophysics*, 290:496–502, October 1994.
- [57] H. T. Janka and E. Mueller. The first second of a Type II supernova: Convection, accretion, and shock propagation. *Astrophysical Journal Letters*, 448:L109–+, August 1995.
- [58] H. T. Janka and E. Mueller. Neutrino heating, convection, and the mechanism of type-ii supernova explosions. *Astronomy and Astrophysics*, 306:167+, February 1996.

- [59] W. Keil, H. T. Janka, and E. Mueller. Ledoux convection in protoneutron stars—a clue to supernova nucleosynthesis? *Astrophysical Journal Letters*, 473:L111–+, December 1996.
- [60] R. Kippenhahn and A. Weigart. *Stellar Structure and Evolution*. Springer Verlag, New York, 1994.
- [61] R. Kuhfuss. A model for time-dependent turbulent convection. *Astronomy and Astrophysics*, 160:116–120, 1986.
- [62] L.D. Landau and E. M. Lifshitz. *Fluid Mechanics*. Pergamon Press, Oxford, 2nd edition, 1987.
- [63] N. Langer. Non-local treatment of convection and overshooting from stellar convective cores. *Astronomy and Astrophysics*, 164:45–50, August 1986.
- [64] J. M. Lattimer and J. Cooperstein. Limits on the neutrino magnetic moment from SN 1987A. *Physical Review Letters*, 61:23–26, July 1988.
- [65] C. D. Levermore and G. C. Pomraning. A flux-limited diffusion theory. *Astrophysical Journal*, 248:321–334, August 1981.
- [66] T. J. Loredo and D. Q. Lamb. Neutrinos from SN 1987A - implications for cooling of the nascent neutron star and the mass of the electron antineutrino. *New York Academy Sciences Annals*, 571:601–630, 1989.
- [67] T. J. Loredo and D. Q. Lamb. Implications of the supernova 1987A neutrinos for supernova theory and the mass of nu/e. In *Supernovae. The Tenth Santa Cruz Workshop in Astronomy and Astrophysics, held*

*July 9-21, 1989, Lick Observatory. Editor, S.E. Woosley; Publisher, Springer-Verlag, New York, 1991. LC # QB856 .S26 1989. ISBN # 0387970711. P.405, 1991, pages 405+, 1991.*

- [68] A. Maeder. Stellar evolution. III. the overshooting from convective cores. *Astronomy and Astrophysics*, 40:303–310, May 1975.
- [69] R. McCray. Supernova 1987A revisited. *Annual Reviews of Astronomy and Astrophysics*, 31:175–216, 1993.
- [70] B. S. Meyer and J. S. Brown. Survey of r-process models. *Astrophysical Journal Supplement*, 112:199+, September 1997.
- [71] B. S. Meyer, G. J. Mathews, W. M. Howard, S. E. Woosley, and R. D. Hoffman. r-process nucleosynthesis in the high-entropy supernova bubble. *Astrophysical Journal*, 399:656–664, November 1992.
- [72] A. Mezzacappa and S. W. Bruenn. A numerical method for solving the neutrino Boltzmann equation coupled to spherically symmetric stellar core collapse. *Astrophysical Journal*, 405:669–684, March 1993b.
- [73] A. Mezzacappa and S. W. Bruenn. Stellar core collapse - a Boltzmann treatment of neutrino-electron scattering. *Astrophysical Journal*, 410:740–760, June 1993c.
- [74] A. Mezzacappa and S. W. Bruenn. Type II supernovae and Boltzmann neutrino transport - the infall phase. *Astrophysical Journal*, 405:637–668, March 1993a.
- [75] A. Mezzacappa, A. C. Calder, S. W. Bruenn, J. M. Blondin, M. W. Guidry, M. R. Strayer, and A. S. Umar. An investigation of neutrino-

- driven convection and the core collapse supernova mechanism using multigroup neutrino transport. *Astrophysical Journal*, 495:911+, March 1998.
- [76] D. Mihalas, R. P. Weaver, and J. G. Sanderson. On iterative solutions of the lte model atmosphere problem. *Journal of Quantitative Spectroscopy and Radioactive Transfer*, 28:53–59, July 1982.
  - [77] E. Mueller and H. T. Janka. Gravitational radiation from convective instabilities in Type II supernova explosions. *Astronomy and Astrophysics*, 317:140–163, January 1997.
  - [78] E. S. Myra and S. A. Bludman. Neutrino transport and the prompt mechanism for Type II supernovae. *Astrophysical Journal*, 340:384–395, May 1989.
  - [79] E. S. Myra, S. A. Bludman, Y. Hoffman, I. Lichenstadt, N. Sack, and K. A. Van Riper. The effect of neutrino transport on the collapse of iron stellar cores. *Astrophysical Journal*, 318:744–759, July 1987.
  - [80] A. Nordlund. On convection in stellar atmospheres. *Astronomy and Astrophysics*, 32:407+, June 1974.
  - [81] M. Rayet, M. Arnould, M. Hashimoto, N. Prantzos, and K. Nomoto. The p-process in Type II supernovae. *Astronomy and Astrophysics*, 298:517+, June 1995.
  - [82] C. Spruit, A. Nordlund, and A. M. Title. Solar convection. *Annual Reviews of Astronomy and Astrophysics*, 28:263–301, 1990.

- [83] R. F. Stellingwerf. A simple model for coupled convection and pulsation. *Astrophysical Journal*, 303:119–129, April 1986.
- [84] M. Takahara and K. Sato. Supernova 1987A and constraint on the mass and lifetime of tau neutrinos. In *Atmospheric Diagnostics of Stellar Evolution. Chemical Peculiarity, Mass Loss, and Explosion. Proceedings of the 108th. Colloquium of the International Astronomical Union, held at the University of Tokyo, Japan, September 1-4, 1987. [Lecture Notes in Physics, Volume 305]* Editor, K. Nomoto; Publisher, Springer-Verlag, Berlin, New York, 1988. ISBN # 3-540-19478-9. LC # QB806 .I18 1987, P.428, 1987, pages 428+, 1988.
- [85] K. Takahashi, J. Witt, and H. T. Janka. Nucleosynthesis in neutrino-driven winds from protoneutron stars II. the r-process. *Astronomy and Astrophysics*, 286:857–869, June 1994.
- [86] G. Testor. Which star in the complex Sk-69 202 is the supernova 1987 A progenitor? *Astronomy and Astrophysics*, 190:L1–L4, January 1988.
- [87] F. K. Thielemann, M. Hashimoto, and K. Nomoto. Explosive nucleosynthesis in SN 1987A. II - composition, radioactivities, and the neutron star mass. *Astrophysical Journal*, 349:222–240, January 1990.
- [88] F. K. Thielemann, K. Nomoto, and M. A. Hashimoto. Core-collapse supernovae and their ejecta. *Astrophysical Journal*, 460:408+, March 1996.
- [89] S. E. Thorsett, Z. Arzoumanian, M. M. McKinnon, and J. H. Taylor.

The masses of two binary neutron star systems. *Astrophysical Journal Letters*, 405:L29–L32, March 1993.

- [90] F. X. Timmes, S. E. Woosley, D. H. Hartmann, R. D. Hoffman, T. A. Weaver, and F. Matteucci. 26Al and 60Fe from supernova explosions. *Astrophysical Journal*, 449:204+, August 1995.
- [91] F. X. Timmes, S. E. Woosley, and Thomas A. Weaver. The neutron star and black hole initial mass function. *Astrophysical Journal*, 457:834+, February 1996.
- [92] A. P. Trofimenko and V. S. Gurin. Gravitational radiation associated with anticollapse and supernova explosions. *Astrofizika*, 34, 83-89 (1991), 34:83-89, 1991.
- [93] E. P. J. Van Den Heuvel and J. Van Paradijs. Intrinsic kicks at birth are required to explain the observed properties of single and binary neutron stars. *Astrophysical Journal*, 483:399+, July 1997.
- [94] J. van Paradijs and E. McClintock. *X-ray binaries*, page 58. Cambridge University Press, Cambridge, 1995.
- [95] R. M. West, A. Lauberts, H. E. Schuster, and H. E. Jorgensen. Astrometry of SN 1987A and Sanduleak-69 202. *Astronomy and Astrophysics*, 177:L1–L3, May 1987.
- [96] J. R. Wilson and R. W. Mayle. Convection in core collapse supernovae. *Physics Reports*, 163:63–78, 1988.
- [97] J. R. Wilson and R. W. Mayle. Report on the progress of supernova research by the Livermore group. *Physics Reports*, 227:97+, 1993.

- [98] S. E. Woosley, D. H. Hartmann, R. D. Hoffman, and W. C. Haxton. The nu-process. *Astrophysical Journal*, 356:272–301, June 1990.
- [99] S. E. Woosley and W. C. Haxton. Supernova neutrinos, neutral currents and the origin of fluorine. *Nature*, 334:45–47, July 1988.
- [100] S. E. Woosley and Robert D. Hoffman. The alpha-process and the r-process. *Astrophysical Journal*, 395:202–239, August 1992.
- [101] S. E. Woosley and T. A. Weaver. The evolution of massive stars. II explosive hydrodynamics and nucleosynthesis. *Astrophysical Journal*, 101:181–235, 1995.
- [102] S. E. Woosley, J. R. Wilson, G. J. Mathews, R. D. Hoffman, and B. S. Meyer. The r-process and neutrino-heated supernova ejecta. *Astrophysical Journal*, 433:229–246, September 1994.
- [103] D. R. Xiong. Time-dependent convection theory generalized for nonradial oscillations of stars. *Acta Astronomica Sinica V.25:3, P. 223, 1984, 25:223+, 1984.*
- [104] D. R. Xiong. Stellar convection. (*IAU, Asian-Pacific Regional Astronomy Meeting, 5th, Sydney, Australia, July 16-20, 1990, Proceedings. A92-17077 04-90) Astronomical Society of Australia, Proceedings (ISSN 0066-9997), vol. 9, no. 1, 1991, p. 26-31., 9:26-31, 1991.*
- [105] A. Yahil. Self-similar stellar collapse. *Astrophysical Journal*, 265:1047–1055, February 1983.
- [106] S. Yamada and K. Sato. Numerical study of rotating core collapse in supernova explosions. *Astrophysical Journal*, 434:268–276, October 1994.

# Vita

Joseph Chen-Yu was born in Morgantown, West Virginia on December 5, 1969, the son of Ming Kang Wang and Luan Luan Wang. He has a younger sister, Ruth and a younger brother, Daniel. After graduating from Forest High School in Ocala, Florida in June 1987, he entered the Massachusetts Institute of Technology, majoring in Physics with a concentration in Chinese language. He received his Bachelor of Science in May 1991. In September 1991 he entered a Graduate Program in the Department of Astronomy in the University of Texas at Austin. He received his Master of Arts in Astronomy from the University of Texas at Austin in May 1994.

He married Suchen Liao on November 15, 1996. She received a Master of Arts in Child Welfare from the Chinese Cultural University in Taipei, Taiwan, Republic of China and is currently a doctoral student in the Early Childhood Education program at the University of Texas at Austin. They have a daughter Rebecca Si-Ning Wang, who was born on March 8, 1998.

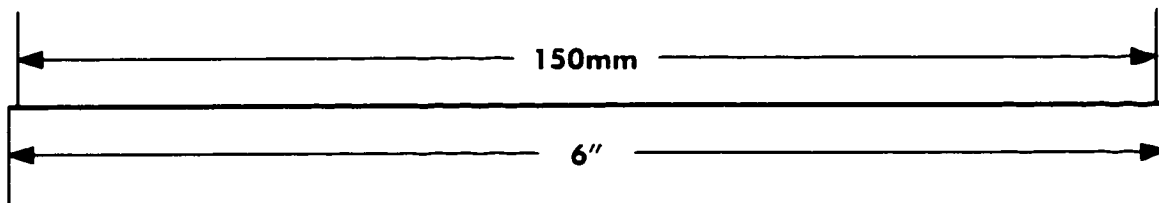
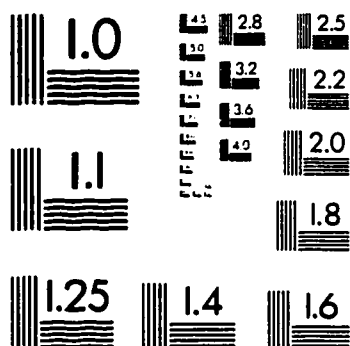
Permanent Address: c/o Luan Luan Wang  
1405 Raa Avenuc  
Tallahassee, Florida 32303

This dissertation was typeset with  $\text{\LaTeX} 2\epsilon$ <sup>1</sup> by the author.

---

<sup>1</sup> $\text{\LaTeX} 2\epsilon$  is an extension of  $\text{\LaTeX}$ .  $\text{\LaTeX}$  is a collection of macros for  $\text{\TeX}$ .  $\text{\TeX}$  is a trademark of the American Mathematical Society. The macros used in formatting this dissertation were written by Dinesh Das, Department of Computer Sciences, The University of Texas at Austin.

# IMAGE EVALUATION TEST TARGET (QA-3)



APPLIED IMAGE, Inc.  
1653 East Main Street  
Rochester, NY 14609 USA  
Phone: 716/482-0300  
Fax: 716/288-5989

© 1993, Applied Image, Inc., All Rights Reserved

